THE HONG KONG
POLYTECHNIC UNIVERSITY
香港理工大學
Pao Yue-kong Library
包玉剛圖書館

Copyright Undertaking

This thesis is protected by copyright, with all rights reserved.

By reading and using the thesis, the reader understands and agrees to the following terms:

1. The reader will abide by the rules and legal ordinances governing copyright regarding the use of the thesis.
2. The reader will use the thesis for the purpose of research or private study only and not for distribution or further reproduction or any other purpose.
3. The reader agrees to indemnify and hold the University harmless from and against any loss, damage, cost, liability or expenses arising from copyright infringement or unauthorized usage.

IMPORTANT

If you have reasons to believe that any materials in this thesis are deemed not suitable to be distributed in this form, or a copyright owner having difficulty with the material being included in our database, please contact lbsys@polyu.edu.hk providing details. The Library will look into your claim and consider taking remedial action upon receipt of the written requests.

Pao Yue-kong Library, The Hong Kong Polytechnic University, Hung Hom, Kowloon, Hong Kong

http://www.lib.polyu.edu.hk

MECHANISTIC STUDY OF BECLIN1-TARGETING AUTOPHAGY MODULATORS TO INHIBIT LUNG CANCER CELL PROLIFERATION

CHEN JINGYI

PhD

The Hong Kong Polytechnic University

2023

The Hong Kong Polytechnic University
Department of Applied Biology and Chemical Technology

Mechanistic Study of Beclin1-targeting Autophagy Modulators to Inhibit Lung Cancer Cell Proliferation

Chen Jingyi

A thesis submitted in partial fulfilment of the requirements
for the degree of Doctor of Philosophy

December 2022

CERTIFICATE OF ORIGINALITY

I hereby declare that this thesis is my own work and that, to the best of my knowledge and belief, it reproduces no material previously published or written, nor material that has been accepted for the award of any other degree or diploma, except where due acknowledgement has been made in the text.

Signature:

Name of student： Chen Jingyi

Abstract

Abstract:

Lung cancer is the most common cause of cancer-related death in the world. There are 2 main subtypes of lung cancer. The most common type is Non-small-cell Lung Cancer (NSCLC), which accounts for 85% of all lung cancer cases and includes adenocarcinoma, squamous cell carcinoma, and large cell carcinoma. The second major subtype is Small-cell Lung Cancer (SCLC), accounting for the remaining 15%. For early-stage or localized lung cancer, curative surgery and many effective drugs are available to push the 5-year survival rate to the impressive level of 52.6%. For advanced or metastatic stage, therapeutic options are rather limited with the 5-year survival rate dropping to the dismal level of 3.5%. Novel therapeutic strategies are urgently needed.

Epidermal Growth Factor Receptor (EGFR) is a major drug target for non-small-cell lung carcinoma (NSCLC). Tyrosine Kinase Inhibitors (TKIs) like erlotinib are potent inhibitors of EGFR and have achieved impressive clinical success against NSCLC. However, NSCLC cells readily develop resistance to TKIs by acquiring mutations in EGFR or other oncogenes. Novel strategies to inhibit EGFR are needed to overcome this urgent problem of TKI resistance.

SCLC is characterized by highly proliferative and metastatic lung cancer, making it ineligible for surgery in most cases. Current outcome of clinical treatment for SCLC

is poor since lack of known predictive or diagnostic biomarkers and poor response to standard therapies. SCLC is usually sensitive to initial chemotherapy but prone to recurrence and acquired drug resistance. Upon receiving treatment, the median survival time (MST) of SCLC patients is only 8-20 months(Puglisi, Dolly et al. 2010). Therefore, it is challenging but necessary to develop effective therapeutics for SCLC.

Autophagy is an evolutionarily conserved catabolic process for recycling or degrading organelles and cellular macromolecules and plays important roles in regulating cell survival and death. Autophagy acts like a double-edged sword in cancer and exerts both positive and negative effects in a context-dependent manner. It was reported that inhibiting autophagy could suppress lung cancer progression, especially at the early stage, making autophagy is an interesting and potential target for cancer therapy.

Our lab designed a series of all-hydrocarbon stapled peptides (Tat-SPs) targeting at interfere with Beclin 1 self-association to promote the interaction between Beclin 1 and Atg14L/UVRAG. Here I present data to show that one lead peptide Tat-SP4 upregulated autophagy activity, and promotes two overexpressed membrane proteins, EGFR and c-Met, endolysosomal trafficking as well as inhibits the downstream signaling pathway. Tat-SP4 shows potent anti-proliferative efficacy in different lung cancer cell lines and exhibit synergistic effect with EGFR-TKIs in NSCLC cell lines.

The cell death induced by Tat-SP4 could be rescued by digoxin, a cardioglycoside that blocks the Na^+/K^+ ATPase and is accompanied by the morphological features similar to that of autosis. We also found that Tat-SP4 partially depolarized mitochondria membrane potential, increased intracellular reactive oxygen species, inhibited the mitochondrial OXPHOS activity and induced mitochondrial permeability transition pore (mPTP) opening. Meanwhile, intracellular calcium homeostasis was disrupted when lung cancer cells were challenged by Tat-SP4, which is characterized by a release of Ca^{2+} from ER followed by increase in Ca^{2+} level in mitochondria and cytoplasm. In SCLC cell-based xenograft model, Tat-SP4 significantly inhibited tumor growth without obvious toxicity.

In conclusion, our novel designed Beclin-1 targeting stapled peptides have shown potent anti-proliferative efficacy in lung cancer model both *in vitro* and *in vivo*, suggesting that our study provides a new strategy to target autophagy for lung cancer treatment. Our stapled peptides may offer an approach orthogonal to the existing regimen of tyrosine kinase inhibitors (TKIs) that directly inhibit the kinase activity of EGFR. Thus, our stapled peptides may potentially serve as the prototype for a new class of therapeutic agents that can be used in conjunction with existing therapies toward better treatment for lung cancer.

Publications arising from the thesis

Chen, J., X. Zhang, S. Gao, N. Li, V. Keng and Y. Zhao (2022). "A Beclin 1-targeting stapled peptide synergizes with erlotinib to potently inhibit proliferation of non-small-cell lung cancer cells." Biochemical and Biophysical Research Communications 636: 125-131.

Gao, S., N. Li, X. Zhang, **J. Chen**, B. C. B. Ko and Y. Zhao (2023). "An autophagy-inducing stapled peptide promotes c-MET degradation and overrides adaptive resistance to sorafenib in c-MET+ hepatocellular carcinoma." Biochemistry and Biophysics Reports 33: 101412.

Li, N., X. Zhang, **J. Chen**, S. Gao, L. Wang and Y. Zhao (2023). "Perturbation of Autophagy by a Beclin 1-Targeting Stapled Peptide Induces Mitochondria Stress and Inhibits Proliferation of Pancreatic Cancer Cells." Cancers 15(3): 953.

Acknowledgements

It's a sunny and slightly breezy Saturday afternoon. I am sitting in my study room, recalling the four years of my PhD study, and writing this acknowledgment to appreciate the people who supported, helped, encouraged, and accompanied me.

At first, I would like to express the appreciation from the bottom of my heart to my supervisor, Professor Zhao Yanxiang. My first impression of Prof. Zhao is that she loves to laugh and is approachable. Your personality makes everyone respect you and feel close to you at the same time, which makes us get along very well at work. When we discussed about my project, you always gave me guidance and advice with rigorous and profound research logic and rich professional knowledge. I also thank you for being strict with me in my research, which has helped me to gradually approach the standard of a qualified researcher. You also gave me proper care and understanding in my life, so that I rarely experienced any conflict between life and study in these four years. Because of your olive branch and platform, I had the chance to feel the charm of research.

I'd like to thank all the lab members who were coloring the four years of my PhD study. Many thanks to Dr. Wu Shuai, as a senior member of our lab, you gave me encouragement when I joined our lab. I am very grateful to Dr. Qiu Xia who patiently taught me experiment skills at the beginning of my research. Dr. Qiu is also like a sister,

caring and enlightening me when I encountered frustrations in my life. I would like to thank Dr. Li Na and Miss. Wang Lei for their support and assistance in my animal experiments. Thank you, Dr. Zhang Xiaozhe, for your willingness to discuss project with me and share experimental methods without reservation. Your cheerful personality has brought a lot of laughter to my life. Thanks to Miss. Gao Shan for accompanying me to write the thesis together and sharing stress with each other. Thanks to Miss. Feng Yu, who is very well organized and have organized many wonderful activities to enrich our after-lab life. Very grateful to Dr. Yang xian, Miss. Zhang Shuqi, Miss. Yu Yingting, Mr. Allen Leung, and Mr. Zheng Siqiong, you provided support and help with the routine lab work. Because of you, my PhD study were different and colorful.

I would like to thank Dr. Zhang Huan and Dr. Li Chang for leading me to open the door of scientific research to explore the richness of science.

I really appreciate my parents who love me dearly. I would like to thank them for nurturing me to be independent, cheerful, and kind person, and these characters are the most valuable assets in my life. Whenever I was faced with a choice, my parents always encouraged me to pursue my dreams courageously and always fully trust and respect my decisions. They give me strength when I am in trouble and can cheer for me when I am making progress. At all times, I could feel their selfless love and support for me.

My deep love and thanks will be given to my husband, Dr. Huang Wei, who accompanied me from my undergraduate to today and will be with me for a long time to come. Fortunately, over the years, we have been there for each other at every important moment. I'm happy that we have grown together and seen each other get better. Your unconditional acceptance and love are a warm haven for me. Looking forwards to our wonderful coming life.

Thank everyone that is reading my acknowledgement for your patience and interest.

Table of contents

List of figures and tables

Figures

Tables

Abbreviations

AD	Alzheimer’s disease
ALK	Anaplastic lymphoma kinase
AM	Amiloride
AZD	Osimertinib
BCL-2	B cell lymphoma 2
BRAF	B-Raf proto-oncogene
BTC	Beta-cytokine
CCD	Coiled-coil domain
CPPs	Cell-penetrating peptides
CQ	Chloroquine
CSCs	Cancer stem cells
DLL3	Delta-like protein 3
DMEM	Dulbecco’s Modified Eagle’s Medium
ECAR	Extracellular acidification rate
ECD	Evolutionarily conserved domain
EGF	Epidermal growth factor
EGFR	Epidermal growth factor receptor
EPR	Epiregulin
ER	Endoplasmic reticulum
ETC	Electron transport chain
Fer-1	Ferrostatin-1
GSDMD	Gasdermin D
GSDME	Gasdermin E
GTP	Guanosine triphosphatease
HCQ	Hydroxychloroquine
HEK293T	Human embryonic kidney cells

HER2	Human epidermal growth factor 2
IC50	Half-maximal inhibitory concentration
KRAS	Kirsten rat sarcoma
LPS	Lipopolysaccharide
MET	MET proto-oncogene
MHV	Mouse hepatitis virus
MLKL	Mixed lineage kinase domain-like
mPTP	Mitochondrial permeability transition pore
MTT	(3-(4,5-Dimethylthiazol-2-yl)-2,5-Diphenyltetrazolium Bromide
MβCD	Methyl-beta cyclodextrin
Nec-1	Necrostatin 1
NLS	Nuclear localisation signal peptide
OCR	Oxygen consumption rate
OXPHOS	Oxidative phosphorylation
PBS	Phosphate buffered saline
PI	Propidium iodide
PS	Phospholipid phosphatidylserine
RB1	Retinoblastoma 1
RIP1	Receptor-interacting protein 1
ROS	Reactive oxygen species
ROVA-T	Rovalpituzumab tesirine
RPMI1640	Roswell Park Memorial Institute 1640 Medium

1. Introduction

1.1 Lung cancer

Lung cancer is one of the most popular malignant tumors in the world and is a major cause of cancer-related death in many countries. According to the cancer statistics for Asia countries, lung cancer is the most commonly diagnosed cancer and has the highest mortality rate, and it causes more deaths than prostate, breast and colorectal cancers combined(Huang, Ngai et al. 2022).

1.1.1 Types of lung cancer

Lung cancer can be classified into two major categories: small cell lung cancer (SCLC) and non-small cell lung cancer (NSCLC) (Figure 1.1). Non-small cell lung cancer is more common and currently accounts for approximately 85% of all lung cancer cases (Novello, Barlesi et al. 2016). Non-small cell lung cancer can be further divided into squamous cell carcinoma (squamous cell carcinoma), adenocarcinoma, and large cell carcinoma based on histology. Compared with small cell carcinoma, NSCLC cells grow slowly and diffuse and metastasis slowly.

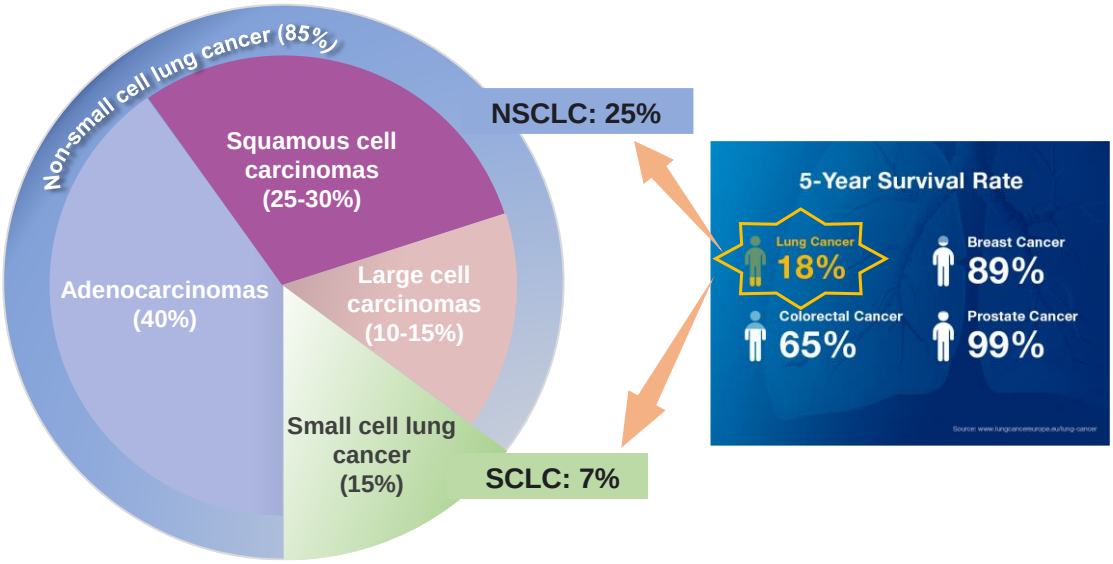

Figure 1.1 The subtypes and 5-year survival rate of lung cancer.

SCLC is the most malignant type of lung cancer and account for about 15% of all lung cancer cases(Jänne, Freidlin et al. 2002). Occurrence of SCLC is closely related to long-term smoking The male-to-female incidence of small cell lung cancer is now close to 1:1 in the United States (Govindan, Page et al. 2006). SCLC cells are very small and shaped like oat grains, therefore they are also known as oat cell carcinoma. SCLC cells are malignant epithelial cells with scant cytoplasm and unclear cell boundaries. SCLC is derived from the hormonal cells of the lung with dedifferentiation properties. The doubling time and growth rate of SCLC are much faster than those of NSCLC. SCLC has the characteristics of rapid progression, early metastasis, and easy recurrence. SLCL is extremely aggressive and with earlier widespread to submucosal lymphatic vessels and regional lymph nodes. Most SCLC patients are diagnosed at advanced stage or hematogenous metastases (Saltos, Shafique et al. 2020).The 5-year survival rate is only 7% and 2-year survival rate is 10-20%(Simon and Wagner 2003).

SCLC is more sensitive to chemotherapy and radiotherapy than other types of lung cancer, treating it is challenging due to its high relapse rate and drug resistance rate. After treatment, the median survival time of patients at limited stage is about 15 months to 20 months, and the median survival time of patients at extensive stage is 8 months to 13 months(Davies, Lara et al. 2004).

Lung adenocarcinoma is the most common type of non-small cell lung cancer and is a glandular epithelial malignancy. Lung adenocarcinoma is more likely to occur in women and non-smokers and adenocarcinoma accounts for 40% of all NSCLC cases (Couraud, Zalcman et al. 2012). Adenocarcinoma cells and their nucleus are large, and the ratio of nucleoplasm is higher. Also, the boundaries of adenocarcinoma cells are unclear. Most lung adenocarcinoma starts from the bronchial mucosa epithelium and a small part of lung adenocarcinoma starts from the mucinous glands of the large bronchi. Lung adenocarcinoma has no special symptoms in the early stage. Chest pain, shortness of breath and pleural effusion are symptoms often seen in patients with advanced lung cancer or in patients who have had intrathoracic regional dissemination.

Lung squamous cell carcinoma is the second most common type of lung cancer, accounting for 25% to 30% of primary lung cancer cases (Perez-Moreno, Brambilla et al. 2012). Unlike lung adenocarcinoma, squamous cell carcinoma of the lung is more common in older men and is closely related to smoking. Lung squamous cell carcinoma

originates from the bronchi and is always located in central lung, with a tendency to spread to the thoracic cavity. The pathology is mainly due to chronic stimulation and injury of bronchial columnar epithelial cells, loss of cilia, squamous metaplasia of basal cells, dysplasia and hypoplasia, which eventually results in mutation that lead to cancer (2012). Since lung squamous cell carcinoma develops and metastasizes slowly, there are more chances for lung cancer patients to be treated with surgical resection, and its 5-year survival rate is higher. However, lung squamous cell carcinoma is less sensitive to radiotherapy and chemotherapy than small cell undifferentiated carcinoma(Gridelli, Ardizzoni et al. 2010).

The incidence of large cell carcinoma (LLC) is not high, accounting for about 10%-15% of non-small cell lung cancer cases. According to the new version of the classification of large cell lung carcinoma by the World Health Organization (WHO), it contains several subtypes, such as clear cell large cell carcinoma, basaloid large cell lung carcinoma, pulmonary lymphoepithelial neoplasia, giant-cell lung carcinoma, rhabdoid phenotype large cell lung carcinoma, and large cell neuroendocrine lung carcinoma. It appears as a highly undifferentiated or immature large cell under the microscope(Pardo, Martinez-Peñuela et al. 2009). Large cell lung cancer is often located in the upper lobe of the lungs, mostly in the surrounding type, with a large volume, clear boundaries and rare cavities, and without the tendency to be surrounded or centered(Popper 2011).

The clinical symptoms of large cell lung cancer are similar to those of other types of lung cancer and include cough, hemoptysis, chest pain, but large cell lung cancer has additional clinical features. Firstly, compared with squamous cell carcinoma and adenocarcinoma, large cell lung carcinoma has poor differentiation, rapid proliferation and short course of disease, and it has invasive growth and rapid development. It is a highly malignant neuroendocrine tumor, and lymphatic and hematogenous metastasis may occur at an early stage, invading adjacent lobes. Secondly, most of the large cell lung cancers patients are male, many of whom have a long history of smoking (Muscat, Stellman et al. 1997). Besides, peripheral tumor lesions are more common in large cell lung cancer, accounting for more than 80% of all large cell lung cancer cases. The tumor has no cavities, and its diameter of the tumor is usually above 8cm.

1.1.2 The cause of lung cancer

Lung cancer is also known as bronchial lung cancer since most lung cancer originates from the bronchial mucosa. Over the past 5 decades years, lung cancer incidence and mortality rates are rising rapidly in many countries, particularly in industrialized countries.

Cell carcinogenesis is closely linked to the mutations in genetic information including epigenetics and DNA that disrupt the normal functions of cells, including cell

survival, programmed cell death (such as apoptosis), and DNA repairment. The greater the accumulation of genetic damage, the higher the risk of cancer(Kastan 2008). Although the etiology and pathogenesis of lung cancer is still not well understood, the following factors are considered closely related to the cause of lung cancer.

Smoking (cigarettes, pipes or cigars) is the main risk factor in inducing lung cancer, especially squamous cell carcinoma and undifferentiated small cell carcinoma(Mason, Murray et al. 2015). It has been proven that more than 70 carcinogens are present in cigarette smoke, including benzopyrazole, NNK, 1,3-butadiene, and some radioactive materials(Hecht 2012). Compared with non-smokers, smokers are 4-10 times more likely to develop lung cancer and it is 10-25 times more likely for severe smokers. It has been reported that 85% of lung cancer patients have a history of smoking(Peto, Boreham et al. 1996). Besides, secondhand smoke increases the risk of lung cancer in non-smokers by 20-30% (Taylor, Najafi et al. 2007).

Asbestos is a recognized carcinogen and dust-like asbestos have a serious adverse effect on health. Asbestos fibers flying in the air can be inhaled into the lungs of the human body and after 20 to 40 years of incubation period. Asbestos fibers will induce some lung diseases, such as pneumoconiosis, lung cancer and pleural cancer(O'Reilly, Mclaughlin et al. 2007).

It is reported that less than 10% of lung cancer is associated with genetic factors.

In other words, if one's immediate family members have lung cancer, the prevalence will be higher than those without a family history of lung cancer(Yang, Holloway et al. 2013). The disease may be regulated by multiple genes (Larsen and Minna 2011).

1.1.3 Oncogenic driver mutations in NSCLC and SCLC development

It has been found that most NSCLC patients present genetic alterations in certain oncogenic drivers. Figure 1.2 shows the incidence of common oncogenic driver mutations in NSCLC. Common oncogenic divers in NSCLC include kirsten rat sarcoma (KRAS), epidermal growth factor receptor (EGFR), anaplastic lymphoma kinase (ALK), human epidermal growth factor 2 (HER2), ROS proto-oncogene 1 (ROS1), B-Raf proto-oncogene (BRAF) and MET proto-oncogene (MET). Molecular testing is to screen the common oncogene mutations and is one of the most important and necessary guidelines to develop a treatment plan for patients with advanced lung adenocarcinoma(Chevallier, Borgeaud et al. 2021). Therefore, it is important to establish a well understanding of the biology of these oncogenic drivers. In this part, I will only introduce the most frequent oncogenic mutations in clinical practice and the oncogenic diver mutations involved in my project.

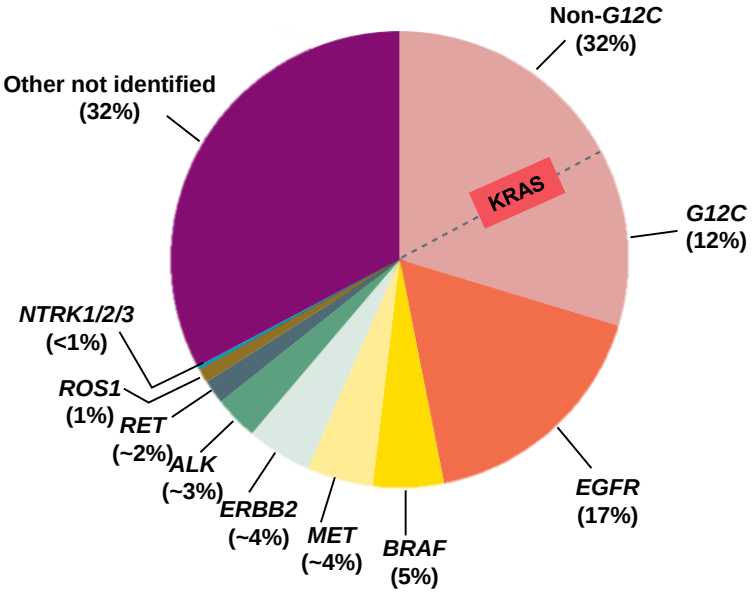

Figure 1.2 Genetic driver mutations for NSCLC

1.1.3.1 KRAS

The kirsten rat sarcoma (KRAS) represent the most frequent human oncogenes. KRAS mutation exists in 29% of NSCLC patients. The most common mutations are located at codons 12 and 13. The KRAS G12C subtype is detected in 13% smoker, while the KRAS G12D subtype is more common in non-smokers(Hong, DuBois et al. 2020). KRAS is a member of the RAS gene family and is a kind of small guanosine triphosphate (GTP)ase. KRAS protein functions as a central regulator at downstream of growth factor receptor signaling to regulate cell proliferation and differentiation. KRAS is an important protein at downstream of the EGFR signaling pathway. Mutations of the KRAS gene can directly initiate the downstream of the EGFR pathway and indirectly initiate the PI3K pathway, leading to more rapid development of NSCLC and drug failure targeting the upstream of EGFR Pathway(Lee, Lee et al. 2014). It has

been found that KRAS gene mutations are related to EGFR mutation status, which means that KRAS mutations can occur in the case of EGFR gene mutations, but the incidence is significantly lower than in patients with the wild-type EGFR gene(Cheng, Alexander et al. 2012). Clinical statistics shows that KRAS mutations are associated with resistance to first-generation TKIs and conventional chemotherapy(Eberhard, Johnson et al. 2005).

1.1.3.2 EGFR

The incidence of mutation in the epidermal growth factor receptor (EGFR) is about 19% among NSCLC patients. EGFR mutations are commonly found in women, non-smoking, lung adenocarcinoma and Asian patients. The mutation site of EGFR is located at exons 18-21. EGFR 19 exon deletion and 21 exons L858R point mutations are most common, they can induce activation of tyrosine kinase domain and are sensitive to tyrosine kinase inhibitors(TKIs)(Sequist, Martins et al. 2008). However, T790M mutation in exon 20 can result in acquired resistance to EGFR-TKIs(Onitsuka, Uramoto et al. 2010). There are also other mutations for EGFR, such as △LRE and G719R.

EGFR is a glycoprotein widely expressed on the cell surface of human tissue. It function as a tyrosine kinase receptor that mediates multiple signal transduction pathways and transmits extracellular signals into cells, thereby regulating cell growth

and differentiation. EGFR is a member of the HER/ErbB family of receptors and EGFR (ErbB-1/HER-1), Her-2/neu (ErbB-2), Her3 and Her-4 belong to the HER/ErbB family. It has been reported that increased gene copy number or overexpression of EGFR can promote normal cell transformation and metastasis of malignant tumors.

Human EGFR gene is located on chromosome7, and EGFR consists of three parts. An extracellular domain, located at the N-terminus, contains a ligand binding site, a transmembrane region consists of 23 amino acid residues, and the intracellular region at the C-terminus contains a tyrosine kinase domain(Bishayee 2000). The activation of EGFR involves two important steps. Firstly, EGFR will be activated by binding of specific ligands. Ligands that specifically bind to EGFR include epidermal growth factor (EGF), transforming growth factor alpha (TGFα), bidirectional regulatory protein, beta-cytokine, heparin-binding EGF-like growth factor and epiregulin. Upon binding of the ligand to EGFR, monomer EGFR will undergo dimerization to form a homo- or heterodimer. The dimerized EGFR undergoes cross-linking phosphorylation of several tyrosine residues in the C-terminal domain of EGFR and stimulates downstream signal transduction(Yarden and Schlessinger 1987).

1.1.3.3ALK

The incidence of anaplastic lymphoma kinase (ALK) gene rearrangements in NSCLC is about 3%-5%(Soda, Choi et al. 2007). ALK posotivity is commonly found

in young adenocarcinoma, non-smoking or light smoking NSCLC patients. ALK gene rearrangements are often repulsive to EGFR or KRAS mutations(Gainor, Varghese et al. 2013). ALK is a transmembrane receptor tyrosine kinase which involve in various cancer signaling pathways such as Ras/MAPK、PI3K/AKT and JAK/STAT signaling pathway. Activation of the NSCLC ALK gene results from ALK chromosomal rearrangements, whereby the ALK tyrosine kinase region forms a fusion gene with the 5' terminal echinoderm microtubule-associated protein-like 4. The 5' terminal fusion gene undergoes an oligomerization reaction, resulting in ALK tyrosine kinase activation independent of ligand, leading to downstream pathway activation(Solomon, Wilner et al. 2014).

1.1.3.4 Met

c-MET has been confirmed as one of the important driving genes for NSCLC. Met alteration are found in approximate 4% of NSCCL. There are three main MET mutations, MET amplification, MET exon 14 mutation, and MET overexpression. Among them, MET amplification is one of the important reasons for resistance to three generations of EGFR-TKIs for NSCLC and about 15%-20% of patients who have acquired-resistance to TKIs can be detected with MET amplification(Drilon, Cappuzzo et al. 2017). MET exon 14 mutation may happen in the absence of EGFR, KRAS or ALK mutations and it is reported that, in China, MET exon 14 mutation accounts for only about 0.9% of lung adenocarcinoma cases(Liu, Gou et al. 2016).

c-MET is a transmembrane receptor with autophosphorylation activity encoded by MET gene and its ligand is HGF. Dimerization and tyrosine phosphorylation of c-MET will happen after binding of HGF to c-MET, which will activate its downstream signaling pathway, such as Ras/MAPK, PI3K/Akt and MET/ERK. The activation of c-MET plays an important role in cell proliferation, cell migration, invasion of blood vessels and angiogenesis. When c-MAT pathway is under normal status, it can control tissue differentiation and repair. However, abnormal activation of c-MET pathway will result in tumor cell proliferation and metastasis(Paumelle, Tulashe et al. 2002).

1.1.3.5 ASCL1

Acoete-scute homologue 1(ASCL1) is a major regulator of the differentiation of neuronal and neuroendocrine cell. It was found that ASCL1 is expressed in 75% of SCLC(Borromeo, Savage et al. 2016), therefore ASCL1 is a potential therapeutic target for high-grade neuroendocrine lung cancer. ASCL1-positive SCLC usually expresses a full set of neuroendocrine markers. ASCL1 expression is closely linked to not only delta-like ligand 3 (DLL3, an inhibitory ligand of Notch pathway) expression, but also RE1 silencing transcription factor (REST, a protein inhibiting the differentiation of neuronal cells and neuroendocrine cells). Deletion of ASCL1 expression is more common in recurrent tumors.

1.1.3.6 TP53/RB1

It has been found that inactivating mutations of TP53 and RB1 is an important initiating molecular event in the pathogenesis of SCLC. The frequency of biallelic loss of *TP53* and *RB1* is up to 100% and 93% of SCLC, respectively(George, Lim et al. 2015). Other inactivating mutations of TP53 and RB1, including mutations, translocations, homozygous deletions, loss of heterozygosity, occur frequently(George, Lim et al. 2015). p53 is a carcinoma suppressor protein encoded by the TP53 (human) gene. p53 not only can bind specifically to DNA sequences and participate in transcriptional regulation, but also plays a role in a wide range of cellular activities, including DNA repair, cell cycle arrest and apoptosis. RB1 mainly take part in regulating cell cycle and cell differentiation, and the high frequency mutations of RB1 are only found in SCLC.

1.1.3.7 TP73

TP73 is a homolog of TP53. 13% of SCLC patients have TP73 gene mutation or rearrangement(George, Lim et al. 2015). The rearranged N-terminal truncated *p73* transcript variant exerts a dominant repressive effect on wild-type p73 and p53(George, Lim et al. 2015), indicating that TP73 may be a new potential therapeutic target for SCLC.

1.1.3.8 MYC

The MYC family includes three members, MYC, MYCL and MYCN. Amplification of oncogene MYC occurs in approximately 20% of SCLC patients(George, Lim et al. 2015). MYC acts as a transcription activator driving the expression of genes that regulate cell cycle and development. MYC amplification is also linked to low survival rate in SCLC(de Cássia S. Alves, Meurer et al. 2014). The three MYC genes are mutually exclusive and can drive the development and progression of SCLC with different expression patterns(Kim, Dunn et al. 2019). Aurora kinase has been identified as a key kinase leading to the amplification of MYC in SCLC cell lines. Suppression of AURKA and AURKB selectively inhibits the proliferation of SCLC cells overexpressing MYC (Kim, Wu et al. 2016).

1.1.4 Molecular pathways involved in SCLC development

Respiratory epithelial cells contain multiple nests of stem cells, and most SCLC arise from the differentiation of stem cells into neuroendocrine cells. Cancer stem cells (CSCs) are tumorigenic and have various of the features of embryonic stem cells and. In CSCs, some conserved cellular signaling pathway involved in cell proliferation and survival are continuous activated. The known molecular pathways involved in SCLC development and progression include cell cycle regulation, receptor kinase/PI3K signaling, transcriptional regulation and Notch signaling/Neuroendocrine differentiation(George, Lim et al. 2015). Various gene alterations were found in each signaling pathways in SCLC patients. SCLC was initially considered to be molecularly

homologous because absence of tumor protein p53 (*TP53*) and retinoblastoma 1 (*RB1*) and neuroendocrine epithelial differentiation of cells was prevalent in almost all SCLC cases(George, Lim et al. 2015). Later, by categorizing and analyzing RNA-seq data from SCLC tumors, Rudin et al. found that molecular subtypes of SCLC could be defined by differential expression of transcription factors ASCL1, NEUROD1, POU2F3 and YAP1. The classification includes SCLC-A、SCLC-N、SCLC-P and SCLC-Y(Rudin, Poirier et al. 2019).

1.1.4.1 Receptor Kinase/PI3K Signaling

Mutations in the PI3K-AKT-mTOR signaling pathway are reported in approximately 40% of SCLC patients. The PI3K-AKT-mTOR pathway plays an important role in cell proliferation, survival, migration and chemoresistance in SCLCL(Umemura, Mimaki et al. 2014). The incidence of kinase gene mutations is lower in SCLC than that in NSCLC. One study including 51 SCLC samples showed that genetic alteration in PI3K/AKT/mTOR pathway were found in 36% of the SCLC tumors, and mutations in PI3CA (encoding the catalytic subunit of PI3K), PTEN, AKT, RICTOR and mTOR were detected in the SCLC samples(Umemura, Mimaki et al. 2014). The inhibitor of PI3K/AKT/mTOR signaling pathway significantly suppress proliferation of SCLC with genetic alterations in PI3K signaling pathway(Umemura, Mimaki et al. 2014).

1.1.4.2 Notch Signaling/Neuroendocrine Differentiation

Notch function as a tumor suppressor gene in SCLC that negatively regulates the neuroendocrine differentiation. However, Notch genes act as oncogenes in NSCLC(Saunders, Bankovich et al. 2015). Inactivating mutations of Notch signaling occur in approximately 25% of SCLC patients(George, Lim et al. 2015). Notch signaling plays a vital role in inducing cell cycle arrest, inhibiting NE cell phenotypic transformation, and is a master regulator of tumor suppressors and neuroendocrine differentiation in SCLC. Therefore, inactivation of Notch signaling leads to cell hyperproliferation and promote neuroendocrine differentiation of SCLC cells. Delta-like protein 3 (DLL3) regulated by ASCL1 acts as an suppressor ligand of Notch signaling pathway and is commonly upregulated and aberrantly expressed on the plasma membrane in SCLC but is not expressed in normal cells(Saunders, Bankovich et al. 2015) Rovalpituzumab tesirine (ROVA-T) is an antibody-drug targeting to DLL3 that shows significant anti-cancer efficacy in relapsed refractory SCLC(Rudin, Pietanza et al. 2017).

1.1.5 Treatment strategy for lung cancer

Lung cancer is a serious threat to human health. Lung cancer is the malignancy with the highest incidence and mortality rate in China. (Zhang, Zheng et al. 2018). Clinically, SCLC and NSCLC are classified according to treatment methods and prognostic effects. Due to the differences in pathology and biology, treatment strategies

for of SCLC and NSCLC are also different. SCLC is more sensitive to chemotherapy and radiation than NSCLC. Treatment strategies for large cell lung cancer, adenocarcinoma, and squamous cell carcinoma are similar. Traditional treatment methods for lung cancer are surgery, radiation, and chemotherapy. Recently, immunotherapy, targeted therapy and other methods have made new progress. Among the various treatment methods, the effect of surgery is the best, but only 20%-30% lung cancer patients are suitable for surgery. Chemotherapy is the earliest and most widely used method for treating cancer, and it is the most mature treatment at present, but its side effects are obvious. Clinical studies have found that most lung cancer patients are diagnosed at mid- to advanced stages, so most have missed the period of surgery. At present, molecular targeting inhibitors of different driving genes and immunotherapy are now making important advances in the treatment of lung cancer.

Surgery is still the most ideal method at present, although it is only suitable for lung cancer patients without metastasis and in good health. For patients in stages I &II of lung cancer, it has been confirmed that surgical eradication therapy is the most effective strategy. With the rapid development of lung surgery techniques, for patients at a higher stage of lung cancer, comprehensive treatment based on surgical treatment is advocated(Van Raemdonck, Schneider et al. 1992). According to some reports, the 5-year survival rate after surgery is 30%-40% for NSCLC and comprehensive treatment after surgery can significantly improve the treatment effect for higher stage

NSCLC(Smythe 2003).

Chemotherapy has become a vital treatment strategy for advanced lung cancer. Because of the lack of specific clinical manifestations in the early stage of lung cancer, most lung cancer patients are diagnosed in the advanced stage, therefore many patients missed the best time for surgery. SCLC cells divide rapidly, so they are more sensitive to chemotherapy drugs. Combination chemotherapy with etoposide and cisplatin (EP) has been the first-line chemotherapy regimen for limited-stage SCLC(Lara Jr, Natale et al. 2009). Combination chemotherapy regimen with platinum and irinotecan and EP is mainly for extensive stage SCLC(Noda, Nishiwaki et al. 2002). Although SCLC is sensitive to chemotherapy, patients are prone to develop drug resistance and relapse after chemotherapy. For some patients with relapse, combination with topotecan can be considered as second-line therapy. For NSCLC, the third-generation cytotoxic drugs, including paclitaxel, gemcitabine, and docetaxel, combined with platinum-based chemotherapy are still the standard first-line chemotherapy. With third-generation cytotoxic drugs combined with platinum-based chemotherapy, the median survival is improved to 7.4-8.2 months and one-year survival rate is improved to 31%-36% for NSCLC(Schiller, Harrington et al. 2002). Compared with single-agent sequential therapy, combination chemotherapy using platinum-based drugs can significantly control the clinical progression of lung cancer, prolong the median survival period, and improve the patients' life quality(Ohe, Ohashi et al. 2007). However, the side effects of

combined chemotherapy are relatively large, such as nausea and vomiting, hair loss, and decreased immunity and long-term use of platinum drugs can lead to acquired-drug resistance.

Radiotherapy is valued in clinics because it can increase the local control rate, reduce local recurrence, and improve overall survival (OS). Currently, radiotherapy is considered to improve survival in limited-stage SCLC. Compared with chemotherapy alone, chemotherapy combined with radiotherapy significantly improve the survival rate of SCLC patients(Pignon, Arriagada et al. 1992). SCLC patients are prone to intracranial metastases. Prophylactic cranial radiotherapy can reduce the incidence of brain metastases in SCLC patients and prolong OS. For extensive-stage SCLC, a randomized controlled study showed that prophylactic cranial radiotherapy can reduce the incidence of brain metastases and improve the one-year survival rate (Slotman, Faivre-Finn et al. 2007). Surgery is the first option for early-stage NSCLC, but radiotherapy is one of the most efficient treatments for patients with stages III or IV disease. Radiotherapy alone can improve the median survival time of 10 months in patients with stages III or IV non-small cell lung cancer(Rowell and Williams 2001). Radiotherapy can be performed alone, but due to its limited efficacy, it is often used in combination with other treatments.

Tumor molecular targeted therapy refers to the design of therapeutic agents that

target the main cancer-causing molecules of interest. After drug enters the body, it specifically targets to oncogenic molecules, downregulates the expression of receptors or inactivation of downstream genes. Molecular targeted therapy can reverse the ability of cancer cell to differentiate, inhibit tumor angiogenesis, and cause cancer cell ischemia to induce apoptosis and necrosis. Tumor molecular targeted therapy has become a research hotspot in the treatment of lung cancer with in-depth research on the molecular biology and gene level of tumors.

Several studies have examined the role of molecularly targeted therapy in SCLC. Bevacizumab is an angiogenesis inhibitor. The results of a study showed that the first-line treatment of metastatic-stage of SCLC with EP regimen combined with bevacizumab can prolong the median progression-free survival (PFS)(Tiseo, Boni et al. 2015). Anlotinib is a multi-target tyrosine kinase inhibitor. Compared with placebo(0.7 months), anlotinib significantly extended PFS (4.1 months) and reduced the risk of cancer development by 81% in third-line and beyond treatment of SCLC(chengY 2018). Apatinib is a specific TKI binding to vascular endothelial growth factor receptor 2 (VEGFR2). A clinical study showed that the PFS and OS of patients with metastatic-stage SCLC who were treated with apatinib were 3 months and 5.8 months, respectively, (Xu, Huang et al. 2019).

Molecular targeted therapy has made the most important breakthrough in NSCLC in the past decade. Targeted therapy for NSCLC is mainly focused on tyrosine kinase

receptors since EGFR mutations are the most popular oncogenic drivers among NSCLC patients. FDA-approved EGFR TKIs are listed in Table 1.1. Up to date, three generations of TKIs targeting EGFR have been developed. The first generation of EGFR-TKIs include gefitinib and erlotinib. For NSCLC patients with EGFR mutation, the effectiveness of gefitinib or erlotinib is 70%-80%, while for EGFR wide type NSCLS patients, it is only 10%~20%(Kosaka, Yatabe et al. 2004). The second generation of EGFR-TKIs include Afatinib and Dacomitinib. Afatinib is an irreversible inhibitor of both EGFR and HER2 and it can disrupt downstream information transmission, thereby preventing cancer cell proliferation and inducing apoptosis. Compared with gefitinib, dacomitinib significantly improves progression-free survival over gefitinib in NSCLC patients with EGFR mutation. The third generation of EGFR-TKIs is Osimertinib (AZD9291). It has been clinically used to treat advanced NSCLC patients with T790M EGFR mutation and metastasis and can further prolong the median PFS of patients(Soria, Ohe et al. 2017). Although the third generation of EGFR-TKIs brings huge survival benefits to patients of advanced lung cancer, drug resistance may occur among NSCLC patients after a period of third-generation EGFR-TKIs application and the most commonly induced mutation is EGFR-C797S(Niederst, Hu et al. 2015). The molecular targets of targeted therapy approved by FDA for NSCLC treatment also include ALK, MET, RET, KRAS, NTRK and ROS1. The corresponding targeted agents for different molecular targets are shown in Table 1.1.

Table 1.1 FDA-approved therapeutic drugs targeting at different gene mutations for lung cancer.

Actionable mutation	FDA approved therapy	Comparator	ORR(%)	mPFS (months)	mOS (months)
KRAS	Sotorasib	No	32%	6.3	12.5
EGFR	Erlotinib	chemotherapy	64%	9.7	22.9
	Gefitinib	Carboplatin/Paclitaxel	74%	10.8	27.2
	Afatinib	Cis/Pemetrexed	56%	11.1	28.2
	Dacomitinib	Gefitinib	75%	14.7	34.1
	Osimertinib	Erlotinib/Gefitinib	80%	18.9	38.6
ALK	Crizotinib	Platinum/Pemetrexed	74%	10.9	NR
	Certinib	Platinum/Pemetrexed	73%	16.6	51.3
	Alectinib	Crizotinib	83%	25.7	Immature
	Brigatinib	Crizotinib	74%	24	47.6
	Erntrectinib	No	77%	19	NR
NTRK	Larotrectinib	No	70%	NA	NA
	Entrectinib	No	70%	NA	NA

Immunotherapy for lung cancer includes immune checkpoint inhibitors, cancer vaccines and adoptive T cell therapy. Immune checkpoint inhibitors have made the most progress in immunotherapy for lung cancer. Nivolumab (Opdivo), pembrolizumab (Keytruda), and cemiplimab (Libtayo) are PD-1 inhibitors, while Atezolizumab (Tecentriq) and durvalumab (Imfinzi) are PD-L1 inhibitors, which are approved by the FDA to be used in patients in different stages of NSCLC. Atezolizumab (Tecentriq) and durvalumab (Imfinzi) that target PD-L1 can be used as a part of the first-line treatment for advanced SCLC, along with chemotherapy with etoposide and cisplatin. CTLA-4 is another immunotherapy target. Ipilimumab is a CTLA-4 inhibitor that is not used alone. In clinical treatment, ipilimumab is usually combined with nivolumab to treat advanced NSCLC. Atezolizumab (Tecentriq) and durvalumab (Imfinzi) along with etoposide and a platinum chemotherapy drug, such as carboplatin or cisplatin, can be used as the first-

line treatment for advanced SCLC. Immune checkpoint inhibitors are usually used as consolidation therapy or adjuvant therapy in clinical trials, which can provide better treatment effect.

At present, chemotherapy is still the basis of lung cancer treatment. Chemotherapy can reduce tumor size and relieve clinical symptoms of lung cancer patients, but after chemotherapy, patients are prone to fatigue, anorexia, nausea and vomiting, poor mood, and reduced quality of life. The first-line standard chemotherapy regimen can prolong the survival of lung cancer patients, but the efficacy has reached a plateau. Chemotherapy regimens are not suitable for advanced lung cancer patients with poor physical condition because of the obvious side effects of chemotherapy. Molecular targeted therapy has the characteristics of high efficiency and low adverse effect and has become a new hot spot in the treatment of advanced NSCLC. However, there are currently no molecular targeted therapies approved by the FDA as clinical treatment strategies for SCLC. Screening for driver genes is essential before deciding on molecularly targeted therapy. The corresponding molecular targeted drugs are selected according to the driver genes of cancer. However, genetic mutations occur at very high frequency in cancer cells, patients with NSCLC who have received a period of targeted therapy may experience acquired drug-resistance. Immunotherapy has made great progress in the treatment of lung cancer in recent years. Compared to chemotherapy, immunotherapy has a lower incidence of adverse reactions, but immune-related adverse

reactions can occur in almost all systems and organs in the body. Immunotherapy is usually combined with chemotherapy to achieve better treatment effect. However, due to the complexity of the immune system and tumor microenvironment, the pathogenesis of immune-related adverse reactions caused by immunotherapy have not been thoroughly studied.

1.2 Autophagy and its role in lung cancer

1.2.1 Autophagy is an essential cellular catabolic process

Autophagy is an evolutionarily conserved catabolic process that packs cytosolic content into double-membraned vesicles termed autophagosomes and traffics these vesicles to lysosomes for degradation and recycling. According to the process of occurrence, autophagy is classified into three subtypes: macroautophagy, microautophagy and chaperone-mediated autophagy. Autophagy is commonly referred to as macroautophagy(Glick, Barth et al. 2010).

Autophagy is an intracellular “self-eating” process and is composed of five steps: induction, elongation, autophagosome formation, fusion of autophagosome and lysosome as well as degradation (Figure1.3). Autophagy can be triggered by various stimulus, such as nutrient starvation and stress signals. With the initiation of autophagy, a bilayer lipid vesicle called phagophore is formed. Phagophore is not enclosed but

shaped like a bowl and is likely to originate from membrane-based organelles, such as endoplasmic reticulum (ER) and/or the trans-Golgi and endosomes(Axe, Walker et al. 2008, Simonsen and Tooze 2009). Then phagophore extends continuously and engulfs cytosolic cargo, such as damaged organelles, invaded pathogens, and protein aggregates, forming an intact double-membraned vesicle named as autophagosome. Subsequently autophagosome fuses with the lysosome to form an autolysosome, during which the inner membrane of the autophagosome is degraded by lysosomal enzymes. The cargo in the autophagosome is also degraded, and degradation products such as amino acids and fatty acids are transported to the cytosol for recycle(Mizushima 2007).

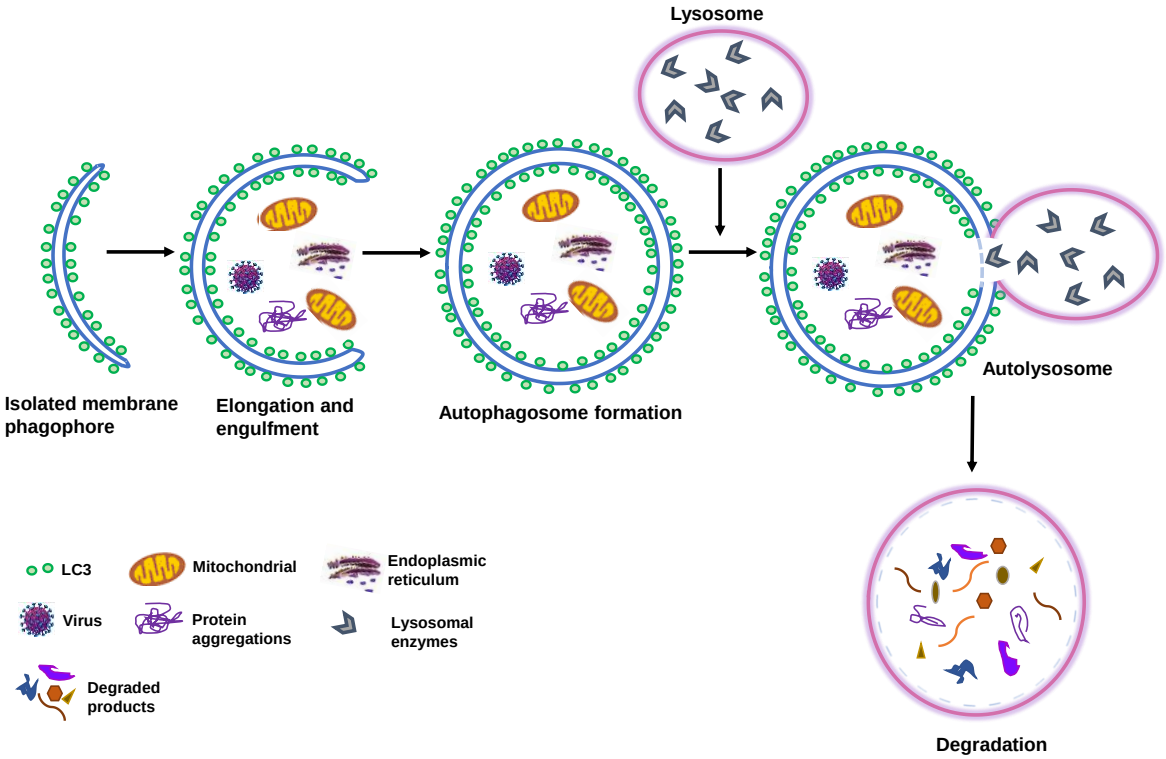

Figure 1.3 Autophagy flux under normal condition

The autophagy process takes part in maintaining cellular homeostasis. Based on

the steps of autophagy flux, the functions of autophagy mainly include sequestrating intracellular harmful cargos, depredating these harmful cargos and recycling degradation products. At the early stagy of autophagy flux, some abnormal intracellular components or invaded pathogenic organisms are sequestrated via autophagosome. For instance, ER stress can trigger autophagy and in return, autophagosome packs abnormal ER, which helps to relieve ER stress and protect cell from ER stress-induced cell death(Bernales, McDonald et al. 2006). Autophagy plays a crucial role in depredating misfolded proteins and damaged organelles, which is mediated by the ubiquitin–proteasome system. Mitophagy is a selective autophagy, in which damaged mitochondria are selectively eliminated via autophagy(Kim, Rodriguez-Enriquez et al. 2007). Autophagy plays a role in innate immune response to invaded pathogens as well. Some pathogenic organisms, such as *Legionella pneumophila*, *Coxiella burnetti*, *Brucella abortus*, and *Porphyromonas gingivalis*, take advantage of autophagy for their replication(Pizarro-Cerdá, Moreno et al. 1998, Finlay, Dorn et al. 2001, Berón, Gutierrez et al. 2002). Phagosomes engulf these pathogenic organisms first, followed by fusion with autophagosomes, and this process provides a protective vacuole for pathogenic organisms to replicate(Swanson and Fernandez-Moreia 2002). It has been reported that mouse hepatitis virus (MHV) infection could induce autophagosome formation and inhibiting autophagy leads to decreased MHV replication(Jackson, Giddings Jr et al. 2005). In some cases, autophagy exerts a defensive function against some viruses(Tallóczy, Jiang et al. 2002). Autophagy contributes a lot to the clearance

of intracellular harmful cargos. One pathology of Alzheimer's disease (AD) is accumulation of intracellular tau aggregates and extracellular β-amyloid. Many studies have evidenced impaired autophagy in AD and a latest study has reported that faulty autolysosome acidification is the culprit(Lee, Yang et al. 2022). In response to starvation, acute autophagy will be triggered and it plays an important role in cell survival through recycling necessary amino acids(Onodera and Ohsumi 2005). The functions of autophagy in physiological activities are not limited to the above.

1.2.2 Role of autophagy in cancer

In normal cells and tissue, the role of autophagy is tissue dependent. Similarly, autophagy functions as either a suppressor or a promoter of cancer, which is context dependent.

Autophagy is considered as a tumor inhibitor since autophagy is very important for eliminating intracellular damaged DNA and misfolded proteins as well as clearance of excessive oxidative stress, which are the major causes of tumor initiation and progression. There are some studies supporting autophagy as a tumor inhibitor. Beclin1 is a key protein for initiating autophagy. Knocking down Beclin1 in mice made the mice prone to tumor(Qu, Yu et al. 2003). Genomics screening showed that the monoallelic loss of autophagy gene *ATG6/BECN1* is very common in various cancer types, such as prostate, breast, and ovarian cancers(Aita, Liang et al. 1999, Liang, Jackson et al. 1999). Besides, heterozygous mutation of *Becn1* led to increased susceptibility to liver and

lung cancer and long latency lymphomas in mice(Qu, Yu et al. 2003). In the liver, autophagy dysfunction results in chronic death of hepatocytes and inflammatory response, which are fuse of liver cancer(Sun and Karin 2013). In addition to Belcin1, p62/ SQSTM1 is another protein related to the suppressive role of autophagy in cancer. In autophagy-defective cells, p62/SQSTM1 is abnormally accumulated, while genetically silencing p62/SQSTM1 decreased ROS toxicity and DNA damage caused by autophagy inactivation. p62 deficiency inhibited tumorigenesis in *Ras* driven lung carcinomas(Duran, Linares et al. 2008), indicating that suppressing p62/SQSTM1 accumulation due to autophagy dysfunction was a potential target for inhibiting lung cancer tumorigenesis. However, the molecular mechanism of p62 on tumorigenesis is still ambiguous, it is proved that p62 is also involved in other oncogenic pathways, such as NRF2, mTOR, and NF-κB(Duran, Linares et al. 2008). Autophagy inhibits necrosis and chronic inflammation mediated by endogenous HMGB1, protecting against tumor initiation(Tang, Kang et al. 2010). Taken these current studies together (not limited to what has been discussed above), autophagy suppresses tumorigenesis.

Autophagy acts as a tumor promoter through conferring both intracellular and microenvironmental stress tolerance(Degenhardt, Mathew et al. 2006). Metabolic alteration in cancer cells is well known and cancer cells need increased metabolism and biosynthesis to meet their excessive cell proliferation and to overcome the hypoxic tumor microenvironment. Under hypoxic and nutrient-deprived state, autophagy is

upregulated to recycle energy and biosynthesis components for cancer cell survival and proliferation. In human pancreatic tumors, the basal level of autophagy is upregulated to promote energy production. In contrast, downregulating autophagy inhibit the growth of pancreatic cancer cells and lead to tumor elimination as well as prolong survival in pancreatic cancer xenograft models(Yang, Wang et al. 2011). Autophagy is usually enhanced in RAS-driven cancers and takes part in different stages of tumor development, including initiation, invasion and metastasis(Guo, Chen et al. 2011). In chemotherapy and radiation therapy, rare ovarian cancer cells enter dormancy state with the protection from autophagy, which may result in tumor recurrence(Lu, Luo et al. 2008). Combining anti-cancer drugs, such as TKIs inhibitors and chemotherapy drugs, with autophagy inhibitors can achieve better anti-tumor efficacy than anti-cancer drugs alone treatment.

Taken together, the function of autophagy in cancer is variable and depends on the context. Cancer cells not only can upregulate autophagy to meet their energy and biosynthesis demands but also can take advantage of autophagy to survive from therapeutic stress. At the same time, it is undeniable that the contribution of autophagy to the quality control of protein and organelle, which is important to protect normal cells from carcinogenesis, cannot go unnoticed.

1.2.3 Autophagy in lung cancer

In *KRas*^{G12D}—driven lung cancer, autophagy promotes tumor progression, while at the early stage of lung cancer, autophagy suppresses oncogenesis(Rao, Tortola et al. 2014). A study found that genetically inactivated autophagy in mice led to increased tumor foci and transition from lung hyperplasia to lung adenomas, which was due to the accumulated potentially oncogenic event caused by autophagy dysfunction(Rao, Tortola et al. 2014). In the process of tumor progression, autophagy accelerates the transition from adenoma to adenocarcinoma through helping tumor cancer overcome survival stress and meeting their increased energy and biosynthesis demands. In xenograft mice model, tissue-specific silencing *Atg5* in lung could significantly inhibit the progression of *KRas*^{G12D}-driven lung cancer, and mitochondrial dysfunction, oxidative stress and accumulation of damaged DNA were observed in autophagy-defective lung cancers(Rao, Tortola et al. 2014). NSCLC development is related to mutation in genes that regulate mTOR signaling. The negative regulator LKB1 in mTOR pathway has been found to be lost in NSCLC, leading to decrease in tumor suppressing effect and tumor development(Dong, Sun et al. 2013). Mutations in oncogenes is some of the key factors for adenocarcinoma cases. p53, a tumor suppressor gene, generally exists in cytosol and will transport to nuclei under stress. Nucleus p53 but not cytosolic p53 triggers autophagy through mTOR/AMPK signaling(Budanov and Karin 2008). p53 mutation was found in NSCLC. In NSCLC patients, better prognosis is accompanied with higher autophagy level indicted via higher LC3

level(Schläfli, Adams et al. 2016).

Chemotherapy is the first-line treatment strategy for lung cancer. Recently, it has been evident that combination therapies provide better effect for lung cancer patients(Herbst, Morgensztern et al. 2018). Some chemotherapeutic drugs, such as gemcitabine, can enhance autophagy. Gemcitabine was used together with cisplatin for the treatment of lung cancer patients, while a study reported that autophagy induced by gemcitabine could protect lung cancer from apoptosis induced by cisplatin(Wu, Shao et al. 2016). In contrast, blocking autophagy by CQ can increase lung cancer cell susceptibility to chemotherapy. Rapamycin is an autophagy inducer, and it was used in combination with ABT-737 and the results suggested that the combination treatment enhanced apoptosis and autophagy in lung cancer cells(Kim, Moretti et al. 2009). Besides, EGFR-TKIs, the molecular targeting therapy drugs for NSCLC, can induce autophagy.

Autophagy is a double-edged sword in cancer. Anti-cancer effect of autophagy has been found, especially at the early stage of lung cancer. However, it is also supported by many studies that blocking autophagy can enhance cancer cell susceptibility to conventional chemotherapeutic drugs. Although the role of autophagy in cancer is controversial, it is undisputed that autophagy is an interesting and potential target for lung cancer therapy.

1.2.4 Autophagy modulation for cancer therapy

Since autophagy plays the dual roles of tumor suppressor and tumor promoter that provide energy and ingredients for biosynthesis in tumor cells, autophagy modulation is bidirectional for cancer therapy. Rapamycin is a classical autophagy inducer that targets at mTOR pathway. Rapamycin and its analogs including temsirolimus (CCI-779), everolimus (RAD-001), and deforolimus (AP-23573) targeting at mTORC1 have been evaluated in various cancer types. Rapalogs exerted significant anti-cancer effect on lymphoma, renal angiolypomas and neuroendocrine carcinomas. In other cancer types, some clinical trials showed that single agent rapalogs had limited success(Meric-Bernstam and Gonzalez-Angulo 2009). Other autophagy inducers which include ATP-competitive inhibitors of both mTORC1 and mTORC2 and dual PI3K-mTOR inhibitor are more potent autophagy inducer than rapalogs and showed more effective anti-cancer effect(Janes, Limon et al. 2010, Yu, Shi et al. 2010).Metformin is a drug for treating type 2 diabetes. Metformin activates AMPK which in turn phosphorylates mTOR and ULK1 to induce autophagy(Kim, Kundu et al. 2011). Recent works showed that metformin showed anti-cancer effect through suppressing cancer cell proliferation and inducing cancer cell death in various cancer cells, including NSCLC, breast cancer, colorectal cancer endometrial cancer and pancreatic cancer(Kim, Kundu et al. 2011). Some conventional anti-cancer drugs, such as TKIs and chemotherapy drugs can induce autophagy(Abedin, Wang et al. 2007, Li and Fan 2010).

However, up to date, clinical autophagy modulating drugs are inhibitors of autophagy that aim at inhibiting autophagy to sensitize tumor to canonical therapies. Chloroquine and its derivatives are FDA-approved drugs that inhibit late-stage autophagy by disrupting acidification of lysosomes and further degradation. Autophagy inhibitors are always combined with conventional chemotherapeutic drugs in clinical cancer treatment. It has been proved that inhibiting autophagy via Hydroxychloroquine (HCQ) increases chemotherapy cytotoxicity and tumor regression(Chude and Amaravadi 2017). In a colon cancer animal model, CQ in combination with vorinostat inhibited tumor growth(Carew, Medina et al. 2010). Similarly, in a prostate cancer xenograft model, CQ in combination with saracatinib was shown to have greater anti-tumor effect compared with saracatinib-monotherapy treatment in mice(Wu, Chang et al. 2010). Currently, about 30 phase I/II clinical trials are being conducted to evaluate the potential of combination of CQ/HCQ with conventional anti-cancer drugs in a variety of tumor types, and it is not surprising that the therapeutic responses of various cancer are different. The effect of CQ/HCQ in multiple myeloma and glioblastoma was not satisfactory (Verbaanderd, Maes et al. 2017). Although preclinical studies support that CQ and HCQ function as anti-cancer compounds and can sensitize tumor cells to conventional anti-cancer drugs, the anti-cancer efficacy of CQ and HCQ in human patients still needs to be confirmed.

1.3 Beclin1-targeting stapled peptides developed by our lab

1.3.1 The structure and function of Beclin1 in autophagy

Beclin1 is a well-studied positive modulator of autophagy and is the first identified mammalian autophagic gene that regulates the formation of autophagosomes. Belcin1 was discovered in 1998 by Beth Levine's lab when they screened the proteins interacting with anti-apoptotic protein B cell lymphoma 2 (BCL-2)(Liang, Kleeman et al. 1998). Before the discovery of Beclin1, *ATG6/VPS30*, the ortholog of Belcin1, was first found in yeast with the function of regulating vacuolar protein sorting(Tsukada and Ohsumi 1993). The mammalian Beclin1 is composed of 450 amino acids and three key functional domains(Figure1.4)(Li, He et al. 2012) including an N-terminal BH3 domain (residues 105-125), a coiled-coil domain (CCD, residual 174-266), and a C-terminal evolutionarily conserved domain (ECD) (residues 267–337)(Lee, Perugini et al. 2016, Yao, Lee et al. 2016). The BH3 domain contains phosphorylation sites and is required to interact with Bcl-family proteins to suppress autophagy(Oberstein, Jeffrey et al. 2007). The CCD of Beclin1 can interact with itself, forming homodimer and also serves as a platform to recruit other autophagy regulators such as Atg14L and UVRAG to modulate vacuolar protein sorting-associated protein 34 (VPS34) activity(Li, He et al. 2012). The ECD of Beclin1 is responsible for engaging ER and mitochondrial membrane and is required for the binding with VPS34 complex(Furuya, Yu et al. 2005).

Figure 1.4 The domain structure of Beclin1 (Li, He et al. 2012)

Beclin1 acts as an autophagy initiator through recruiting key autophagic proteins to form pre-autophagosome core complex containing Beclin1, Vps34, and Vps15(He and Levine 2010). Belcin1 can form homodimer by itself and heterodimer with Atg14L or UVRAG through homotypic interactions involving its CCD, because the interface of Beclin1 CCD contains antiparallel helices and a series of 'imperfect' a-d' residues pairings at its dimer interface which allows its metastability in form(Li, He et al. 2012). Since the association strength of Beclin1 homodimer is much weaker than that of Beclin 1–Atg14L/UVRAG complex, in the presence of either Atg14L or UVRAG, Beclin1 prefers to form heterodimer with Atg14L(Beclin1-Atg14L complexI) and UVRAG (Beclin1-UVRAG complex II), which enhance autophagy signaling through regulating autophagosome mutation and autolysosome formation, respectively(Figure 1.5) (Wu, He et al. 2018). ECD consists of four α-helices (α1-α4), three pairs of anti-parallel β-sheets (β1-β6), and six intervening loops, and it is shaped like a compact ellipsoid(Huang, Choi et al. 2012). Beclin1 ECD directly associates with lipid membrane and the aromatic finger in ECD surface is responsible for membrane association. Mutations on the aromatic finger, including F359, F360, and W361 of EDC, could inhibit the association with liposomes.(Huang, Choi et al. 2012). Besides, Beclin1 ECD is essential for Vps34 binding, autophagy initiation and tumor suppression.

Mutant Beclin1 losing ECD, failed to immunoprecipitate Vps34 and initiate autophagy. In MCF7 driven xenograft mice model, mutant Beclin1 losing ECD didn't exert any tumor suppressive activity (Furuya, Yu et al. 2005). Beclin1 BH3 domain is responsible for the interaction between Beclin1 and anti-apoptotic Bcl-2 family proteins. Beclin1:Bcl2 interaction prevents Beclin1 from forming pre-autophagosome core complex with Vps34, and Vps15, thus inhibiting autophagy(He and Levine 2010).

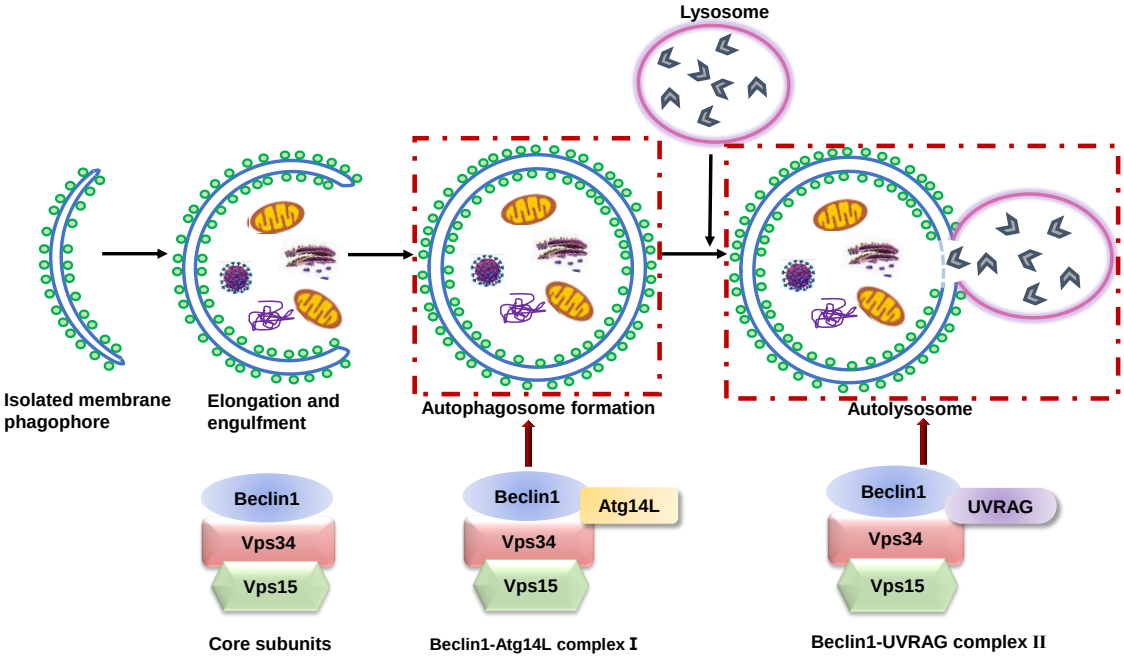

Figure 1.5 Function of Beclin1 in autophagy

Epidermal growth factor receptor (EGFR) is widely expressed in different cells and plays a crucial role in cell proliferation, survival, and differentiation. It has been reported EGFR signaling takes part in regulating autophagy through a non-mTOR dependent pathway(Wei, Zou et al. 2013). Prof. Beth Levine's lab has revealed the relation between the activation of EGFR signaling and autophagy regulation. Some

cell-based assays have shown that EGFR activated by EGF binds to Beclin1 at its ECD and BH3 domain and phosphorylates Beclin1 tyrosine on residues Y229, Y233 and Y352, and the phosphorylation of Beclin1 promotes Belciin1 homodimerization, which diminishes the interaction between Beclin1 and Vps34 and inhibits Beclin1's function in autophagy. The tyrosine phosphorylated Beclin1 by active EGFR tents to recruit Rubicon, which in turn inhibits endolysosomal degradation of EGFR(Matsunaga, Saitoh et al. 2009).

Beclin1 tyrosine phosphorylation induced by active EGFR promotes NSCLC progression(Wei, Zou et al. 2013). Inactivating Beclin1 with three phosphomimetic mutations Y229E/Y233E/Y352E (EEE) inhibits autophagy activity both *in vitro* and *in vivo* and accelerates NSCLC tumor growth(Wei, Zou et al. 2013). In some EGFR-mutant NSCLC cell lines, EGFR-TKI inhibiting phosphorylation of EGFR can disrupt the binding of EGFR with Beclin1 and enhance the interaction of Beclin1 with Vps34, thereby inducing autophagy to inhibit tumor cell growth and tumor progression(Wei, Zou et al. 2013). In other words, active EGFR suppresses autophagy and endolysosomal trafficking through Beclin1 tyrosine phosphorylation, which may promote tumor progression and chemoresistance.

1.3.2 Structure-based rational design of Beclin1-targeting stapled peptides

Beclin1 is an essential component of the autophagic core complex and is essential for the activation of autophagy. *In vitro* experiments have shown that Beclin-1 has inhibitory effect on tumorigenesis by activating autophagy(Fu, Cheng et al. 2013). A single allele deletion of Beclin-1can result in tumorigenesis and interfering with Beclin-1 by hybrid mutagenesis can suppress autophagy in cells, inducing a range of spontaneous tumors such as lymphoma, lung cancer, hepatocellular carcinoma and precancerous lesions in breast cancer(Liang, Jackson et al. 1999). It is directly indicated that the deletion of Beclin-1 leads to a massive increase in the expression of the anti-apoptotic protein Bcl-2, which promotes tumorigenesis in turn (Degenhardt, Mathew et al. 2006). In breast cancer, high expression of phosphorylated keratin suppresses the expression of Beclin-1, inhibiting autophagy, which in turn increases reactive oxygen species (ROS) and DNA damage, and promote tumor development(Kongara, Kravchuk et al. 2010). These findings suggest that targeting Beclin1 to improve autophagic activity for tumor suppression may be an effective strategy in tumor therapy.

Previous structure-based studies in our lab and other labs demonstrated the mechanism that Beclin1 regulates the autophagy through PI3KC3 complex. Our lab previously solved the structure of Beclin1 coiled coil domain by X-ray crystallography and the structure shows the “imperfect” dimer interface of Beclin1 coiled coil domain.

Beclin1 recruits Atg14L and UVRAG in mutually exclusive manner to its coiled coil domain to form Beclin1-Atg14/UVRAG PI3KC3 complexes, which can promote PI3KC3-dependent processes(Liang, Feng et al. 2006, Zhong, Wang et al. 2009). The hydrophobic dimer interface of Beclin1 coiled coil domain determined the metastable homodimeric Beclin1, so the self-association of Beclin1 readily dissociates when Atg14L/UVRAG bind to Beclin1 with more competitive binding ability. The stability of heterodimeric Beclin 1-Atg14L/UVRAG complex is better than that of Beclin1 homodimer (Wu, He et al. 2018).

Based on the structural feature of Beclin1 coiled coil domain, a group of hydrocarbon-stapled peptide segments interacting with Beclin1 coiled-coil domain was designed, aiming at suppressing Beclin1 homodimerization and enhancing Beclin1-UVRAG/Atg14L interaction *in vivo*. The residues 191-205 in the Beclin1 coiled coil domain was applied as a model to design stapled peptides containing an 11-residue segment (Figure 1.6A), which is proposed to bind to the C-terminal residues 231-245 of the Beclin1 coiled-coil domain and can disrupt the self-association of Beclin1. Since the binding site of this template on Beclin1 doesn't compete with the binding site for UVRAG, this segment will not compete with UVRAG for Beclin1 interaction. To improve its cell permeability, stability, and binding affinity to Beclin1, a hydrocarbon stapling was introduced to stabilize the α-helix of the Beclin1-derived peptide. Tat is a well-studied cell penetrating peptide, so we add Tat (YGRKKRRQRRR) to the N-terminal of the peptide to improve cell penetration (Figure 1.6B).

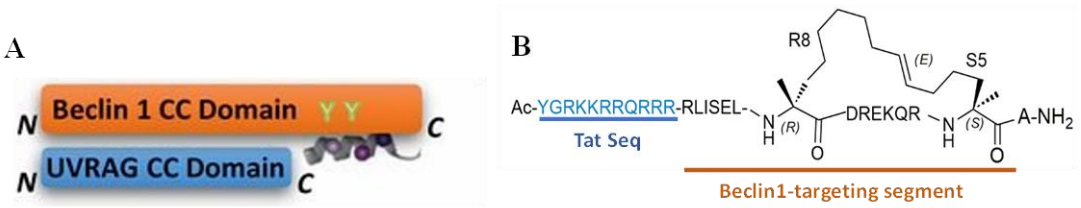

Figure 1.6 The design principle of Beclin1 coiled-coil domain-derived stapled peptides. (A) The small spiral band binding to the C-terminal of the Beclin1 coiled-coil domain refers to the designed α-helical stapled peptide. The hydrocarbon staples stabilizing the α-helical structure are shown as spheres. **(B)** The sequence and chemical structure of Beclin1-targeting stapled peptides interacting with Beclin1 coiled coil domain. The Tat sequence (in blue) is applied to improve cell penetration.

We computationally generated a group of stapled peptides. The first stapled peptide (SP1) was designed as a prototype for further structural modification. We introduced a hydrocarbon stapling with two helical loops at residues 197 and 204 through (i, i+7) to stabilize the α-helix of the Beclin1-derived peptide. Both residues associated with hydrocarbon stapling are located on the outer side of the helix, rather than at the coiled-coil interface, so that hydrocarbon stapling does not interfere with Beclin1 binding. SP1 was introduced onto a Beclin1-coiled homodimer structure to produce a structure-based model of the interaction between SP1 and Belcin (Figure 1.7A). Based on this structure-based interaction model, the binding affinity of SP1 was optimized computationally, while The key residues binding to residues 191-205 of the Beclin1 coiled-coil structural domain remained unchanged. Figure 1.7B is a library of stapled peptide, from SP2 to SP12, with different amino acid residues mutation. As listed in Figure 1.7B, the binding affinity was improved in SP4, SP9 and SP12 by using Ser to replace Gln94 and Ala to replace Val205. Thus, SP4, SP9, and SP12 was selected for further optimization.

A

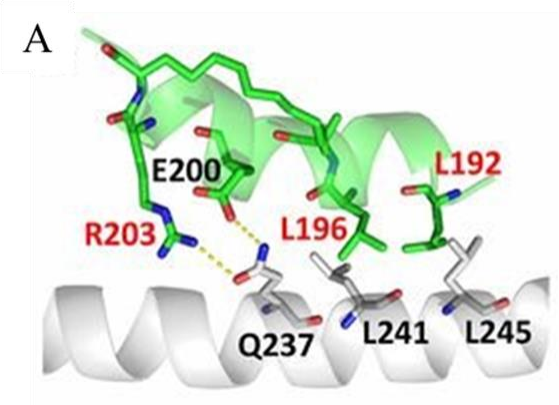

B

Number	Sequence	ΔG_{bind} (Kcal/mol)
SP1	Ac-RLIQEL(R8)DREAQR(S5)V-NH2	-29.75±6.62
SP2	Ac-RLIQEL(R8)DREAQR(S5)S-NH2	-43.69±5.21
SP3	Ac-RLISEL(R8)DREKQR(S5)V-NH2	-47.51±3.96
SP4	Ac-RLISEL(R8)DREKQR(S5)A-NH2	-56.05±6.87
SP5	Ac-RLIQEL(R8)DREKQR(S5)S-NH2	-40.75±5.59
SP6	Ac-RLISEL(R8)DREKQR(S5)S-NH2	-47.40±6.90
SP7	Ac-RLIQEL(R8)DREKQR(S5)R-NH2	-45.77±5.13
SP8	Ac-RLIQEL(R8)DREKER(S5)A-NH2	-49.78±6.34
SP9	Ac-LLISEL(R8)DREKQR(S5)A-NH2	-74.52 ±4.31
SP10	Ac-RLLSEL(R8)DREKQR(S5)A-NH2	-55.69 ±5.15
SP11	Ac-LLLSRL(R8)DREKQR(S5)A-NH2	-50.47 ±5.23
SP12	Ac-LLISQL(R8)DREKQR(S5)A-NH2	-56.05±4.35

Figure 4.2 Structural model of SP1-Beclin1 coiled-coil domain interaction and a library of computationally designed stapled peptide. (A) The hydrogen bonds were labelled with dashed lines. The residues are numbered based on the sequence of Beclin1. **(B)** A library of modified stapled peptides. Mutated residues are in blue color and unchanged residues are in red or black color. Hydrocarbon stapling are introduced at R8 and S5 residues. SP4, SP9, and SP12 with improved binding energy are highlighted in pink background.

Our lab had performed some structural studies and structure-guided functional studies of the Beclin1-targeting staple peptides. The ITC results showed that Tat-SP4 interacts with Beclin1 coiled-coil domain with strongest binding affinity (~6.8μM), among these three modified stappled peptides (Figure 1.8A). Although Tat-SP9 and Tat-

SP12 also interact with Beclin1, their binding affinities with Beclin1 is much weaker (Figure 1.8B&C). Tat segment alone didn't interact with Beclin1 coiled-coil domain (Figure 1.8D), indicating that Tat segment had little effect on the interaction of SPs and Beclin1(Wu, He et al. 2018). Therefore, Tat-SP4 was selected for further functional study.

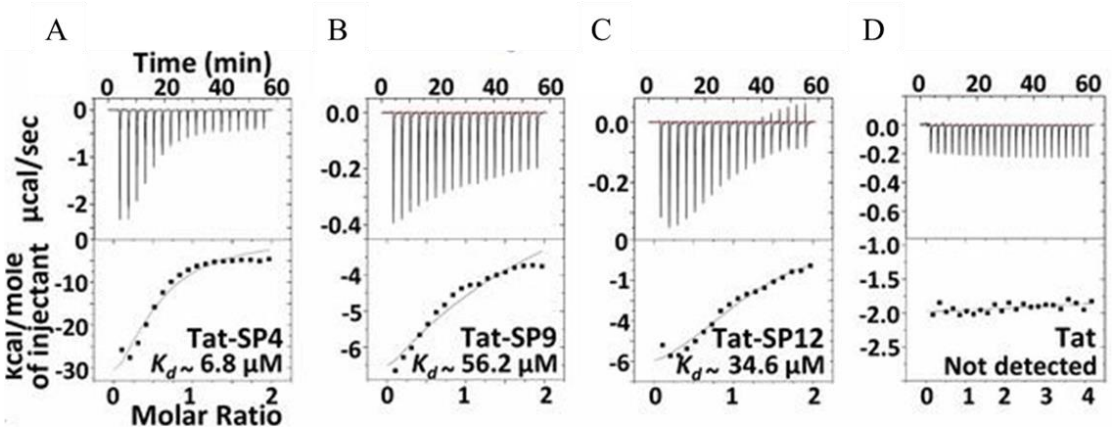

Figure 1.8 Determination of the interaction between Beclin1 and designed peptides with ITC. A. ITC profile of Beclin1 titrated to Tat-SP4. B. ITC profile of Beclin1 titrated to Tat-SP9. C. ITC profile of Beclin1 titrated to Tat-SP12. D. ITC profile of Beclin1 titrated to Tat.

Cell-based functional studies showed that Tat-SP4 could disrupt the self-association of Beclin1 through binding to the Beclin1 coiled-coil domain and promote the redistribution of Beclin1 to form Atg14L/UVRAG-containing Beclin1-Vps34 complexes, which enhanced Vps34-dependent autophagy activity and endocytic trafficking (Figure 1.9). Therefore, our designed stapled peptides significantly suppress Beclin1 self-association and can be used as modulator to regulate Beclin1-dependent autophagy and endolysosomal trafficking.

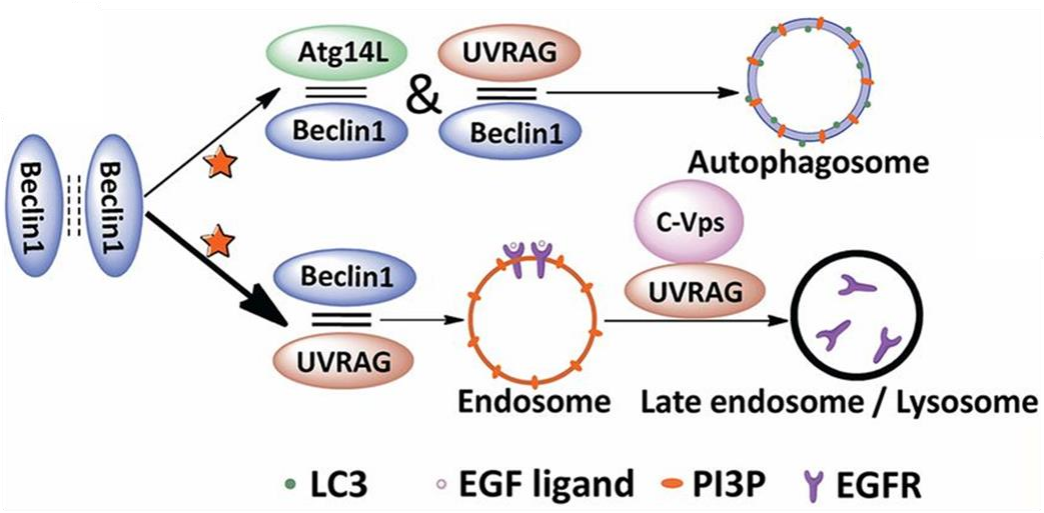

Figure 1.9 The designed Beclin1-targeting stapled peptide enhances autophagy and endolysosomal trafficking. The imperfect interface for the Beclin1 coiled-coil self-association is indicated by the dashed lines. The designed peptides (red stars) disrupt the Beclin1 coiled-coil homodimer and promote the Beclin1-Atg14L or -UVRAG interaction (represent by solids lines), which leading to enhancement of autophagosome and endosome formation.

Since Beclin1 plays a crucial role in tumorigenesis, it is reasonable that our rationally designed Beclin1-targeting stapled peptides have the potential to inhibit the proliferation of cancer cells, especially the cancer cells overexpressing cell surface oncogenic receptors such as EGFR and HER2. We optimized the first-generation stapled peptides, Tat-SP4, to develop the second-generation stapled peptides. To improve the binding affinity to Beclin1, the hydrocarbon stapling was implemented closer to the Beclin1 coiled coil interface and some amino acid that not critical for binding were modified for better conformation. Our previous studies revealed that the optimized Belcin1-targeting stapled peptides not only enhanced autophagy activity and endolysosomal degradation of EGFR and HER2, but also showed potent anti-proliferative efficiency in HER2+ cancer cells(Yang, Qiu et al. 2021). Our previous

findings on the structure of Beclin1 and Beclin1 targeting stapled peptides promote us to investigate the molecular mechanism of anti-proliferative efficacy of our novel designed stapled peptides.

1.3.3 Strategies to generate cell-penetrating stapled peptides for drug discovery

With the development of biotechnology, biomacromolecules such as antibodies, oligonucleotides, peptides, play an important role in the treatment of major diseases such as malignant tumors and autoimmune diseases due to their target specificity and efficiency. However, the practical application of these biomacromolecules is limited by the natural cell membrane barrier. Biomacromolecules can't cross cell membranes into cells to work and can only be used to identify the targets on cell surface and secreted protein targets. Cell-penetrating peptides (CPPs) are usually polypeptide molecules of no more than 30 amino acids that can cross cell membranes independently of specific membrane receptors, and even some CPPs are not energy dependent for entry(Raucher and Ryu 2015). Currently, CPPs have become a powerful vehicle that not only translocate biomacromolecules across cell membrane, but permit CPP cargos to cross plasma membrane through various uptake mechanisms(Xie, Bi et al. 2020). Since last 30 years, CPPs have been evaluated in the research for the drug targeting and introduction. The study found that CPPs have potential applications for disease diagnosis and disease treatment, including cancer, central nervous system disorders,

inflammation and diabetes (Xie, Bi et al. 2020).

CPPs can be classified based on its sequence, origin, function and physical and chemical properties (Table 1.2). The relatively common classification method of CPPs is based on their physicochemical properties: cationic, amphiphilic, and hydrophobic. amphiphilic and hydrophobic.

Table 1.2 The classification, sequence, and origins of some CPPs.

Peptide	Sequence	Origin
Cationic CPPs		
TAT(49-57)	**RKKRRQRRR**	**Protein**
penetratin	**RQIKIWFQNRRMKWKK**	**Protein**
Rev	**TRQARRNRRRRWRERQR**	**Protein**
Amphiphilic CPPs		
MPG	**GLAFLGFLGAAGSTMGAWSQPKKKRKV**	**Chineric**
Pep1	**KETWWETWWTEWSQPKKRKV**	**Chimeric**
hydrophobic CPPs		
C105Y	**VPTLK (PMLKE, VPALR, VSALK, IPALK)**	**Protein**
Bip	**PPR)3, (PPR)4, (PPR)5, (PPR)6**	**Protein**
K-FGF	**SDLWEMMMVSLACQY**	**Protein**

Cationic CPPs usually have a high net positive charge because their sequences are usually rich in arginine, lysine, and histidine. Cationic CPPs can bind to negatively charged glycoprotein on cell membrane and enter cell through a receptor-independent pathway. Transactivator of transcription (TAT, RKKKRRQRRR) from the HIV-1 protein was the first identified cationic CPPs in 1994 (Fawell, Seery et al. 1994). Other common CPPs include acetyl heparin-binding protein derived DPVs, RNA binding

protein derived HIV-1 Rev and BMV Gag, and DNA binding protein derived protamine1 and penetratin(Raucher and Ryu 2015). It was found that the cationic amino acid residues in TAT(49-57) plays critical role in its membrane penetrating capacity, particular its six arginines(Wender, Mitchell et al. 2000). Some studies showed that CPPS containing poly-arginine sequence have the best cell penetrating ability(Wender, Mitchell et al. 2000).

Amphiphilic CPPs usually contain both polar groups and non-polar groups, resulting in both hydrophilic and hydrophobic properties. Most of the amphiphilic CPPs have a high positive charge due to the presence of lysine and arginine residues. Although amphiphilic CPPs are rich in positively charged groups, the cell penetrating capacity is determined by their amphiphilic nature(Milletti 2012). Amphiphilic CPPs accounting for 40% of CPPs and are the most common type. Amphipathic CPPs can be further subdivided into primary-structural amphiphiles, secondary-structural amphiphiles and proline-rich amphiphiles(Milletti 2012). Many primary-structural amphiphilic CPPs are composed of hydrophobic structural domains of some proteins and nuclear localisation signal peptide (NLS). For example, MPG is composed of the SV40 NLS (PKKRKV) and a hydrophobic sequence derived from HIV glycoprotein 41 (GALFLGFLGAAGSTMGA), and Pep-1 is composed of a tryptophan-rich sequence (KETWWETWWTEW) and the SV40 NLS (PKKRKV). The secondary-structural amphiphilic CPPs usually contain includeα-helical and β-folded

structures(Xie, Bi et al. 2020).

Compared with cationic CPPs and amphiphilic CPPs, a relatively small number of hydrophobic CPPs have been reported so far. Hydrophobic CPPs usually contain only non-polar groups, and their hydrophobic groups play an important role in the membrane penetration process. Common amphiphilic CPPs are C105Y, Bip4 and K-FGF (Rhee and Davis 2006, Gomez, Chen et al. 2010).

The cell uptake mechanisms of CPPs and CPP-cargoes are dependent on not only the properties of CPPs and carried cargoes, but also the concentration of CPPs or CPP-cargoes, temperature, pH and cell type. Although there are still many controversies about the cell uptake mechanisms of CPPs, it is generally accepted that CPPs and CPP-cargoes enter cells through endocytosis and direct translocation pathway (Figure1.10). Endocytosis is energy-dependent and is the preferred uptake mechanism for biomacromolecule CPPs or CPP/cargoes(Gao, Mei et al. 2018).

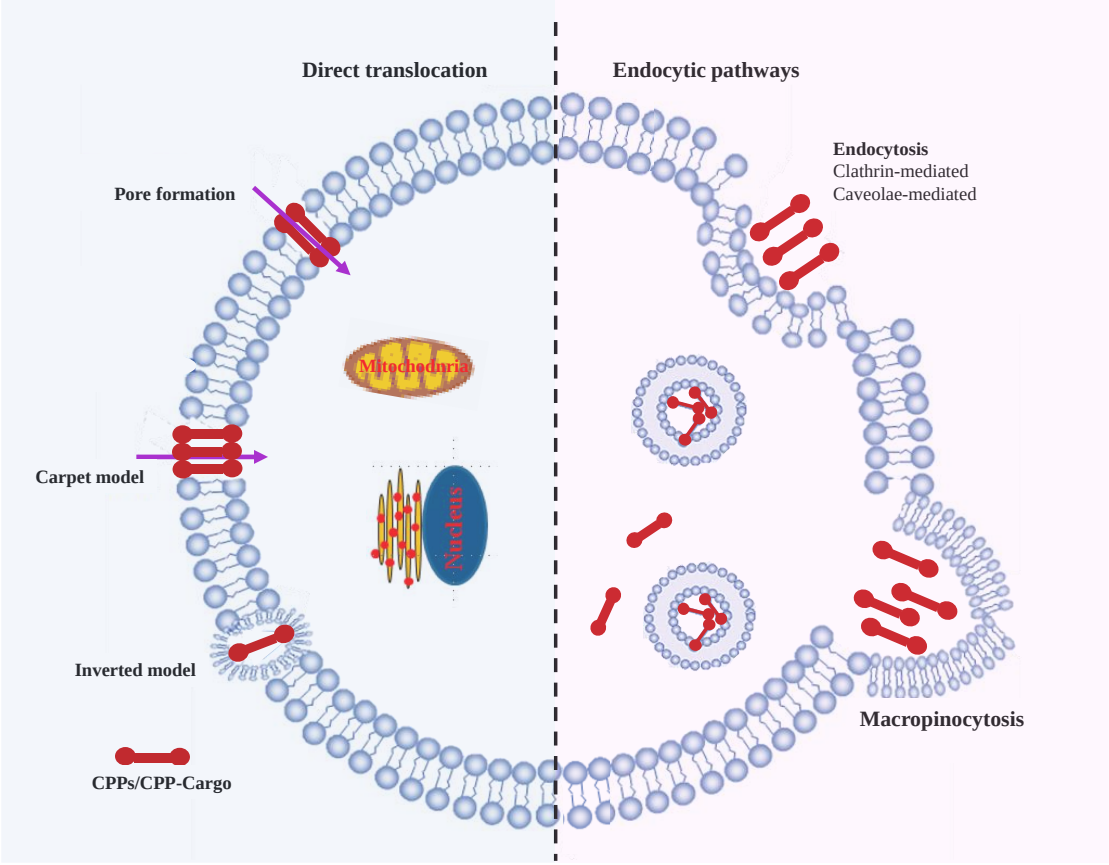

Figure 1.10 The cellular uptake mechanisms of CPPs or CPP-cargoes. CPPs and CPP-cargoes enter cells through endocytosis and direct translocation pathway

Endocytosis include macropinocytosis, caveolin-mediated endocytosis, clathrin-mediated endocytosis, and clathrin- and caveolin-independent endocytosis (LeCher, Nowak et al. 2017), which is shown in Figure 1.10. A study showed that macropinocytosis is the predominant cellular uptake pathway for R8 and TAT and is a typical cellular uptake mechanism of arginine enriched CPPs(Al Soraj, He et al. 2012). There are many molecular mechanisms by which CPPs enter cells through endocytosis. It is widely accepted that receptors on cell surface play critical roles in the process of endocytosis of CPPs/ CPP-cargoes. After CPPs/ CPP-cargoes enter cells mainly through energy-dependence endocytosis, CPPs/ CPP-cargoes have to escape from

endosomes to avoid degrading by lysosomes, otherwise CPPs/ CPP-cargoes trapped in endosomes would not be able to fulfil their biological function.

Direct translocation pathway is energy independent. When CPPs/CPP-cargoes enter the cell via the direct translocation pathway, the positively charged CPPs/CPP-cargoes bind to the negatively charged phospholipid bilayer via electrostatic interaction or hydrogen bonding. Currently, there are different theoretical models for the direct translocation: “Barrel-Stave” mode, “Carpet-like” model and Inverted-micelle model(Islam, Sharmin et al. 2018). The mechanism of direct translocation pathway is usually due to the perturbation and instability of the cell membrane caused by CPPs/CPP-cargoes, resulting in changes in the permeability of the cell membrane. The phospholipid bilayer of the cell membrane and the hydrophobic core of other components on cell membrane are the main barrier for charged CPPs/CPP-cargoes to cross the cell membrane(Pescina, Ostacolo et al. 2018). These features make direct translocation most eligible for CPPs or CPPs with small cargoes into cells.

CPPs have become an important tool in drug delivery as well as disease diagnosis and treatment. Although the FDA has not approve any CPPs-based drugs to date, some preclinical studies have suggested that CPPs has potent potential to serve as a drug delivery platform to improve the therapeutic effect due to the improved drug delivery efficiency, membrane penetration, half-life duration (Table 1.3). Our newly designed

stapled peptides contain a TAT sequence at the N-terminal to improve cell penetration of the peptides. TAT is one of the most well-studied CPPs and some studies have proved that TAT can combine with drugs for application in cancer treatment, antibacterial and antiviral cases. Besides, one study illustrated that TAT conjugated drug can cross the blood-brain barrier(Stalmans, Bracke et al. 2015). Taken together, CPPs have shown great potential for clinical application. Our previous findings also show that our Beclin1 targeting stapled peptides has efficient membrane penetration efficiency and demonstrate potent anti-proliferative efficacy in several cancer cell models, which may stem from the TAT sequence introduced in the N-terminal of the peptides. In my project, I focused on the investigation of the anti-proliferative efficacy and molecules mechanism of our stapled peptides in lung cancer model *in vitro* and *in vivo*.

Table 1.3 Samples of CPP-based therapeutics under clinical development

Compound	CPPs	Cargos	Application	Status
AM-111	**TAT**	**D-JNKI-1**	**Acute inner er heating loss**	**Phase 3**
XG-102	**TAT**	**Dextrogyre peptide**	**Postoperative ocular inflammation**	**Phase 3**
ACPP	**AVB-620**	**Cys5 and Cys7**	**Tumor imaging**	**Phase 1**
P28	**P28**	**Non-HDM2-mediated peptide/inhibitor of p53**	**Central nervous system tumors**	**Phase 1**
P28	**P28**	**P28**	**Solid tumor that resistant standard therapeutic methods**	**Phase1**

2. Objectives

Previous studies in our lab have generated a library of Beclin1-targeting stapled peptides that effectively induce autophagy and enhance endolysosomal degradation. These results led me to hypothesize that these Beclin1-targeting autophagy modulators may have anti-proliferative effect on lung cancer cells through a two-pronged approach. On one hand, these peptides can enhance cellular autophagic response and partially restore physiological homeostasis to inhibit uncontrolled proliferation. On the other hand, these peptides can also enhance the endolysosomal degradation of membrane receptors like EGFR, thus attenuating their oncogenic signaling. With anti-proliferative mechanisms distinct from those targeted by TKIs or mAbs, our Beclin1-targeting stapled peptides may serve as novel complementary agents to potentiate and synergize with existing lung cancer therapies.

To test my hypothesis, I carried out a series of studies ranging from *in vitro* biochemistry and chemical biology to cell- and animal-based *in vivo* validation. There are five objectives in my project.

Objective 1: Comprehensive profiling of autophagy and endolysosomal trafficking activities in diverse lung cancer cell lines upon treatment of Beclin1-targeting stapled peptides

In previous studies, it has been published that our novel designed Beclin1-targeting stapled peptide, Tat-SP4 could enhance autophagy activity in HEK293 cell line and promote endolysosomal trafficking in A549 and H1975 cell lines. In my project, I would like to assess whether Tat-SP4 can effectively upregulate autophagy and enhance endolysosomal trafficking including EGFR degradation and c-Met degradation in different lung cell lines with diverse EGFR genetic background.

Autophagy activity and endolysosomal trafficking including EGFR degradation and c-Met degradation induced by Tat-SP4 treatment will be assessed by *in vitro* biochemical methods including Western Blotting assay and confocal imaging assay. The effect of Tat-SP4 on the downstream signaling of EGFR and c-Met will be checked by Western Blotting assay.

Objective 2: Characterization of Beclin1-targeting stapled peptides as single anti-proliferative agents and the potential synergistic effect between EGFR-TKIs and Beclin1-targeting peptides in lung cancer cell lines

Since our Beclin1-targeting stapled peptides can induce autophagy and promote EGFR degradation in lung cancer cell lines, I hypothesize that Beclin1-targeting stapled peptides could inhibit lung cancer cell proliferation or induce cell death. I plan to

measure the half-maximal inhibitory concentration (IC50) value of Tat-SP4 to assess its cytotoxicity first. Then, 5-day cell proliferation assay and cell colony formation assay will be carried out to evaluate the anti-proliferation effect of Tat-SP4 in lung cancer cell lines.

EGFR-TKIs are approved as first-line treatment for patients with advanced NSCLC, but the acquired drug resistance limits their clinical efficacy. It has been reported that EGFR-TKIs not only can block EGFR signaling transduction through competitively binding to the ATP-binding sites, but also induce autophagy(Han, Pan et al. 2011). And inhibiting TKI-induced autophagy may contribute to resistance to TKI therapy(Wei, Zou et al. 2013). Therefore, I wondered whether Tat-SP4, the autophagy enhancer, can combine with TKIs to receive a synergistic effect on NSCLC treatment. The synergistic effect of EGFR-TKIs and Tat-SP4 will be assessed *in vivo* and *in vitro*. For cell-based study, 5-day proliferation assay will be performed in lung cancer cell lines with the combination treatment of EGFR-TKIs and Tat-SP4. For *in vivo* animal-based study, the synergistic effect of EGFR-TKIs and Tat-SP4 will be assessed in NSCLC cell line-driven xenograft model.

Objective 3: Mechanistic studies to delineate the cell death process induced by Beclin1-targeting peptides

To understand how Beclin1-targeting peptides inhibit proliferation of different lung cancer cell lines, I will characterize the impact of these peptides on different cell death pathways such as apoptosis, necroptosis, ferroptosis and pyroptosis. It is relatively straight forward that using inhibitors for different cell death pathways to elucidate irrelevant cell death pathway. Other experimental methods including Western Blotting assay and flow cytometry analysis will be carried out to investigate the molecular mechanisms of cytotoxicity of Tat-SP4.

Besides, the N-terminal TAT flag of Tat-SP4 is a catonic CPP that may lead to depolarization of plasma membrane potential. To stabilize the plasma membrane potential, some ions such as K^+, Na^+, Ca^{2+} could be transport in or out cells through various ion channels, which may cause intracellular Ca^{2+} homeostasis disruption. The positively charger Tat-SP4 may associate with membrane-bound organelles, such as ER and mitochondria, due to non-specific binding to lipids. Therefore, I will investigate the effect of Tat-SP4 on mitochondria and ER. Intracellular calcium dynamic will be real-time monitored using organelle specific calcium indicators under Tat-SP4 stimulation.

Objective 4: Assessment of the *in vivo* anti-proliferative efficacy of Beclin1-targeting peptides in animal-based lung cancer model

After I delineate the molecular mechanism of cell death induced by Beclin1-

targeting peptide in vitro, it is time to evaluate the anti-proliferative efficacy of Tat-SP4 in animal-based lung cancer model. I will select one tumorigenic lung cancer cell line which is relatively sensitive to Tat-SP4 for nude mice xenograft experiment. And both tumor growth rate and final tumor weight will be measured for assessing the anti-tumor efficacy of our novel designed stapled peptide. Histopathologic analyses are also necessary for checking autophagy marker and tumor morphologic differences.

3. Methodology and materials

3.1 Reagents and antibodies

DMEM and RPMI 1640 (Gibco), FBS (Gibco), hepatocyte growth factor (HGF; Invitrogen). AZD9291, Erlotinib and Olmutinib (Santa Cruz) were dissolved in DMSO with indicated stock concentrations. Epidermal Growth Factor (EGF; Invitrogen), MTT (3-(4,5-Dimethylthiazol-2-yl)-2,5-Diphenyltetrazolium Bromide) (Invitrogen), MitoProbe transition pore assay kit (ThermoFisher), dead cell apoptosis kits with Annexin V (Thermo Fisher), Fura-2, AM (Invitrogen), protease inhibitor cocktail (Roche Diagnostics), trypsin (Invitrogen), Chloroquine (CQ; Sigma-Aldrich),.

Anti-β-actin antibody (Santa Cruz Biotechnology), Anti-LC3 antibody (Abnova), Anti-p62 antibody (Abnova), Anti-Caspase3 antibody (CST), Anti-AKT antibody (CST), Anti-p-AKT antibody (CST), Anti-EGFR antibody (CST), Anti-p-EGFR

antibody (Invirogen), Anti-c-MET antibody (CST), Anti- Gasdermin E antibody(abcam), Anti- cleaved-Gasdermin E antibody (abcam). Anti-Mouse IgG-HRP (Sigma-Aldrich), Anti-Rabbit IgG-HRP (Sigma-Aldrich).

3.2 Cell based experiments

Cell lines and cell culture

Ten lung cancer cell lines are used in this project. A549, H1975, H1993 and H596 cells were purchased from American Type Culture Collection (ATCC). H358, HCC827, SHP-77, H1703 and H146 cells were kindly provided by Stem Cell Bank, Chinese Academy of Sciences. H460 cell was gifted from Prof. Leung Yun-chung, Thomas. All these lung cancer cell lines were cultured in Roswell Park Memorial Institute (RPMI) 1640 Medium (ThermoFisher, A1049101) with the supplementation of 10% Fetal Bovine Serum (FBS) (GibcoTM). Hela cell was cultured with Dulbecco's Modified Eagle's Medium (DMEM) (ThermoFisher, 11965118). All the cells were cultured in 5% CO_2, 37℃ incubators. All these cell lines were regularly tested by staining with Hoechst 33258(Sigma, 861405) to check mycoplasma contamination. Only mycoplasma-negative cells were used in experiments.

IC50 measurements

Lung cancer cell lines were plated in 96-well plates. The number of cells seeded

varies from different cell lines and is dependent on the optimum cell proliferation rate and cell size. After overnight incubation, the cell confluent reached about 70% before adding indicated compounds or peptides. Cells were treated with graded concentrations of compounds or peptides for indicated time periods.

For peptides including Tat-SP4, Tat-SS4 and Tat-SC4 treatment, cell viability was examined by Trypan Blue (ThermoFisher, 15250061) exclusion test after 24 hours post treatment. Trypan Blue exclusion is a common method to distinct the number of live cells from dead cell in cell suspension. The principle is that only live cells with intact cell membranes can exclude trypan blue dye and live cells will have a clear cytoplasm whereas dead cells will have a blue cytoplasm.

For TKIs treatment, cell viability was examined by MTT assay. After treatment with different TKIs for 48 or 72 hours, the medium was replaced by 100ml/well MTT solution at a concentration of 0.5% mg/ml and incubated for 4 hours at 37℃ in a 5% CO_2 incubator. Then, MTT solution was removed and 100ml DMSO was added into each well to dissolve the purple crystal. Cell viability was reflected by absorbance value measured by Bio-Rad Microplate Reader (Model 680, Bio-Rad Laboratories, Hercules, CA, USA) at the wavelength of 570nm.

Each concentration was tested in three independent tests. Data from above assays

was analyzed with control group as 100% and IC50 values were calculated from the curve fitted to duplicate the three concentration-response data sets with Prism 5 software.

Cell proliferation assay

The long-term anti-proliferative efficacy of the peptides were assessed with 5-day cell proliferation assay. Cells were plated into 24-well plates The number of cells seeded varies from different cell lines and is dependent on the optimum cell proliferation rate and cell size. Cells were incubated overnight before adding peptides or different TKIs at indicated concentrations. Cell growth will be monitored daily by Trypan Blue exclusion assay over the course of 5 days after peptide treatment. Based on the viable cell number obtained for each day, a 5-day cell growth curve was drawn with Prism 5 software.

Colony formation assay

A549 cells were seeded at a density of 1000 per well in a 6-well plate cultured and were cultured with medium containing Tat-SP4(20 or 40 μM) or Erlotinib (5 or 10 μM). After 10 days, the medium was removed, and the cells were washed twice with PBS and fixed with 4%PFA at room temperature for 15 min. Then the fixed cells were stained with 0.25% crystal violet at room temperature for 30 min. After that, the cells were washed twice with PBS and air-dried. Subsequently, the plates were scanned for

colony number counting using Image J. All experiments were performed in triplicate.

Transfection

A549 cell was used as transfection host for some image assays to study subcellular distribution of peptides and monitor cellular calcium dynamic in this project. Cells were seeded into confocal dishes or 24-well plate (SPL life science), after overnight adherent the confluency of the cells reached 60%-70%. The designed plasmids were transiently transfected into A549 cells according to the manufacture's instruction of lipofectamine 3000 (ThermoFisher, L3000075). The image study was conducted 24-hour post transfection**.**

Confocal microscopy for live cell imaging

For peptides subcellular distribution experiments, A549 or H1975 cells were stained with 0.5μM Mito Tracker Green (ThermoFisher, M7514) and treated with 20μM rhodamine labelled peptides in complete culture medium at room temperature for 30 minutes. When study the mitochondrial micro-location of peptides, A549 cell were transfected with GFP-TOM20 or GFP-Hsp60, along with GFP vector (as a negative control). After 24 hours transfection, the cells were treated with 20 μM rhodamine labelled peptides at room temperature for 30 minutes. Cells were washed with PBS twice and then put in in complete culture medium. The Hoechst was used to label the nucleus of live cells. The cells were observed using Leica invert confocal

microscope (Leica, TCS-SP8-MP system) with oil immersion objective lens at room temperature under the control of LAS X software (Leica)

Determination of mitochondria membrane potential ($\Delta\psi_m$)

Mitochondrial membrane potential (Δψm) is usually monitored and measured by confocal microscopy or flow cytometry assay. Tetramethylrhodamine Methyl Ester (TMRM) (ThermoFisher, M20036) is a cell-permeant and potentiometric fluorescent dye that is readily accumulated in active mitochondria with negative charge, so the change of ΔΨm can be presented by the change of TMRM fluorescence intensity. When ΔΨm is decreased, TMRM will leak from mitochondria leading to decrease in TMRM fluorescence signal. The optimized working concentration of TMRM range from 10-50nM to avoid auto-quenching. 50nM TMRM was used in this experiment. To measure the change of ΔΨm with peptides treatment, cells were treated with peptides for 2 hours and 50nM TMRM was loaded to cells during the final 30 minutes of treatment. Then cells were wash with PBS twice to remove excess TMRM, followed by trypsinization to collect samples. After centrifugation, the cells were responded with 500μL PBS and sample concentrations were around $5x10^4$ cells/mL. 100μM CCCP was used as a positive control drug to induce mitochondrial. The samples were analyzed by BD Accuri C6 Flow Cytometer (BD Biosciences). TMRM is by the 532nm laser and PE equivalent bandpass filter should be used to detect TMRM.

Mitochondrial membrane potential (Δψm) can also be monitored by confocal microscopy. Cells seeded in confocal dish were loaded with 100nM TMRM for 30 minutes followed by washing with PBS twice to remove excess TMRM. Tat-SP4 was added into culture medium with final concentration of 20μM and then the cells were immediately imaged by Leica invert confocal microscope (Leica, TCS-SP8-MP system) with oil immersion objective lens and imaged at 37 °C/5% CO_2 mini-incubator.

Determination of cellular ROS level

Cellular ROS level was measured by using CellROXTM green Flow Cytometry Assay Kit (ThermoFisher, C10492). CellROX® Green exhibits a strong fluorescence signal after oxidation, but is non-fluorescent in a reduced state, which provides a reliable ROS measurement in live cells. SYTOX® Red Dead Cell stain is cell-impermeant and can be used to distinct live stressed cells from dead cells. 1.5x104 A549 cells were plated in 12-well plate and incubated overnight for adherent. Next day, cell samples would be harvested and then resuspended in complete growth medium with the cell concentration of ~5 × 105 cells/mL. The cell samples were treated with different concentration of Tat-SP4 for indicated incubation time. Then the cell samples were stained with of 500nM CellROX® Green and 5nM SYTOX® Red Dead Cell stain following the protocol in this kit. The cell samples were immediately analyzed by BD Accuri C6 Flow Cytometer (BD Biosciences), and the results were presented by BD Accuri C6 Software.

Oxygen consumption rate (OCR) analysis

The oxygen consumption rate (OCR) is a crucial indicator of normal cellular function. Usually, decreased OCR is associated with disruption of mitochondrial function. We utilized the Seahorse XF24 Extracellular Flux Analyzer to measure cellular OCR in real time, which can directly and continuously quantify the mitochondrial respiration in living cells. This analyzer is instructed with a kind of specific 24-well plate with sensor cartridge. There are four ports in each sensor cartridge, which allows sequential addition of four compounds with unique effect on mitochondrial ETC chain for each well. To study the impact of Tat-SP4 on mitochondrial function, living cells should be sequentially exposed to Tat-SP4 and mitochondrial perturbing reagents, and some key parameters of mitochondrial respiration capacity will be assessed.

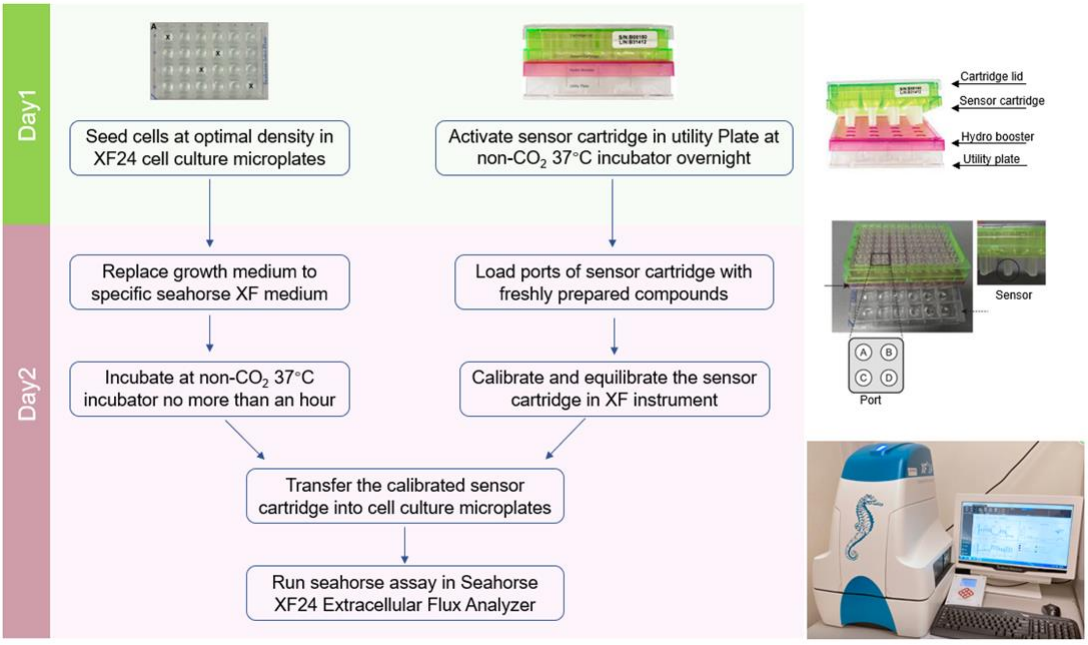

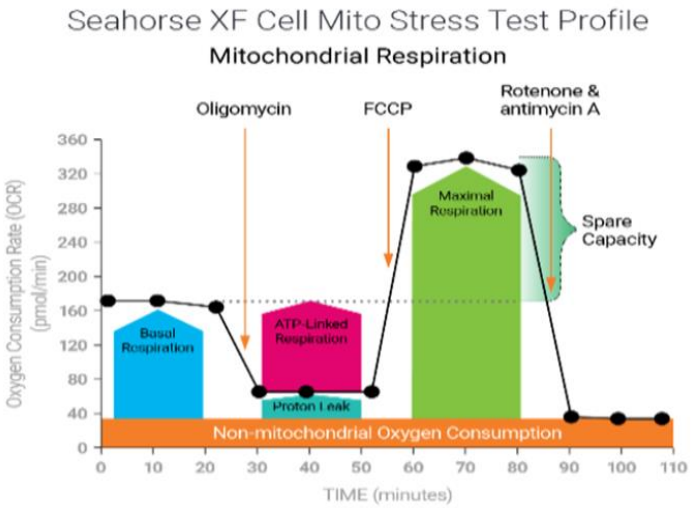

Figure 3.1. Overview of seahorse experiment and Seahorse XF Cell Mitochondrial Stress Test profile

Western blot assay

The desired number of cells were plated in 6-well plate. After overnight adherence, cells were treated with different concentration of peptides or other compounds that used as positive control for indicated incubation period. After incubation, remove the culture medium and cells were washed with ice-cold PBS twice, followed by cell lysis with lysis buffer. The lysis buffer consists of 2% SDS,25% glycerol and 5% β-Me and should be freshly supplement with 1% protease inhibitor cocktail (Bimake, B14001) and 1% phosphatase inhibitor cocktail (Bimake, B15001). The cells were scraped using cell scraper. The cell lysate was transferred into 1.5mL Eppendorf tubes and boiled at 100℃ for 10 minutes. The protein concentration was determined with NanoDrop (Thermo Scientific) at protein mode. 60 μg of the above prepared cell lysate was mixed with 5× SDS sample buffer. The SDS samples were boiled at 100℃ for 5 min before loading. Pre-stained protein standard ladder was used to indicate molecular weight. 10-15μL

SDS sample was loaded into SDS-gel. The voltage for stacking gel is 80V. Once the samples entered separating gel, the samples were run at 100V until the dye reaches the bottom the gel. Next, transferred the samples to 0.45μm PVDF membrane (Bio-Rad) using Mini-Trans-Blot Electrophoretic Transfer Cell (Bio-Rad) at 250mA for 90 minutes. After that, the PVDF membrane was blocked with 5% milk in TBST buffer (137mM NaCl, 20mM Tris, 0.1% Tween 20) at room temperature for an hour to block non-specific binding on the membrane. The blocked membrane was incubated with specific primary antibodies diluted in BSA in TBST buffer at 4℃ overnight. Wash the membrane four times again for 10 minutes each with TBST buffer. The membrane then was incubated with HRP-conjugated secondary antibody at 1:2000 diluted in BSA in TBST buffer for 1 hour at room temperature. Wash the membrane four times again for 10 minutes each with TBST buffer to remove the excess secondary antibody, followed by signal detection with Western HRP Substrate (Millipore) and ChemiDoc Imaging Systems (Bio-Rad).

Apoptosis detection by Annexin V/PI staining

Annexin V/PI staining assay is a common technique for identifying apoptotic cells. Annexin V can bind to anionic phospholipid phosphatidylserine (PS). In healthy cells, PS is only in the cytoplasmic side of the lipid bilayers of plasma membrane. When apoptosis happens, PS will translocate from the inner to the outer side of the lipid bilayers of plasma membrane due to the structural changes of plasma membrane.

PS exposed on the outer side of the lipid bilayers of plasma membrane will bind to fluorescent conjugates of annexin V and apoptotic cell can be identified. Propidium Iodide (PI) is an impermeable nuclear staining dye, which can be used to distinct dead cells from live cells.

The desired number of cells were plated in 6-well plate. After overnight adherence, cells were treated with different concentration of peptides or doxorubicin for indicated incubation period. After treatment, cells were collected by centrifugation and then resuspended with 1X annexin-binding buffer. Stain the cell samples with FITC Annexin V and PI (Thermo Fisher, V13241). The apoptotic cells are Annexin V positive but PI negative, showing green fluorescence only; dead cells are both Annexin V and PI positive; and live cells are both Annexin V and PI negative, showing little fluorescence, which is detected and separated by BD Accuri C6 Flow Cytometer (BD Biosciences). The results were analyzed with BD Accuri C6 Software.

Mitochondrial permeability transition pore (MPTP) detection

The opening of mitochondrial permeability transition pore (mPTP) is closely related to mitochondrial matrix Ca^{2+} accumulation. The MitoProbe Transition Pore Assay Kit (ThermoFisher, M34153) was developed to directly measure mitochondrial permeability transition pore opening independent in mitochondrial membrane potential. The kits provide some reagents. Calcein AM can passively cross cell membrane and

accumulate in cytosol and mitochondria. Once Calcein AM enter cells, its acetoxymethyl esters will be cleaved by intracellular esterase, forming fluorescent dye calcein, which can't cross the mitochondrial or plasma membranes. $CoCl_2$ is used to quench the fluorescence of cytosolic calcein, while fluorescence of the mitochondrial calcein is kept from quenching. When mPTP is opened, mitochondrial contents including calcein will be release into cytosol, then the fluorescence of calcein will be quenched by $CoCl_2$, which can be detected by flow cytometer. Briefly, A549 cells were treated with different concentrations of Tat-SP4 for an hour, followed by cell labeling according to the instruction of this kit. Ionomycin was used as a positive compound to induce mitochondrial calcium overload and subsequent pore formation. The labeled cells were analyzed by BD Accuri C6 Flow Cytometer (BD Biosciences) with 488nm.

Specific organelle calcium dynamic monitoring with genetically encoded Ca^{2+} indicators

Genetically encoded Ca^{2+} indicators used in this experiment include mito-GCaMP5G, cyto-RCaMP1h and G-CEPIA1er. A549 cells were seeded at 6×10^4 cells per well in a 24-well plate. After overnight incubation, cells were transfected with mito-GCaMP5G, cyto-RCaMP1h or G-CEPIA cDNA using Lipofectamine 2000 for 24 hours. SHP-77 cells are suspension cells, so SHP-77cells were plated in 6-well plate to do transfection first. Before imaging, the loading solution was replaced with HBSS buffer with or without $CaCl_2$. SHP-77 cells should be transfected with mito-GCaMP5G, cyto-

RCaMP1h or G-CEPIA cDNA using Lipofectamine 2000 for 36 hours. After 36-hours transfection, SHP-77 cells were collected and evenly plated into 24-well plate in HBSS buffer. Images were collected using an Olympus inverted epifluorescence microscope with a ×20 objective every 3s with specific excitation/emission filter settings.

To monitor subcellular Ca^{2+} dynamics during Tat-SP4 or other agonist induction, A549 cells expressing mito-GCaMP5G, cyto-RCaMP1h or G-CEPIA1er were time-lapse imaged to detect Ca^{2+} flux in mitochondria, cytosol, and ER separately. Tat-SP4 or other agonists was loaded at the 60th second. Data are presented as $\Delta F / F_0$ values (ΔF are fluorescence changes at any time and F0 the baseline value).

3.3 *In vivo* xenograft studies

Animal experiments were carried out according to the guidelines of the Centralised Animal Facilities of the Hong Kong Polytechnic University**.** Male nude mice, 5-6 weeks in age, were purchased from the Centralised Animal Facilities of the Hong Kong Polytechnic University. Exponentially growing SHP-77 cells were harvest and resuspended in PBS with a concentration of 1×10^8 cells per ml. Mixed cell suspensions with Matrigel (Corning, 356237) in a volume ratio of 1:1. 0.5×10^6 SHP-77 cells were injected subcutaneously into the right-lower back of the mice. The tumor volume was calculated by the equation of Length×Width×Width/2. Mice were divided randomly

into two groups (8 animals/group) when the tumor volume reached 50–60 mm^3.Tat-SP4 was administrated intraperitoneally at 40mg/kg every day. The mice in control group were injected with PBS since Tat-SP4 was diluted in PBS. Their tumor volumes were measured every other day. Treatments were continued until tumors volume in mice in control group reached the maximum volume allowable according to the Centralised Animal Facilities of the Hong Kong Polytechnic University. At the end of the experiment, mice were killed, and both tumors and vital organs were harvested for analysis. Tumor weights were measured after resection.

4. Results

4.1 Comprehensive profiling of autophagy and endolysosomal trafficking activities in diverse lung cancer cell lines upon treatment of Tat-SP4

4.1.1 Tat-SP4 induces autophagy in lung cancer cell lines

In our lab's published paper, it has been proved that Tat-SP4 could induce autophagy in HEK293 cells(Wu, He et al. 2018). According to previous studies about the impact of Tat-SP4 on autophagy activity, I wondered whether Tat-SP4 also functions as autophagy enhancer in lung cancer cell lines. LC3 is essential for the maturation of the membrane of autophagosomes and exist in two forms LC3-I and LC3-II. LC3-I is

found in cytoplasm and will be converted into lipidated LC3-II to initiate formation and elongation of the autophagosome. Therefore, elevated LC3-II level is the standard of the enhanced autophagic flux. Similarly, monitoring p62 level is also a common practice for assess autophagy activity since p62 is not only a selective autophagy receptor but also an autophagy substrate, which can be degraded by autophagolysosome. Thus, a decrease in p62 level is considered as an indicator of upregulated autophagic activity. However, p62 is not as sensitive as LC3-II in some cell model.

Our results show that treatment of A549, H1975 and SHP-77 cells with Tat-SP4 for 12 hours induced significant autophagic response. In A549 cells and H1975 cells, the NSCLC cell lines, the addition of Tat-SP4(15 and 30 μM) to cell medium lead to a significant increase LC3-II level in a dosage dependent manner (Figure 4.1A&B, D&E). CQ is an inhibitor for lysosomal degradation and is used to block LC3-II degradation in autolysosome. In the presence of CQ, the increase in LC3-II level became much stronger under Tat-SP4 treatment (Figure 4.1A&B, D&E). However, Tat-SP4 treatment didn't induce noticeable change in p62 level, either in the presence or absence of CQ (Figure 4.1A&C, D&F). Similar results were obtained in SHP-77, the SCLC cells, treated with Tat-SP4 at 5 and 10 μM for 12 hours. Tat-SP4 treatment led to significant increase of LC3-II level in dosage-dependent manner (Figure 4.1G&H). Similar increase was observed when chloroquine (CQ), a lysosomal inhibitor, was added together with Tat-SP4 (Figure 4.1G&H). On the other hand, Tat-SP4 treatment didn't

induce noticeable change in p62 level (Figure 4.1G & I). Such disparity between LC3-II and p62 has been reported in previous studies by us and others (Li, He et al. 2012, Wu, He et al. 2018, Yang, Qiu et al. 2021). It is commonly accepted that changes in LC3-II is more sensitive to autophagy induction while p62 can be influenced by many other factors such as the Keap-NRF2 anti-oxidative stress pathway (Komatsu, Waguri et al. 2007, Lim, Lachenmayer et al. 2015, Deng, Lim et al. 2020). In a summary, Tat-SP4 induced significant autophagic response in both NSCLC and SCLC cells.

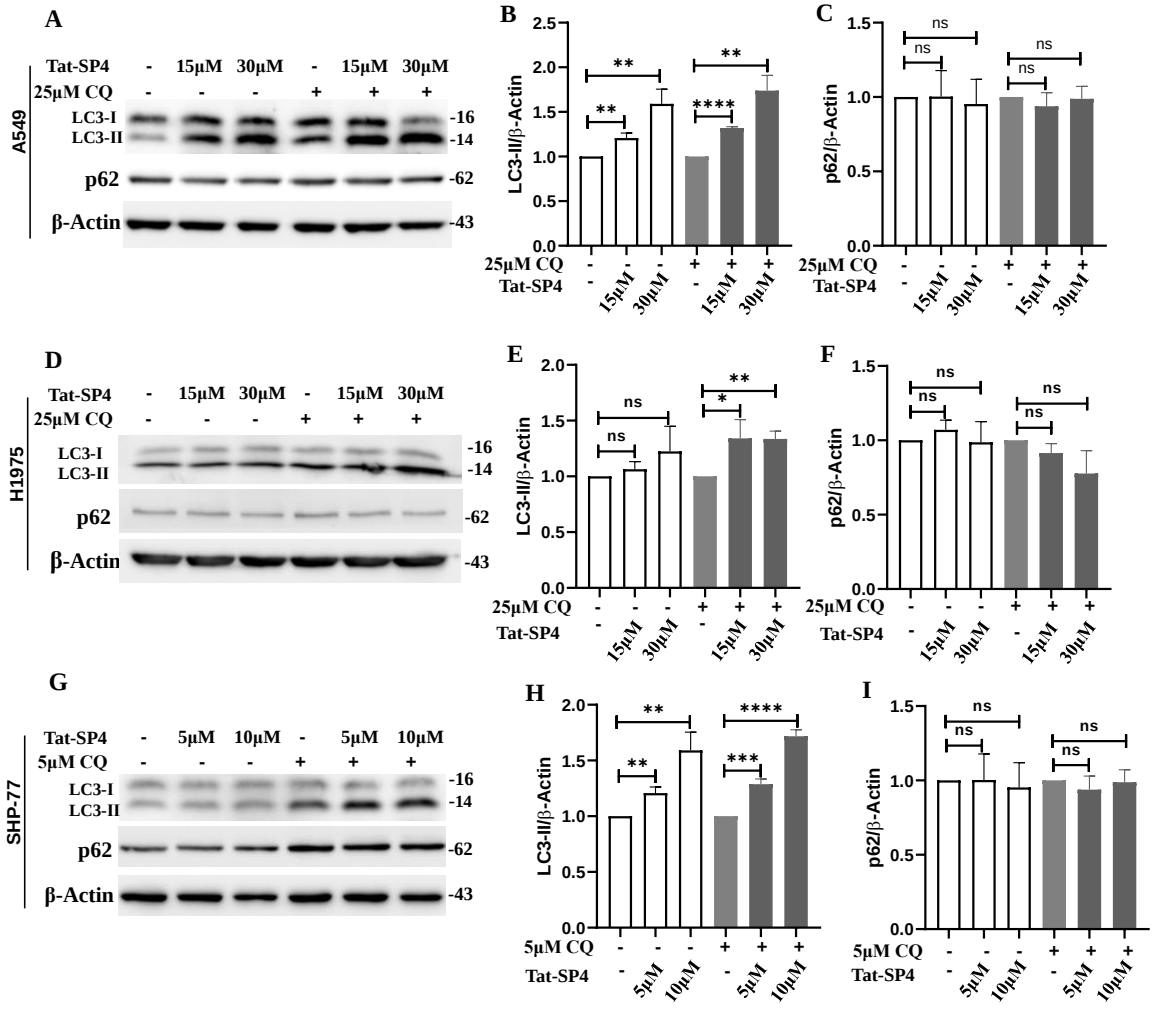

Figure 4.1 Tat-SP4 promotes autophagy in lung cancer cells. (A, D and G) Western blot to evaluate the LC3 level and p62 level in A549(A), H1975**(D)** and SHP-77**(G)** cells after treatment with 15 μM and 30 μM (in A549 and H1975 cells) or 5 μM and 10 μM (in SHP-77 cells) Tat-SP4 for 12 hours, in the presence or absence of 5 μM or 25μM CQ. **(B, E and H)** Quantification of LC3 lipidation profiles from the western blot data. **(C, F and I)** Quantification of p62 levels from the western blot data. The levels of LC3-II or p62 were normalized to the actin level. Data are presented as mean ± SEM (n = 3). Data are presented as mean ± SEM (n = 3). *P<0.05, **P<0.01, ***P<0.001, ****P<0.0001; unpaired t-test.

4.1.2 Tat-SP4 significantly enhances endocytic degradation of EGFR and attenuates the oncogenic EGFR signal transduction

Previous studes have confirmed that Tat-SP4 promots degradative endolysosomal trafficking (Wu, He et al. 2018). The impact of Tat-SP4 on endolysosomal EGFR degradation in A549 cells was characterized by confocal imaging assay and Western Blotting assay. To visualize the EGFR level, A549 cells were immunostained with fluorescent EGFR antibody followed by Tat-SP4 and Tat-SC4 treatment for 6 hours and then the samples were imaged by confocal microscope. The confocal imaging results showed that after 12-hour serum-starvation, most endogenous EGFR is translocated in plasma membrane and the EGFR fluorescence intensity was significantly decreased after Tat-SP4 but not Tat-SC4 treatment, indicating that Tat-SP4 induced EGFR endocytic degradation (Figure 4.2 A).

EGFR activation is essential for its downstream signaling transduction, so we measured the total amount and phosphorylation level of both EGFR and its downstream target Akt (Tomas, Futter et al. 2014) to assess whether EGFR degradation induced by Tat-SP4 would attenuate the EGFR signaling pathway. As shown in Figure 4.5B, in A549 cells, addition of EGF induced EGFR phosphorylation and activated EGFR downstream protein, Akt, which was proved by the elevated p-Akt level under Tat-SP4 treatment (Figure 4.2B). In contrast, Tat-SP4 treatment alone at 20 μM significantly reduced the overall level of EGFR although the level of Akt remained steady (Figure

4.2B). Furthermore, Tat-SP4 completely abolished the phosphorylation signals of EGFR and Akt as soon as 1 hour after treatment and this effect remained for more than 6 hours. Adding both EGF and Tat-SP4 to A549 cells led to even faster EGFR degradation without affecting the Akt level (Figure 4.2B). In presence of Tat-SP4, the phosphorylation of EGFR and Akt induced by EGF at 0 hour was quickly abolished after 1 hour and remained absent after 6 hours (Figure 4.2B).

Similar results were obtained in H1975 cells as Tat-SP4 treatment alone led to faster degradation of EGFR and complete abolishment of its phosphorylation (Figure 4.2C). However, Tat-SP4 only moderately reduced the phosphorylation signal for Akt in H1975 cells, in distinct contrast to the complete abolishment observed in A549 cells (Figure 4.2C). Co-treatment of H1975 cells with EGF and Tat-SP4 further promoted EGFR degradation but the EGFR phosphorylation induced at 0 hour was only moderately reduced by Tat-SP4 (Figure 4.2C). Furthermore, the phosphorylation level of Akt remained largely steady and was not affected by the co-treatment of EGF and Tat-SP4 (Figure 4.2C). This notable difference between A549 and H1975 may be related to their distinct TKI sensitivity, with robust downstream Akt activity in H1975 to overcome EGFR-targeted TKIs.

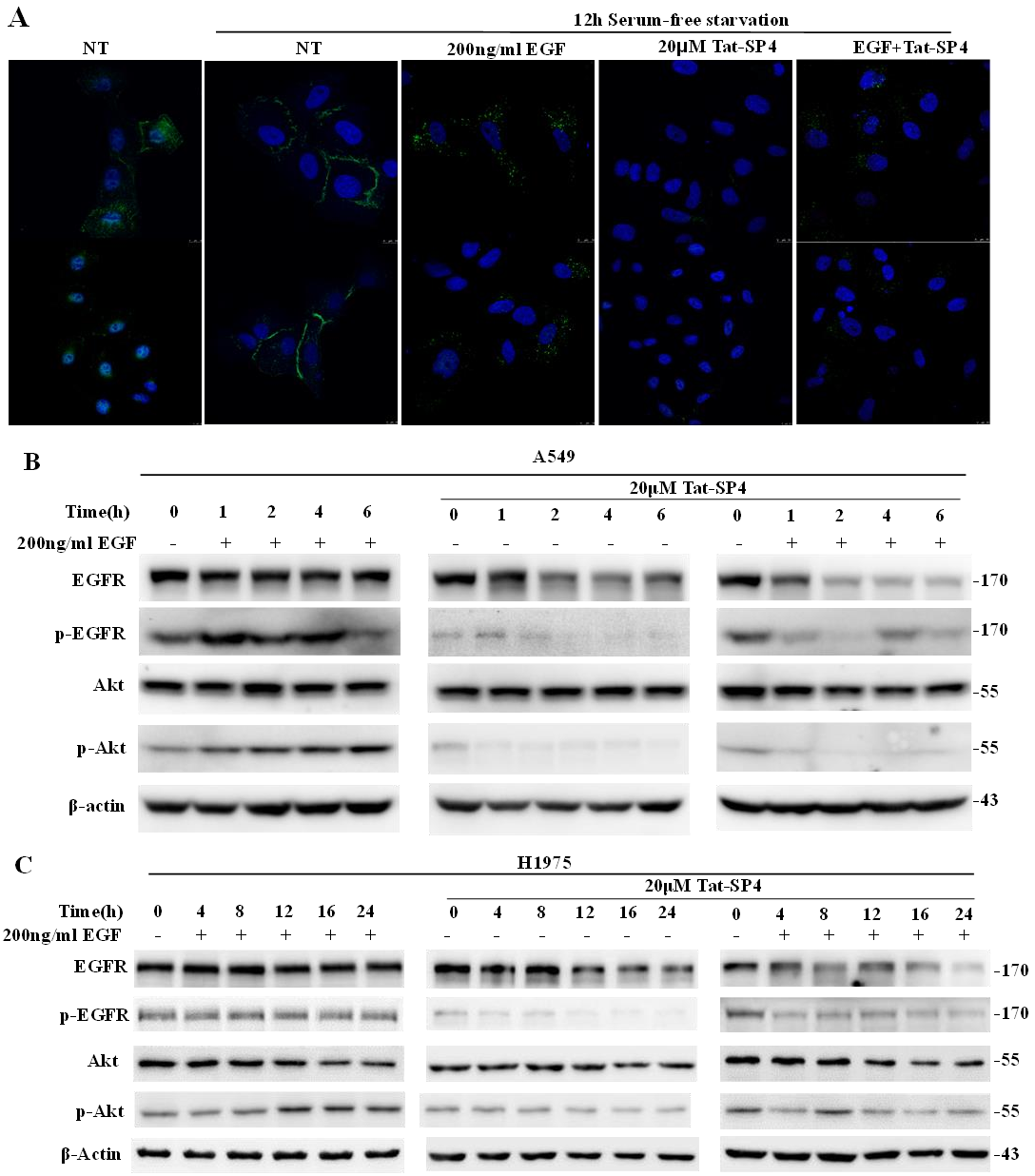

Figure 4.2 Tat-SP4 promotes EGFR degradation and attenuated the oncogenic EGFR signal transduction. (A). Immunofluorescence imaging of EGFR in A549 cells. A549 cells were serum-starved for 12 hours and then treated with 200ng/ml EGF alone and 20 μM Tat-SP4 for 6 hours, in the presence or absence of 200 ng/ml EGF. A549 cells were fixed with 4% PFA, permeabilized with 0.1% TritonTM X-100 and blocked with 1% BSA. After that, cells were incubated with EGFR primary antibody, followed by Alexa Fluor 488 secondary antibody, and examined under the Leica SP8 MP microscope. (Scale bar: 10 μm) **(B and C)**. The impact of Tat-SP4 on EGFR degradation and attenuated the oncogenic EGFR signaling transduction in A549**(B)** and H1975**(C)** cells. A549 and H1975 cells were serum-starved for 12 hours and then treated with 200 ng/ml EGF alone and 20 μM Tat-SP4, in the presence or absence of 200 ng/ml EGF. The proteins level in the cell lysate was analyzed by Western blot at indicated time points.

4.1.3 Tat-SP4 significantly enhances endocytic degradation of c-Met and attenuates the oncogenic c-Met signal transduction

The c-Met receptor is found to be overexpressed and activated in cancers such as lung cancer, liver cancer and breast cancer. It has been studied that crosstalk between c-Met and EGFR is usually associated with acquired-drug resistance to EGFR-TKIs in patients with NSCLC. I assessed the impact of Tat-SP4 on c-Met degradation in lung can cancer cell lines, which was characterized by confocal imaging assay and Western Blotting assay. To visualize the c-Met, EBC-1 cells were immunostained with fluorescent c-Met antibody and Golgi 97 antibody followed by Tat-SP4 treatment for 2 or 4 hours and then the samples were subjected to confocal microscope. The confocal imaging results showed that after 12-hour serum-starvation, most endogenous c-Met translocated in plasma membrane and with increased duration of Tat-SP4 treatment, perinuclear c-Met pool was stable and accumulated in the Golgi, while membrane spanning c-Met were diminished, most remarkably at 4 hours, indicating that Tat-SP4 treatment promoted the degradation of c-Met on plasma membrane but has little effect on perinuclear c-Met pool(Figure 4.3 A).

To assess to efficacy of Tat-SP4 on c-Met degradation, total c-Met level was western blotted after Tat-SP4 treatment and the results showed that when serum starved A549 cells were exposed to 100 ng/ml HGF, a 50% reduction in c-Met level was detected at the latest time point. Besides, the downstream protein Akt was

phosphorylated with HGF treatment. When cells were treated with Tat-SP4, c-Met was degraded in a time-dependent manner and its downstream Akt was not activated, which is independent on HGF stimulation (Figure 4.3 B). Therefore, Tat-SP4 prompted the degradation of c-Met on plasma membrane and inhibited its downstream protein, Akt, activation. The effect of Tat-SP4 on enhancement of endocytic degradation is general for membrane spanning proteins.

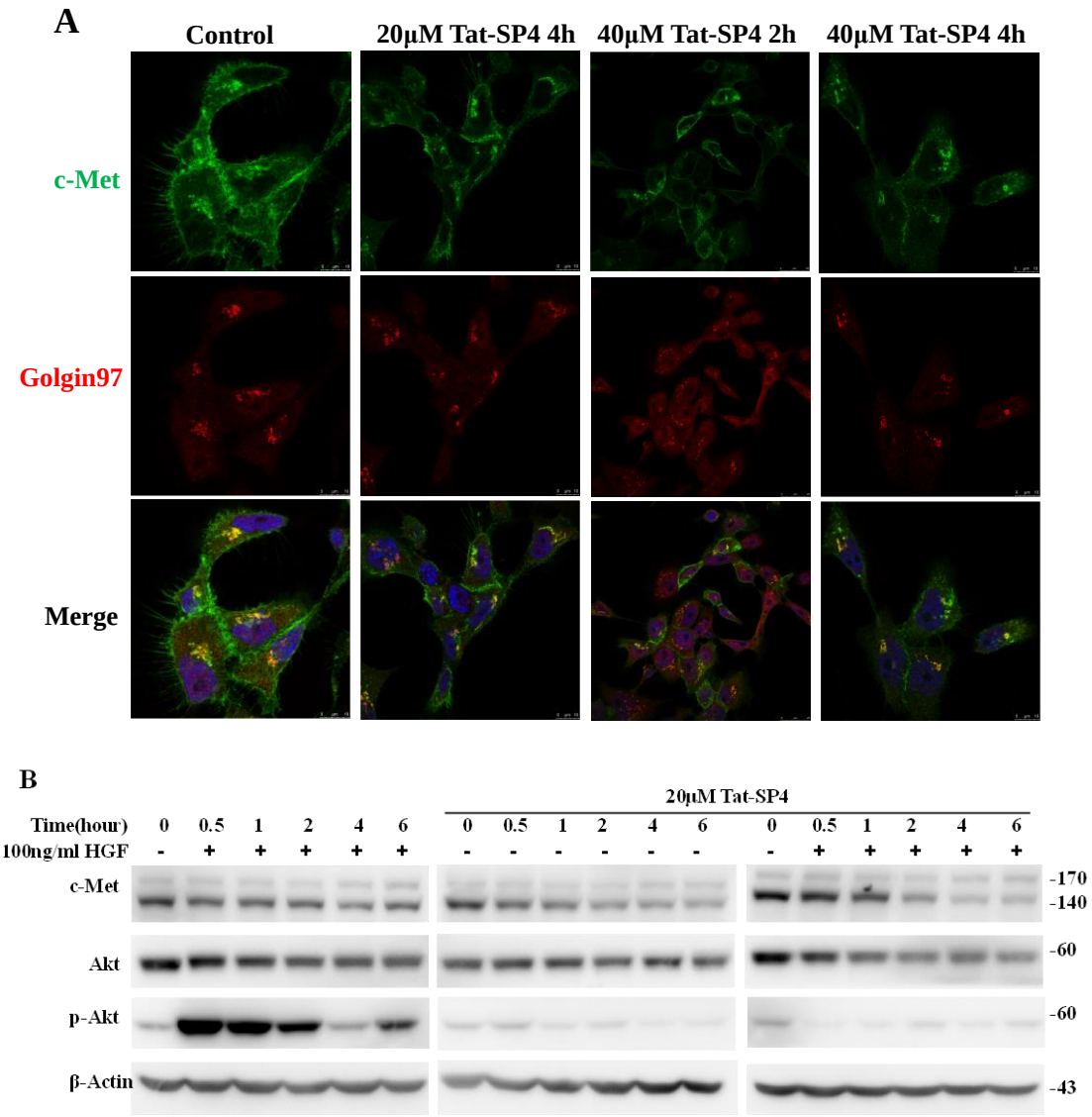

Figure 4.3 Tat-SP4 promotes c-Met degradation and attenuated the oncogenic c-Met signal transduction. (A) Immunofluorescence imaging of c-Met in EBC-1 cells. EBC-1 cells were serum-starved for 12 hours and then treated with 100 ng/ml HGF alone and Tat-SP4(20 μM or 40 μM), in the presence or absence of 100 ng/ml HGF. EBC-1 cells were fixed with 4% PFA, permeabilized with 0.1% Triton X-100 and blocked with 1% BSA. After that, cells were incubated with c-Met and Golgin97 primary antibody, followed by Alexa Fluor 488 and Alexa Fluor 555 secondary antibody, and examined under the Leica SP8 MP microscope. (Scale bar: 10μm) **(B)** The impact of Tat-SP4 on c-Met degradation and attenuated the oncogenic c-Met signaling transduction. A549 cells were serum-starved for 12 hours and then treated with 100 ng/ml HGF alone and 20 μM Tat-SP4, in the presence or absence of 100 ng/ml HGF. The proteins level in the cell lysate was analyzed by Western blot at indicated time points.

4.2 Characterization of Tat-SP4 as single anti-proliferative agents and potential synergistic effect between EGFR-TKIs and Tat-SP4 in lung cancer cell lines

4.2.1 Determination of IC50 of Tat-SP4 in lung cancer cell lines

The anti-proliferative efficacy of Tat-SP4 was assessed in different lung cancer cell lines, which was reflected by IC50 values. The IC50 was determined by measuring cell viability using trypan blue exclusion method after 24-hour treatment with the designed peptides at indicated concentrations. The results showed that Tat-SP4 showed significant anti-proliferative efficacy on lung cancer cells with IC50 values of Tat-SP4 range from 7 μM to 50 μM (Figure 4.4A-D). And small cell lung cancer cell lines, SHP-77 cells (7.66 μM) and H146 (17.62 μM) cells are much more sensitive to Tat-SP4 among these four subtypes of lung cancer cell lines. In Beas-2B cells, a normal bronchial epithelial cell, the IC50 value of Tat-SP4 is high to ~95 μM, which is much higher than the IC50 value of Tat-SP4 in lung cancer cell lines (Figure 4.4E). I also measured the IC50 values of the control peptides including Tat-SC4 and Tat-SS4 in A549 cell lines. Tat-SC4 that is an unmodified peptide with scrambled sequence and Tat-SS4 that has the same sequence as Tat-SC4 but contains a hydrocarbon staple like Tat-SP4. As shown in Figure 4.4 E and F, the IC50 values of either Tat-SC4 or Tat-SS4 failed to be estimated since they were out of the range of the concentration setting, so the cytotoxicity of Tat-SC4 and Tat-SS4 can be ignored.

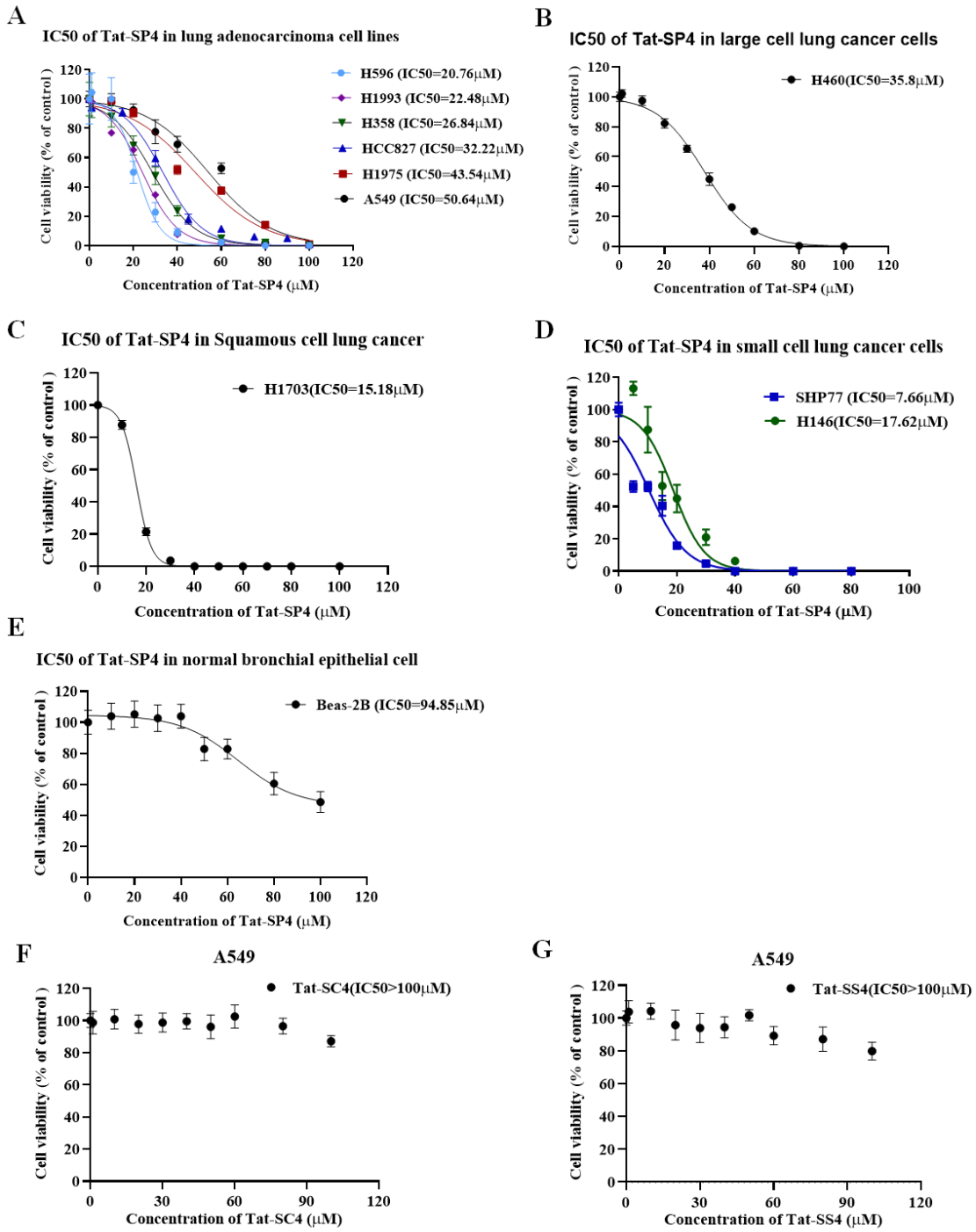

Figure 4.4 Anti-proliferative efficacy of Tat-SP4 in lung cancer cell lines. (A) IC50 of Tat-SP4 in lung adenocarcinoma cell lines. **(B)** IC50 of Tat-SP4 in large cell lung cancer cell line. **(C)** IC50 of Tat-SP4 in squamous cell line. **(D)** IC50 of Tat-SP4 in small cell carcinoma cell lines. **(E)** IC50 of Tat-SP4 in normal bronchial epithelial cell. **(F)** IC50 of Tat-SC4 in A549 cell lines. **(G)** IC50 of Tat-SS4 in A549 cell lines. Data represents mean ± SEM of three replicates.

4.2.2 Long-term anti-proliferative efficacy of Tat-SP4 in lung cancer cell lines

To further determine the long-term anti-proliferative efficacy of Tat-SP4 in lung cancer cell lines, I performed five-day proliferation assay with Tat-SP4 treatment in A549, H1975 and SHP-77 cells. A549 H1975, and SHP-77 cells seeded into 24-well plate were treated with indicated concentrations of Tat-SP4 or Tat-SC4 on Day0. The number of survived cells were counted with trypan blue exclusion method from Day1 to Day 5 to draw 5-day cell proliferation curves. The results showed that Tat-SP4 treatment at 40 μM reduced the proliferation of H1975 cells by ~30% but such effect was statistically insignificant in A549 cells (Figure 4.5 A& B). This trend corroborates the different IC50 values we obtained for A549 and H1975 cells, with H1975 cells being slightly more sensitive to Tat-SP4. As shown in Figure 4.5C, Tat-SP4 treatment at 10 μM reduced the proliferation of SHP-77 cells by ~50%, since SHP-77 is much more sensitive to Tat-SP4 than other lung cancer cell line tested in my project.

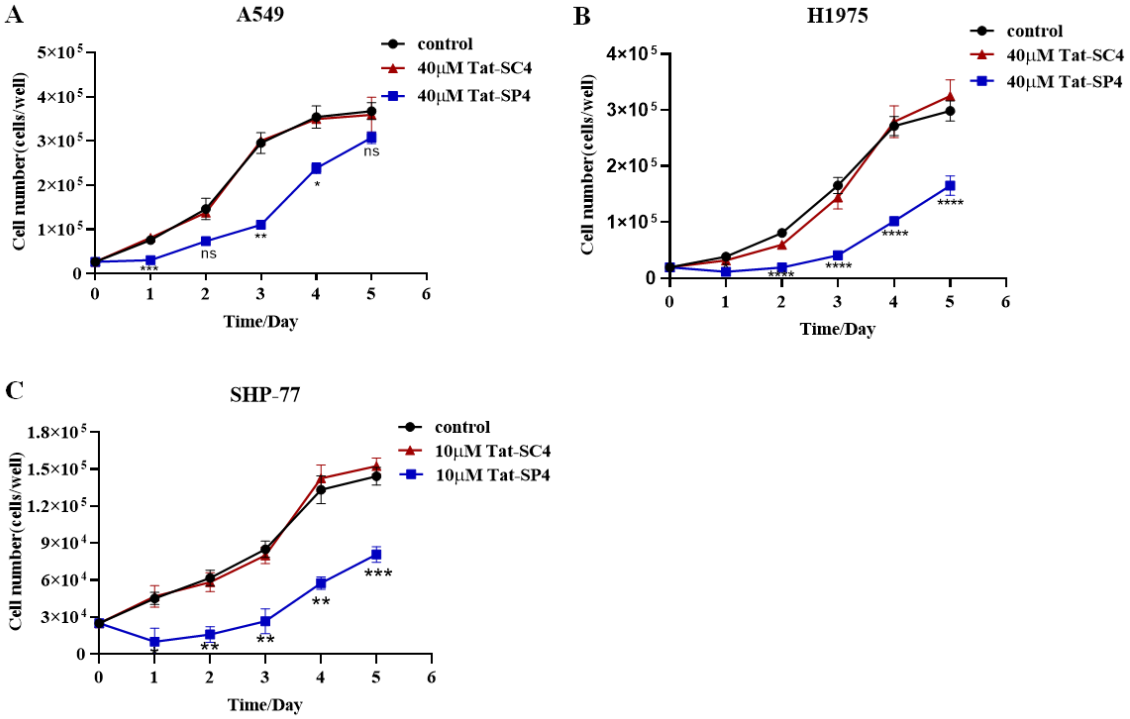

Figure 4.5 Tat-SP4 inhibited A549, H1975 and SHP-77 cell proliferation. (A) 5-day cell proliferation curve of A549 cells with 40 μM Tat-SP4/Tat-SC4 treatment. **(B)** 5-day cell proliferation curve of H1975 cells with 40 μM Tat-SP4/Tat-SC4 treatment. **(C)** 5-day cell proliferation curve of SHP-77 cells with 10 μM Tat-SP4/Tat-SC4 treatment. Cell viability was measured with trypan blue hemocytometry every 24 hours. Data represent mean ± SEM of three replicates. *P<0.05, **P<0.01, ***P<0.001, ****P<0.0001; unpaired t-test.

Besides, I performed classical colony formation assay in A549 cell lines. A549 cells were plated in 6-well plate at very low density to ensure the colony would be formed from a single cell. Then A549 cells were treated with indicated concentrations of Tat-SP4 and Erlotinib for 10 days and the culture media was replaced by fresh treatment media every 72 hours. After 10 days, cells were fixed by 4%PFA and stained by crystal violet. The crystal violet staining results showed that both Erlotinib and Tat-SP4 inhibited colony formation of A549 cells in a dosage-dependent manner (Figure 4.6). Taken together, the results of 5-day proliferation assay and colony formation assay showed significant long-term inhibition of Tat-SP4 in lung cancer cell lines.

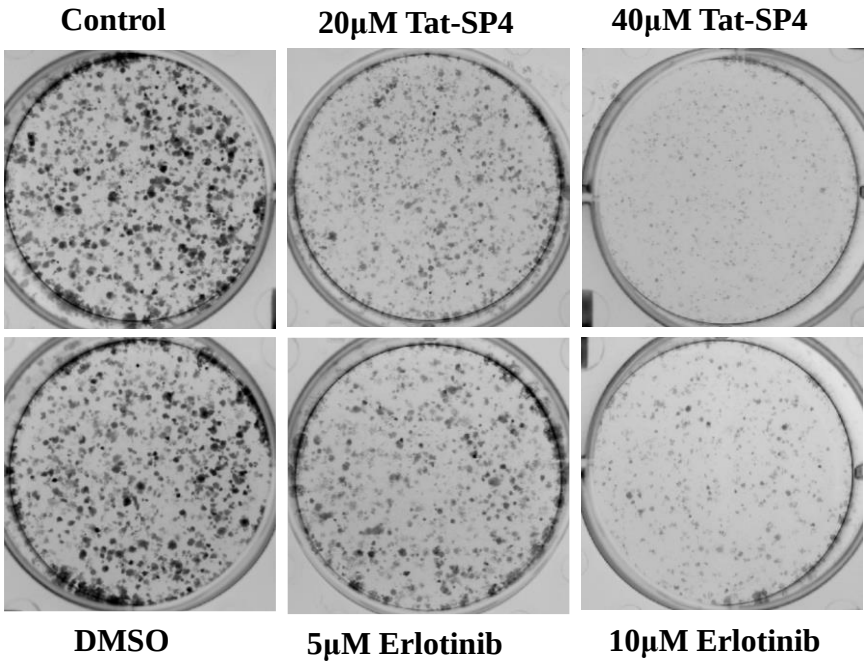

Figure 4.6 Tat-SP4 inhibited colony formation in A549 cells. A549 cells were seeded at a density of 500 per well in a 6-well plate and were cultured with media containing 20 μM/40 μM Tat-SP4 and 5 μM/10 μM Erlotinib for 10 days. After 10 days, cells were fixed by 4%PFA and stained by crystal violet.

4.2.3 Combination of Tat-SP4 and Erlotinib exhibits synergetic effect on inhibition of NSCLC cell proliferation

EGFR-TKIs were approved as first-line clinical treatment for patients with advanced NSCLC, however patients usually got acquired-drug resistance after receiving a period of monotherapy. I wonder whether our stapled peptides could combine with EGFR-TKIs to improve its anti-tumor efficacy or overcome its drug resistance. Firstly, the response of different lung cancer cell lines, including A549, H1975 and SHP-77, towards EGFR-TKIs was assessed, employing a cell viability assay with MTT method. The results showed that the cytotoxicity of AZD9291 and Olmutinib is more potent than the cytotoxicity of Erlotinib in both A549 and H1975 cell lines (Figure 4.7 A&B). Interestingly, SHP-77 cells, a SCLC cell line can't be killed by Erlotinib even at very high concentration, which indicated that SHP-77 cells were totally resistant to the first-generation EGFR-TKI, Erlotinib (Figure 4.7 C). Besides, SHP-77 cells were not sensitive to either AZD 9291 or Olmutinib (Figure 4.7 C). In a word, these three EGFR-TKI compounds failed to significantly inhibit SHP-77 cell proliferation, which may be due to the very low expression level of EGFR in SCLC cell lines.

A

A549

EGFR-TKIs	48h IC50	72h IC50
Erlotinib	23.88μM	8.338μM
AZD 9291	3.82μM	1.79μM
Olmutinib	8.82μM	4.53μM

B

H1975

EGFR-TKIs	48h IC50	72h IC50
Erlotinib	43.63μM	30.33μM
AZD 9291	0.55μM	0.34μM
Olmutinib	0.87μM	0.57μM

C

SHP-77

EGFR-TKIs	48h IC50	72h IC50
Erlotinib	N/A	N/A
AZD 9291	15.07μM	18.61μM
Olmutinib	18.91μM	24.4μM

Figure 4.7 Summary of IC50 of EGFR-TKIs in A549, H1975 and SHP-77 cell lines. Cells were seeded at 96-well plate and cultured in media containing different EGFR-TKIs. After 48 hours and 72 hours, cell viability of A549 cells and H1975 cells were assessed by MTT assay and MTS assay was used to assess the cell viability of SHP-77 cells (suspension cells). Data represents mean ± SEM of three replicates.

Erlotinib is one of the first-generation TKIs approved for $EGFR^+$ NSCLC (Tsao, Sakurada et al. 2005, Thai, Solomon et al. 2021). Among different NSCLC cell lines and clinical tumor samples, sensitivity to Erlotinib is critically dependent on EGFR genotype, with certain activating mutations such as L858R and exon 19 deletions conferring particular sensitivity while exon 20 insertions and T790M causing insensitivity (Lynch, Bell et al. 2004, Pao, Miller et al. 2004, Kobayashi, Boggon et al. 2005). A549 and H1975 cells are not expected to be highly sensitive to erlotinib due to the wild-type or L858R/T790M mutant EGFR they harbor respectively. Our trypan blue exclusion assay showed that the IC50values of Erlotinib in A549 and H1975 cells were ~13.2 μM and ~9.9 μM respectively, thus validating their insensitivity (Figure 4.8A&B). Tat-SP4 enhanced the anti-proliferative efficacy of erlotinib in dosage dependent manner, reducing the IC50 value to ~8.2 μM in A549 and ~4.8 μM in H1975 cells after 30 μM Tat-SP4 was added (Figure 4.8A&B). five-day proliferation assay was also conducted in A549 and H1975 with combinative treatment of Tat-SP4 and Erlotinib and the results further validated such synergy. For A549 cells, treatment by 10 μM Erlotinib alone only reduced cell proliferation by ~30% but combination treatment of 10μM Erlotinib plus 25 μM Tat-SP4 completely abolished cell proliferation (Figure 4.8C). Similar results were obtained for H1975 cells, with the combination treatment of Erlotinib at a lower dosage of 5 μM plus 25 μM Tat-SP4 already sufficient to complete abolish cell proliferation (Figure 4.8D). This heightened sensitivity is likely due to H1975 being more vulnerable to both Erlotinib and Tat-SP4. Taken together, combining

Erlotinib and Tat-SP4 exhibited synergetic effect on inhibition of NSCLC cell proliferation regardless of their EGFR phenotype.

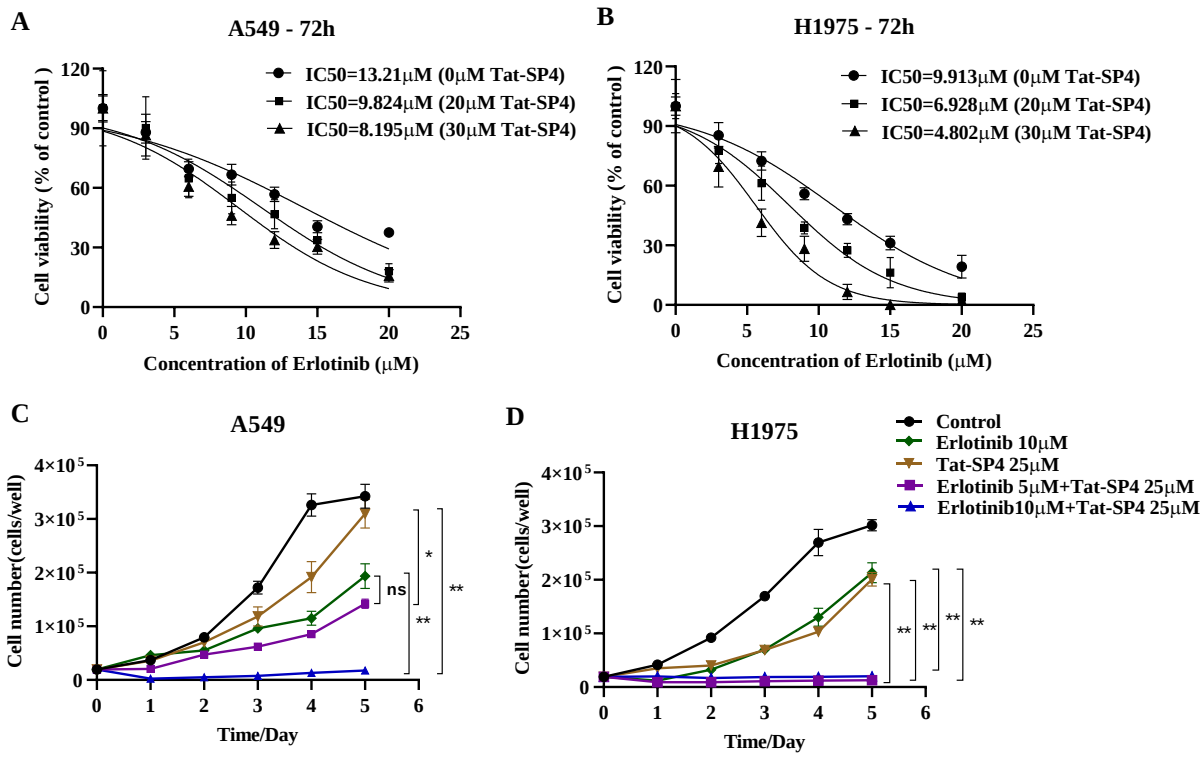

Figure 4.8 Combining Erlotinib and Tat-SP4 exhibited synergetic effect on inhibition of NSCLC cell proliferation. (A-B) The cell viability after different concentrations of Erlotinib with 20 μM or 40 μM Tat-SP4 for 72h in A549 cells**(A)** and H1975 cells **(B)**. Cell numbers were counted by the Trypan Blue exclusion method. **(C-D)** Cell proliferation assay was carried out for five days in A549 cells**(C)** and H1975 cells **(D)** after treatment with Erlotinib (10μM), Tat-SP4(25 μM) or the combination (5 μM/10 μM Erlotinib and 25 μM Tat-SP4). Cells were treated with the indicated treatments at day 0 and the viable cells were counted by the Trypan Blue exclusion method every 24 hours. Data represent mean ± SEM of three replicates. *P<0.05, **P<0.01, ***P<0.001, ****P<0.0001; unpaired t-test.

4.3 Tat-SP4 triggers necrotic cell death that is only rescued by an inhibitor of autosis

It has been demonstrated that Tat-SP4 significantly inhibited the proliferation of lung cancer cells, and I next designed some cell-based experiments to investigate the molecular mechanisms of this process.

4.3.1 Tat-SP4 induces lung cancer cell death not through apoptosis, pyroptosis, ferroptosis or necroptosis.

The anti-proliferative effect of Tat-SP4 on lung cancer cells is to induce cell death instead of to arrest cell cycle. I investigated which type of cell death pathway including apoptosis, pyroptosis and ferroptosis were involved in the Tat-SP4 induced cell death. Firstly, flow cytometry with annexin V/propidium iodide (PI) staining was applied to investigate whether cell death induced by Tat-SP4 was associated with apoptosis. Annexin V specifically binds to anionic phospholipid phosphatidylserine (PS), a marker of apoptotic cells. PS is only in the inner leaflet of the plasma membrane in healthy cells, but PS will translocate to the outer leaflet of the plasma membrane during apoptosis. PS exposed on the outer leaflet of the plasma membrane will bind to fluorescent Annexin V and apoptotic cell can be identified. PI is an impermeable nuclear staining dye, so PI stains nucleus only when the plasma membrane integrity is lost, which is usually because of necrotic cell death. Flow cytometry experiments with annexin V and PI staining reveled that over 40% of A549 cells underwent non-apoptotic

cell death after Tat-SP4 treatment at 40μM for 3 hours while only less than 3% showed apoptosis. When A549 cell were treated with Tat-SP4 40 μM for 6 hours, over 80% of A549 cells underwent non-apoptotic cell death while 6% showed apoptosis (Figure 4.9A). Similar results were obtained in H1975 and SHP-77 cells. In H1975 cells, about 15% of H1975 cells underwent non-apoptotic cell death after Tat-SP4 treatment at 40 μM for 3 hours while only less than 1% showed apoptosis. When H1975 cell were treated with Tat-SP4 40 μM for 6 hours, over 20% of H1975 cells underwent non-apoptotic cell death while 1% showed apoptosis (Figure 4.9A). When SHP-77 cell were treated with Tat-SP4 at 10 μM for 3 hours, over 30% of SHP-77 cells underwent non-apoptotic cell death while 5% showed apoptosis. Over 40% of SHP-77 cells underwent non-apoptotic cell death after Tat-SP4 treatment at 10 μM for 6 hours while only less than 1% showed apoptosis.

To further assess whether Tat-SP4 induced apoptosis in NSCLC cells, I used western blots to track the cleavage of PARP and caspase 3, two hallmark events in apoptosis (Galluzzi, Vitale et al. 2018). The result showed that doxorubicin, a known inducer of apoptosis, triggered cleavage of PARP and caspase 3 in A549 cells (Figure 4.9B). In contrast, no such cleavage was observed after Tat-SP4 treatment at 40 μM, a dosage sufficient to induce significant cell death (Figure 4.9B). I also assessed the effect of Z-VAD-FMK, a pan-caspase inhibitor, on Tat-SP4- induced cell death, and it was shown that Z-VAD-FMK effectively rescued apoptotic cell death induced by cisplatin

in A549 and SHP-77 cells but showed no such effect against the Tat-SP4-caused cell death (Figure 4.9C&D). In summary, Tat-SP4 induced necrotic cell death in lung cancer cells.

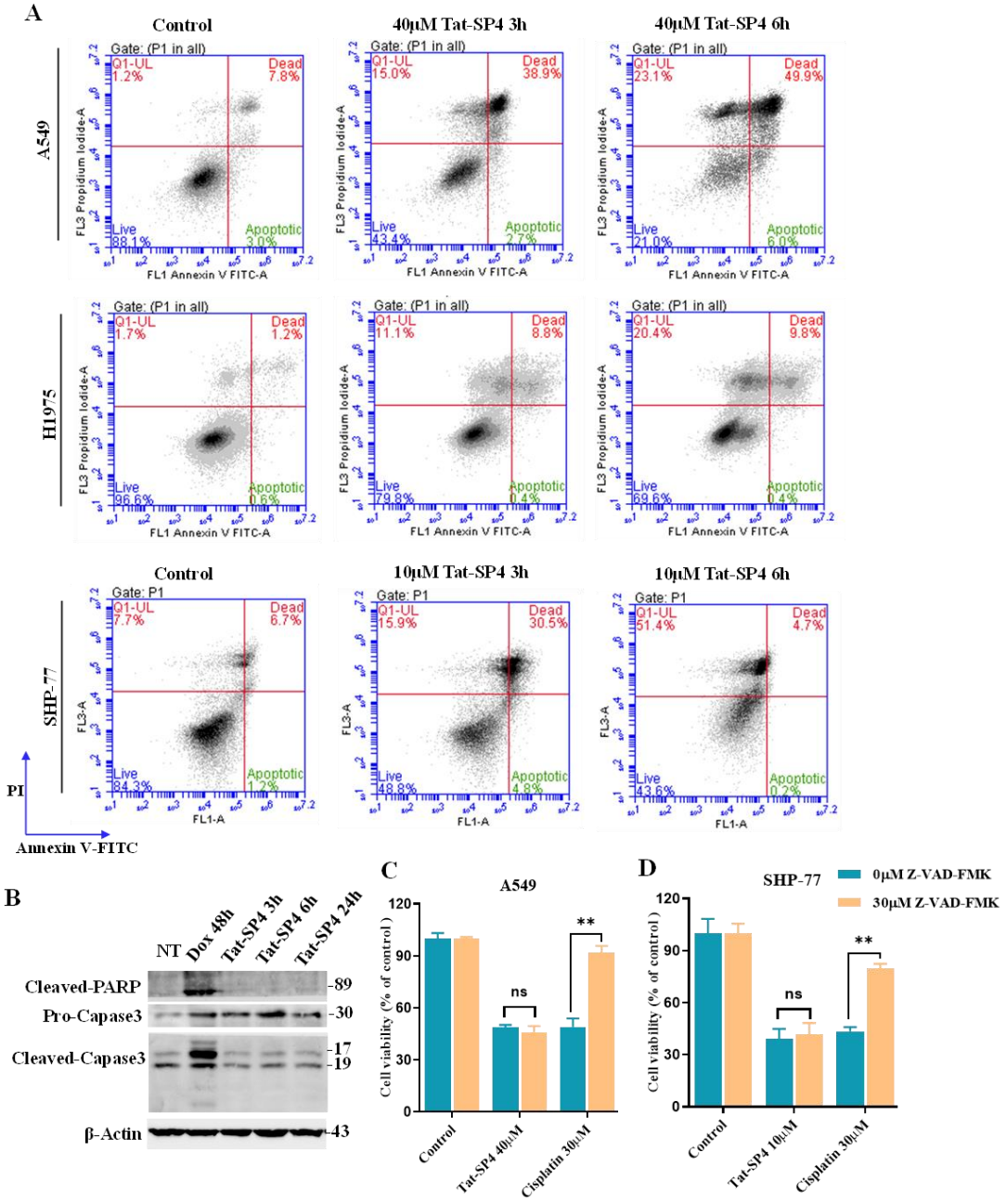

Figure 4.9 Tat-SP4 induce cell death with necrotic features. **(A)** Flow cytometry analysis with Annexin V/PI staining in A549, H1975 and SHP-77 cells treated with Tat-SP4 for indicated time periods. After 3 hours and 6 hours Tat-SP4 treatment, the PI-positive staining cell population was significantly increased, but apoptotic cell population was not changed compared with that of vehicle group. **(B)** Western blotting of cleaved-PARP and cleaved-Caspase3 in A549 cells treated with 40 μM Tat-SP4 for different incubation lengths, or 0.5 μM doxorubicin for 48 hours. The level of cleaved-PARP and cleaved-caspase3 was elevated by treatment of 0.5 μM doxorubicin instead of 40 μM Tat-SP4. **(C&D)** Trypan blue exclusion method to assess the viability of A549 **(C)** and SHP-77 cells **(D)** treated with Tat-SP4 or cisplatin for 24 hours, in the absence or presence of Z-VAD-FMK. Data are presented as mean ± SEM (n = 3). *P<0.05, **P<0.01, ***P<0.001, ****P<0.0001; unpaired t-test.

Additionally, I also investigated whether our Beclin1-targeting stapled peptide induced cell death was associated with other programmed cell death pathways, such as pyroptosis, ferroptosis and necroptosis.

Pyroptosis is a form of programmed cell death mediated by Gasdermin proteins, accompanied by the release of a large number of pro-inflammatory factors. There are two identified pyroptosis signal pathway. The canonical pathway dependents on caspase 1-caspase 3- Gasdermin E (GSDME) signaling pathway(Jiang, Qi et al. 2020). Caspase 1 activation is mediated by inflammasomes and activated caspase 1 will cleave caspase 3. Activated caspase 3 cleave GSDME into GSDME-N domain and GSDME-C domain, and GSDME-N domain plays a crucial role in activating pyroptosis by forming pores in the plasma membrane(Rogers, Erkes et al. 2019). The non-canonical pathway is mediated by caspase4/5/11- Gasdermin D(GSDMD) signaling pathway(N, IB et al. 2015). Caspase4/5/11 are activated by cytoplasmic lipopolysaccharide (LPS) and then Gasdermin D can be cleaved by these activated proteins, forming GSDMD-N domain which is necessary for cell membrane perforation and cell rupture (J, Y et al. 2015).

Gasdermin proteins have been suggested to function as tumour suppressors. A549 cells express GSDME protein at a relatively high level, which make it possible to investigate whether Tat-SP4 induced cell death through pyroptosis in A549 cells. I checked the level of GSDME-FL and GSDME-N, as well as its upstream protein

caspase 3 with Western Blot assay. It was reported some TKIs could induce pyroptosis at high dosage(Lu, Zhang et al. 2018). In A549 cells, 60 μM Olmutinib led to the cleavage of GADME and caspase 3 in a time-dependent manner (Figure 4.10A). Interestingly, higher level of GSDEM-N and lower level of GSDEM-FL was detected in the cell lysate of dead cell floating in supernatant (Figure 4.10A). Z-VAD-FMK is a pan-caspase inhibitor and it prevented caspase3 from cleavage when A549 cells were stimulated with Olmutinib, and the level of GSDME-N was significantly decreased, which suggested that Z-VAD-FMK directly inhibit the cleavage of caspase 3 and further prevented GADME from cleavage by cleaved-caspase 3(Figure 4.10B), confirming that 60 μM Olmutinib induced A549 cell death through canonical pyroptosis pathway. Etoposide is a chemotherapeutic drug, which was used as another positive agent to induce pyroptosis. The change of the level of GSDME-N and cleaved- caspase3 under 40 μM etoposide treatment was too slight to discuss its effect on pyroptosis, which may be because the concentration of etoposide used was not high enough to induce pyroptosis (Figure 4.10B). In contrast, 90 μM Tat-SP4 didn't lead to an increase in GSDME-N and cleaved-caspase3 level (Figure 4.10B), indicating that Tat-SP4 induced cell death though non-pyroptosis pathway.

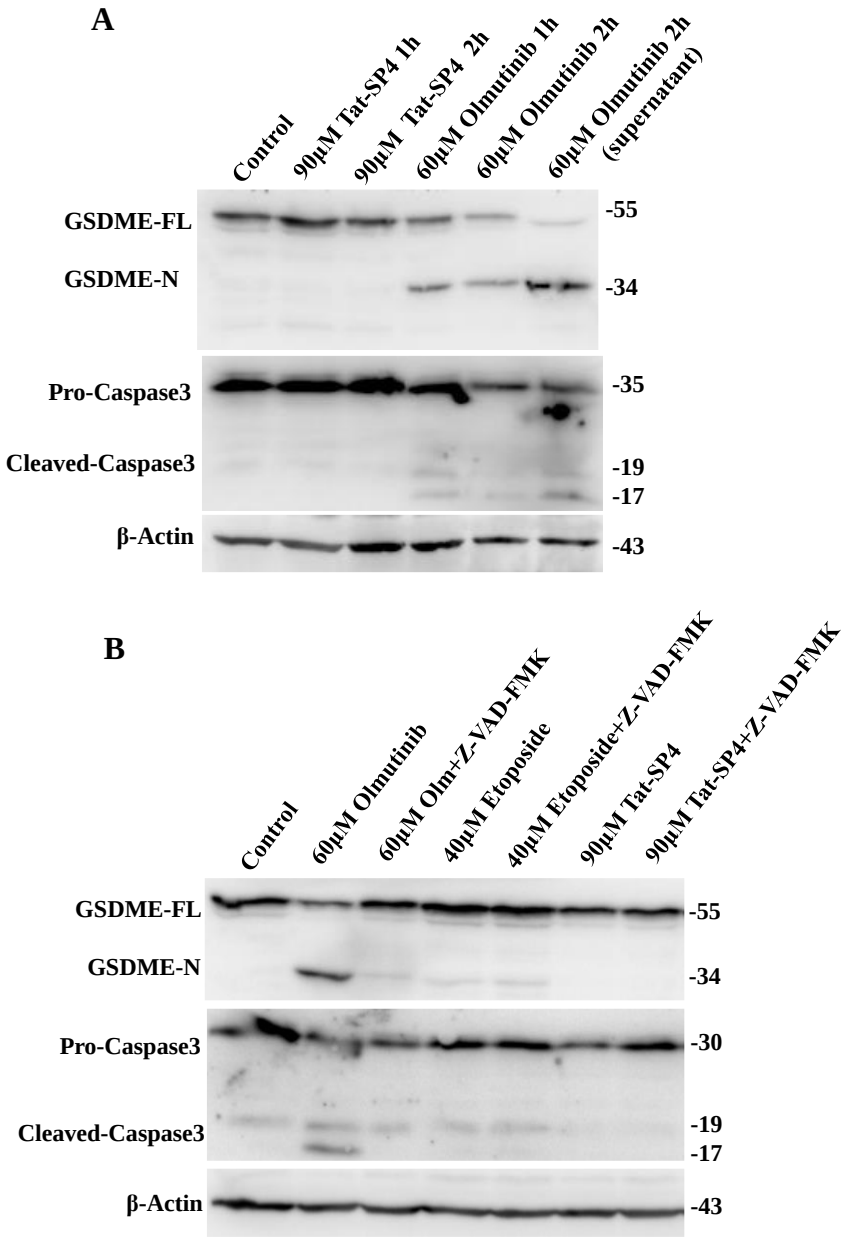

Figure 4.10 Tat-SP4 doesn't induce pyroptosis in A549 cell line. (A) A549 cells were treated with Tat-SP4 and Olmutinib at 90 μM and 60 μM respectively for 1 or 2 hours. Western blotting of GSDME-FL, GSDME-N, Pro-caspase3 and cleaved-caspase3. Action was detected as a loading control. **(B)** Z-VAD-FMK was used to inhibit pyroptosis. A549 cells were treated with 60 μM Olmutinib, 40 μM Etoposide and 90 μM Tat-SP4 for 2 hours in presence or absence of 40 μM Z-VAD-FMK.β-Action was detected as a loading control.

Ferroptosis is an iron-dependent, non-apoptotic form of cell death. It is characterized by excessive intracellular accumulation of lipid hydroperoxides and reactive oxygen species (ROS), as well as shrunken mitochondria with decreased crista and outer mitochondrial membrane rupture. Erastin is an identified small-molecule blocker of System X_{c-} channel, an upstream molecule of ferroptosis. Erastin induces ferroptosis through inhibiting cystine transport mediated by System X_{c-} channel and increasing lipis ROS. Ferrostatin-1(Fer-1) can efficiently prevent erastin-induced lipid ROS accumulation and ferroptosis (Dixon, Lemberg et al. 2012). A549 cells and SHP-77 cells were pretreated with 1 μM Fer-1 for 2 hours followed by Tat-SP4 treatment or Erastin for 24 hours. The cell viability was measured by Trypan Blue exclusion method. As shown in Figure 4.11A and B, Fer-1 prevented both A549 cells and SHP-77 cells from killing by 5 μM Erastin. However, Fer-1 had little protective effect against the cell death induced by Tat-SP4 Figure 4.11A and B.

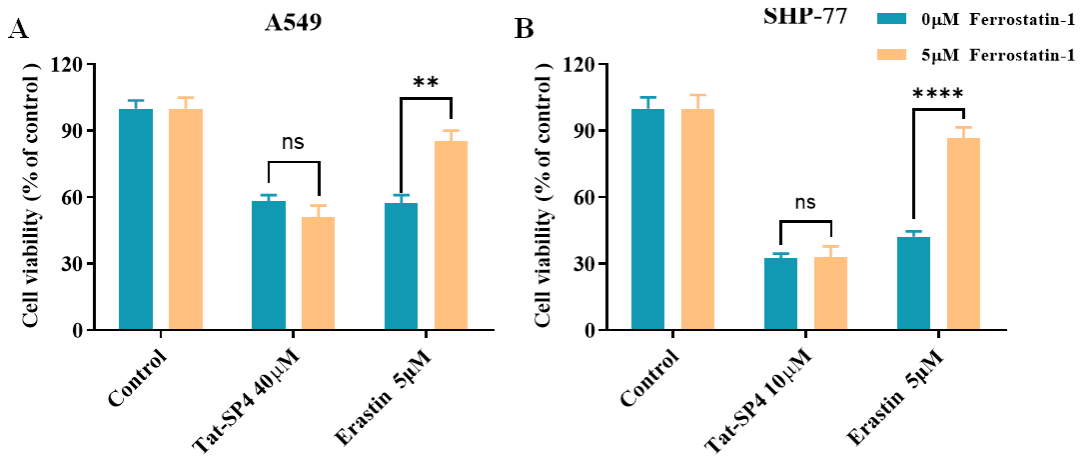

Figure 4.11 Tat-SP4 doesn't induce ferroptosis in A549 and SHP-77 cell lines. **(A)** A549 cells were pretreated with ferroptosis inhibitor, 1 μM Ferrostatin-1(Fer-1), followed by 40 μM Tat-SP4 or 5 μM Erastin treatment for 24 hours. Fer-1 didn't rescue A549 cell death induced by Tat-SP4. **(B)** SHP-77 cells were pretreated with ferroptosis inhibitor, 1 μM Fer-1, followed by 10 μM Tat-SP4 or 5 μM Erastin treatment for 24 hours. Fer-1 didn't rescue SHP-77 cell death caused by Tat-SP4. Data represents mean ± SEM of three replicates. *P<0.05, **P<0.01, ***P< 0.001, ****P<0.0001; unpaired t-test.

Necroptosis is a programmed cell death pathway with the features of apoptosis and necrosis. Necroptosis is regulated by the necrosome complex composed of receptor-interacting protein 1 (RIP1) and RIP3 as well as pseudokinase mixed lineage kinase domain-like (MLKL)(Christofferson, Li et al. 2014).The most studies and characterized necroptosis pathway is mediated via TNFR. TNFR recruits RIPK1 and RIPK3 to form necrosome complex, which promotes the interaction of RIP1 and RIP3 to form necrosome, the key regulator of necroptosis signaling(Xie, Peng et al. 2013). Necrostatin 1 (Nec-1) acts as a specific necroptosis inhibitor through blocking RIPK1. I assessed the cell viability of A549 cells and SHP-77 cells treated with Tat-SP4 in the presence or absence of different concentration of Nec-1. As shown in Figure 4.12A and B, 40 μM and 10 μM Tat-SP4 significantly induced cell death in A549 cells and SHP-

77 cells respectively. Nec-1 had little protective effect against the Tat-SP4-caused cell death (Figure 4.12A&B). Taken together, lung cancer cell death caused by Tat-SP4 doesn't involve necroptosis.

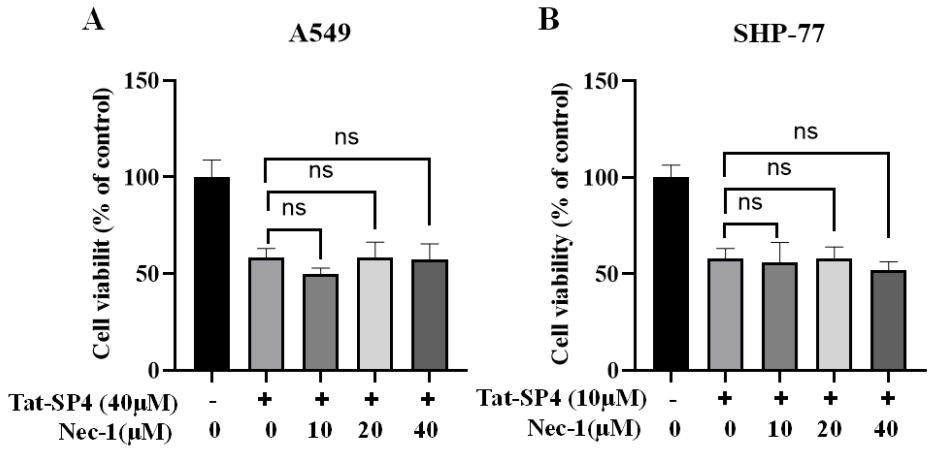

Figure 4.12 Tat-SP4 doesn't induce necroptosis in A549 and SHP-77 cell lines. (A-B) In the presence or absence of Nec-1, A549 **(A)** and SHP-77 **(B)** cells were treated with Tat-SP4 at 40 μM or 10 μM for 24 hours, respectively. Nec-1 didn't rescue A549 or SHP-77 cell death caused by Tat-SP4. Data represents mean ± SEM of three replicates. *P<0.05, **P<0.01, ***P< 0.001, ****P<0.0001; unpaired t-test.

4.3.2 Tat-SP4 exerts anti-proliferative effect that can only be rescued by inhibitors of autosis

Autosis is a type of autophagic cell death and is caused by overactivation of autophagy(Liu and Levine 2015). Autosis can be triggered by prolonged starvation, hypoxia-ischemia, and viral infection with unique morphological changes, such as excessive vacuolization, expansion of perinuclear space, nucleus concavity and eventual rupture of plasma membrane (Liu, Shoji-Kawata et al. 2013, Kheloufi, Boulanger et al. 2015, Zhang, Luk et al. 2019, Yin, Wang et al. 2022, Zheng, Fang et al. 2022). Autosis was first introduced by Beth's lab in 2013. They used an autophagy-

inducing peptide named Tat-Beclin1 to induce autosis *in vivo* and *in vitro*(Liu, Shoji-Kawata et al. 2013). Autosis is dependent on Na^+,K^+-ATPase pump, an ion channel in plasma membrane that essential for generating Na^+ and K^+ gradients across the plasma membrane and functions as a multifunctional signal transducer(Liu, Shoji-Kawata et al. 2013).Conversely, autosis can be inhibited by pharmacological inhibitors of Na^+,K^+-ATPase, such as cardiac glycosides digoxin(Liu, Shoji-Kawata et al. 2013). Therefore, I examined whether digoxin could rescue the necrotic cell death induced by Tat-SP4 in lung cancer cells. A549 and SHP-77 cells in 96-well plate were pretreated with 10 μM or 20 μM digoxin for two hours, followed by the treatment of Tat-SP4 at indicated concentrations for twelve hours. The results showed that digoxin significantly rescued cell death induced by Tat-SP4 in A549 (Figure 4.13 A) and SHP-77 cells (Figure 4.13 B). Thus Tat-SP4 may induce autosis in lung cancer cells.

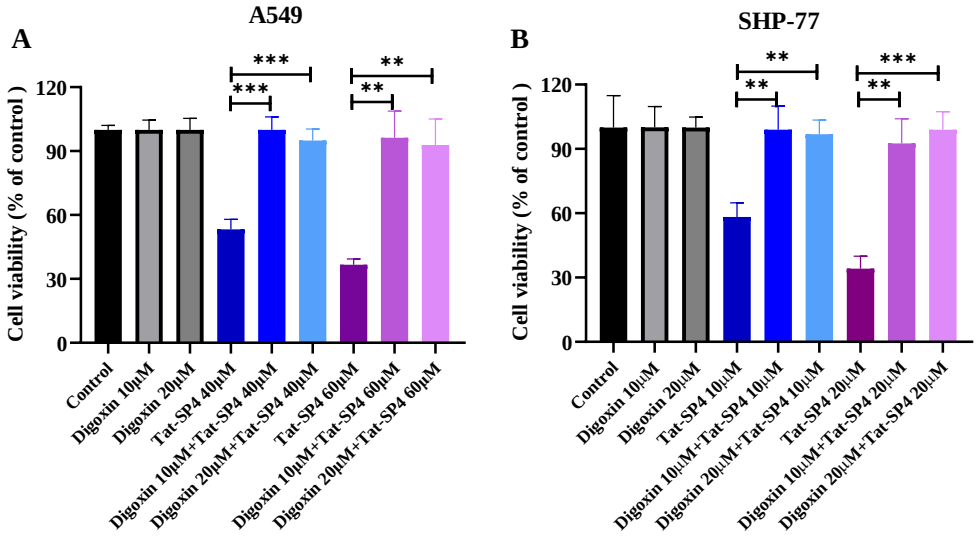

Figure 4.13 Tat-SP4-induced cell death can be rescued by digoxin. A549 **(A)** and SHP-77 **(B)** cells were pretreated with digoxin at indicated concentrations for 2 hours, followed by the treatment of Tat-SP4 at indicated concentrations for 12 hours. Cell viability was measured by Trypan Blue exclusion assay. Data represents mean ±

SEM of three replicates. *P<0.05, **P<0.01, ***P< 0.001, ****P<0.0001; unpaired t-test.

4.3.3 Cells treated with Tat-SP4 shows morphological features of autosis

Cells undergoing autosis showed unique morphological features. Autotic cells in vitro will go through the process of excessive vacuolization, expansion of perinuclear space due to the rapid shrinkage of the nucleus, and eventual rupture of plasma membrane, and cells undergoing autosis remain attached to the culture dish until death (Liu, Shoji-Kawata et al. 2013). To investigate whether necrotic cell death caused by Tat-SP4 showed any morphological features of autotic cells, I performed live cell imaging of A549 cells with the treatment of Tat-SP4(Figure 4.14). During the initial 15 minutes, an increase in vacuolar dynamics and perinuclear accumulation of numerous vacuoles were observed in A549 cells treated with Tat-SP4. Subsequently, the shrinkage of nucleus and a local separation of the inner and outer nuclear membranes were observed, followed by the localized rupture of plasma membrane and extracellular extrusion of cytoplasmic contents. Different from apoptotic or necrotic cells which are ultimately float, cells treated with Tat-SP4 remain attached to the culture dish until death (Figure 4.14).

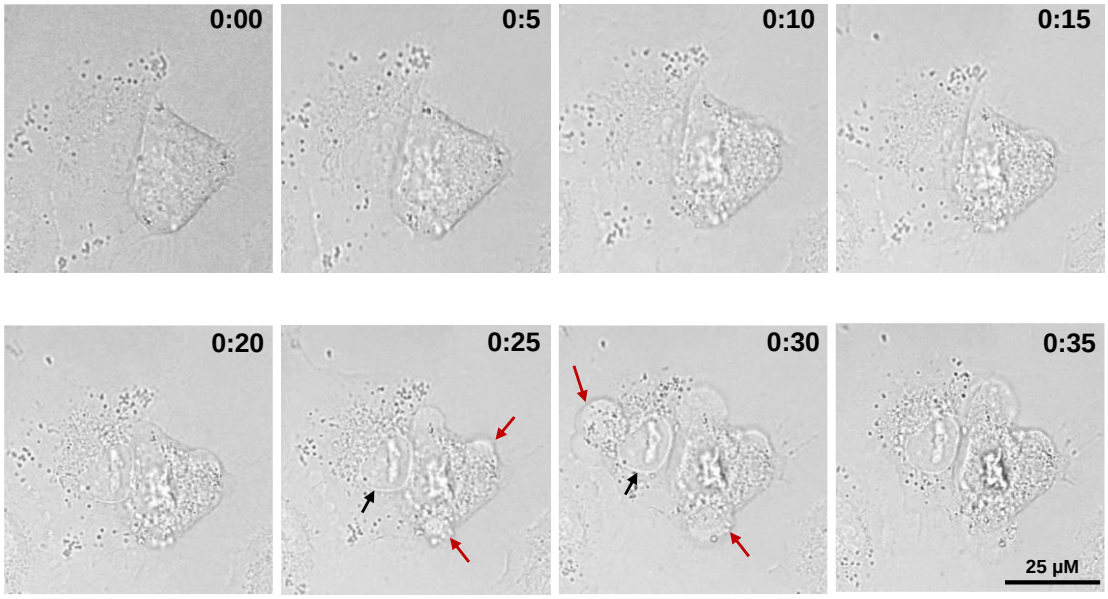

Figure 4.14 Morphological changes of A549 cells treated with Tat-SP4. Live-cell imaging of A549 cells treated with Tat-SP4 at 60 µM (times shown as hh:mm, scale bar: 25 µm). The black arrows show the local separation of the inner and outer nuclear membranes. The red arrows show the localized rupture of cell membrane and released intracellular components.

The flow cytometry data suggests that Tat-SP4 induce necrotic cell death in lung cancer cells. However, the molecular mechanism involved in necrotic cell death is still controversial. Cell death induced by Tat-SP4 can be rescued only by digoxin, a cardioglycoside that blocks Na^+/K^+ ATPase, and some notable autotic morphology changes were observed in A549 cells upon Tat-SP4 induction, suggesting Tat-SP4 may induce cell death through autosis pathway. Although some studies have demonstrated that autosis can be triggered via excessive autophagy and other extreme stress such as hypoxia, mitochondrial damage, and pathogen infection, the molecular mechanism of autosis is not well defined. Thus, I want to explore other possibilities that contribute to the induction of autosis. Since TAT is a cationic CPP that combine with negatively charged phospholipid membranes through electrostatic interaction(Xie, Bi et al. 2020),

it is reasonable to assume that Tat-SP4 may associate with membrane-bound organelles due to non-specific binding to phospholipids. Mitochondria are classical organelles with a phospholipid bilayer membrane structure and mitochondrial dysfunction is a key player in cell death, which attract me to investigate the effect of Tat-SP4 on mitochondria.

4.4 Tat-SP4 causes mitochondria dysfunction and impairs oxidative phosphorylation activity

4.4.1 Tat-SP4 depolarizes mitochondrial membrane potential in a dosage- and time-dependent manner in lung cancer cells

Mitochondria dysfunction usually results from mitochondrial membrane depolarization, increase cellular ROS, inhibition of oxidative phosphorylation (OXPHOS) respiratory chain, decreased mitochondrial enzyme activity, and mtDNA damage. Firstly, the impact of Tat-SP4 on mitochondrial function was assessed through measuring MMP. The dissipation of MMP was monitored via staining with TMRM fluorescent probe whose intracellular distribution is directly related to the membrane potential. A549 cells were transfected with GFP-TOM20 for 24 hours and then stained with 100 nM TMRM for 30 minutes, followed by 40 μM Tat-SP4 treatment. The images of the treated cells were captured immediately after treatment of Tat-SP4 by confocal microscope. The red fluorescence of TMRM were observed in A549 cells, reflecting the impact of Tat-SP4 on the MMP. As shown in Figure 4.15A, the fluorescence of

TMRM in A549 cells was decreased significantly along the time lapse, which indicated that Tat-SP4 depolarized MMP in a time-dependent manner.

Flow cytometry assay was also performed to assess the effect of Tat-SP4 on MMP. Cells were treated with different concentrations of Tat-SP4 for an hour. At the last 30 minutes of incubation, TMRM with final concentration of 100nM was added into cell culture medium. After incubation, the cells were collected according to the protocol described in methodology part and then analyzed by flow cytometer. As shown in Figure 4.15B, CCCP was used as a positive compound to induce MMP depolarization and with Tat-SP4 induction, TMRM fluorescence intensity decreased in A549, H1975 and SHP-77 cells, suggesting Tat-SP4 depolarized MMP in a dosage-dependent manner in lung cancer cells.

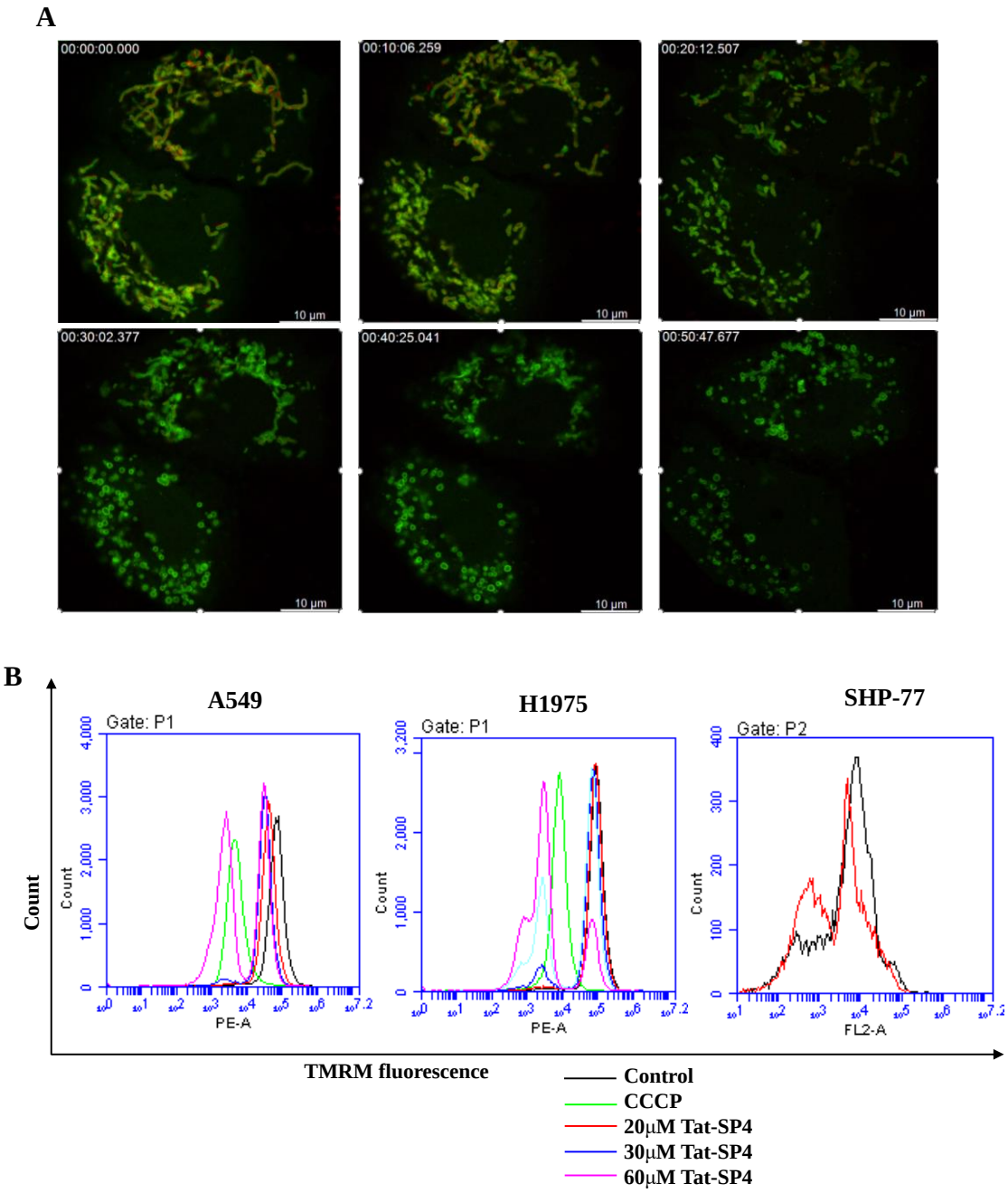

Figure 4.15 Tat-SP4 induces loss of mitochondrial membrane potential in lung cancer cells. (A) A549 cells transiently expressing GFP-TOM20 were stained with TMRM for 30 minutes followed by 30 µM Tat-SP4 treatment. Images were captured by confocal microscope. (Scale bar: 10 µm) **(B)** Representative flow cytometry plot of A549, H1975 and SHP-77 cells treated with indicated concentrations of Tat-SP4 for an hour.

4.4.2 Tat-SP4 impairs mitochondrial oxidative phosphorylation

The homeostasis of MMP plays an important role in maintaining cellular oxidative phosphorylation, so decreased MMP induced by Tat-SP4 may disturb OXPHOS process. To study the effect of Tat-SP4 on mitochondrial function, oxygen consumption rate (OCR), an important indicator for mitochondrial respiration, and extracellular acidification rate (ECAR), largely the result of glycolysis, were measured in response to Tat-SP4 by Seahorse XF24 analyzer in A549, H1975 and SHP-77 cells. The OCR and ECAR was monitored under Tat-SP4 or vehicle, oligomycin (ATP synthase inhibitor), FCCP (uncoupling agent) and rotenone together with antimycin (irreversible inhibitor of complex I and complex III respectively) treatment in order. In A549 cells, both basal OCR and basal ECAR were decreased in a dosage dependent manner when cells were treated with Tat-SP4(Figure 4.16A, B&C). Under energetically stressed conditions caused by FCCP, both maximum mitochondrial respiration and ECAR were also decreased in a dosage dependent manner when cells were treated with Tat-SP4 (Figure 4.16A, B&C). Similar results were obtained in H1975 cells (Figure 4.16D, E&F) and SHP-77 cells (Figure 4.16G, H&I). Taken these data together, it was concluded that Tat-SP4 inhibited mitochondrial OXHOS process as well as impaired on the glycolysis.

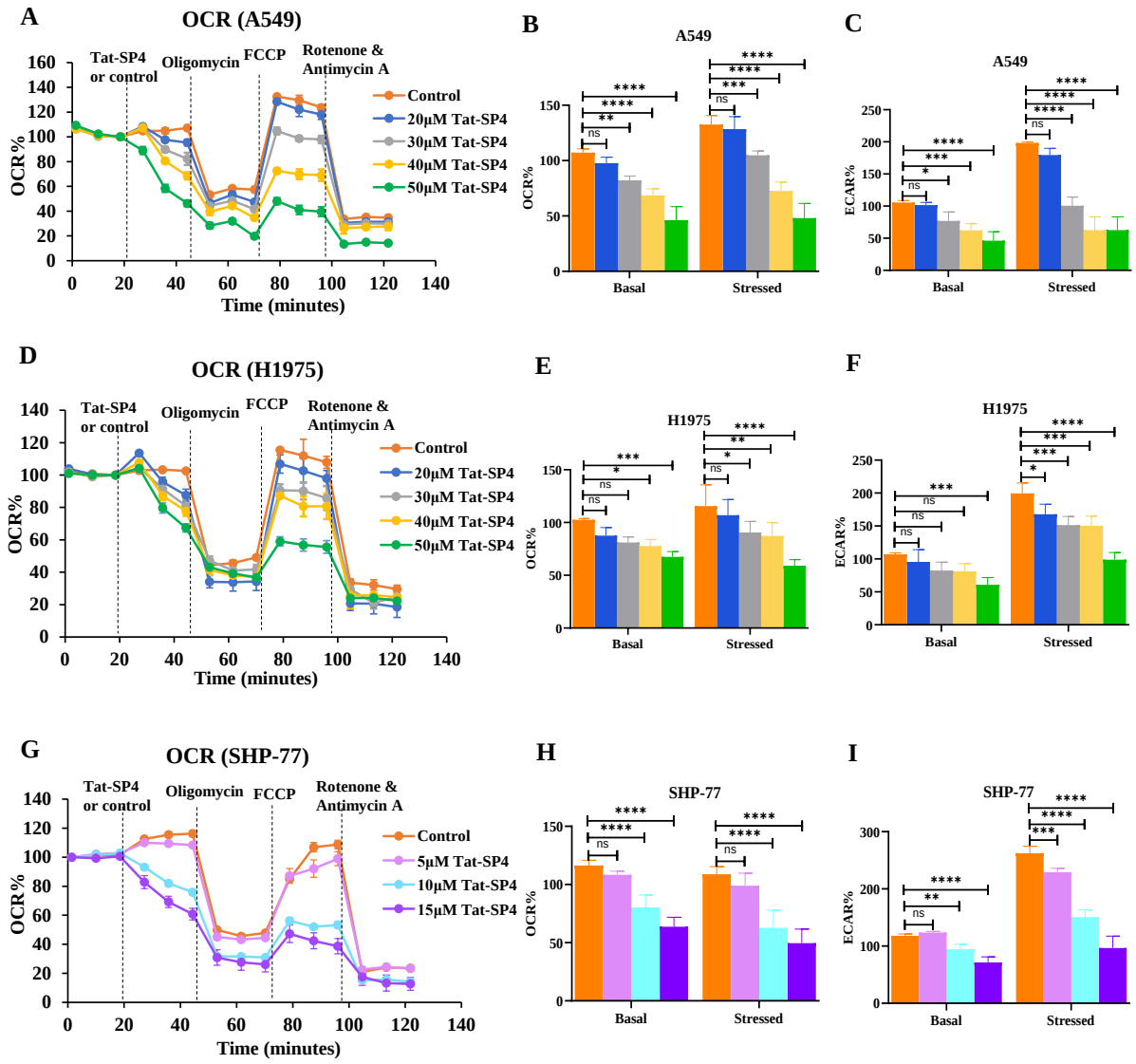

Figure 4.16 Tat-SP4 inhibits the mitochondrial OXPHOS. (A, D and G) OCR was measured using Mito Stress Test with Agilent Seahorse Analyzer. A549**(A)**, H1975**(D)** and SHP-77**(G)** cells were treated with either Tat-SP4 or vehicle (control), 1 μM oligomycin, 1 μM FCCP, and 0.5 μM rotenone and antimycin A sequentially. Each data point represented a real-time OCR measurement. **(B, E and H)** OCR is presented before (baseline) oligomycin addition in A549**(B)**, H1975**(E)** and SHP-77**(H)** cells. **(C, F and I)** ECAR is represented after (stressed) FCCP addition in A549**(C)**, H1975**(F)** and SHP-77**(I)** cells. Data represents mean ± SEM of three replicates. *P<0.05, **P<0.01, ***P< 0.001, ****P<0.0001; unpaired t-test.

4.4.3 Tat-SP4 leads to an increase in cellular ROS level in lung cancer cells

Mitochondria are not only the main site of cellular ROS production, but also the main target organ of ROS attack. The increase of ROS production beyond the cellular scavenging ability will lead to the imbalance of oxidation and anti-oxidation, resulting in oxidative stress. The electron transport chain (ETC) is the main source of cellular ROS production, therefore suppression of OXPHOS generally lead to an increase in cellular ROS level. The ROS level was assessed by CellROX^{TM} green probe with flow cytometer. SHP-77, A549 and H1975 cells were treated with Tat-SP4 at indicated concentrations for an hour, followed by staining process according to the kit protocol. As shown in Figure 4.17, the fluorescence of CellROX^{TM} green was increased when cells were treated with Tat-SP4 at indicated concentrations, indicating that Tat-SP4 increased cellular ROS in a dosage- dependent manner in lung cancer cells.

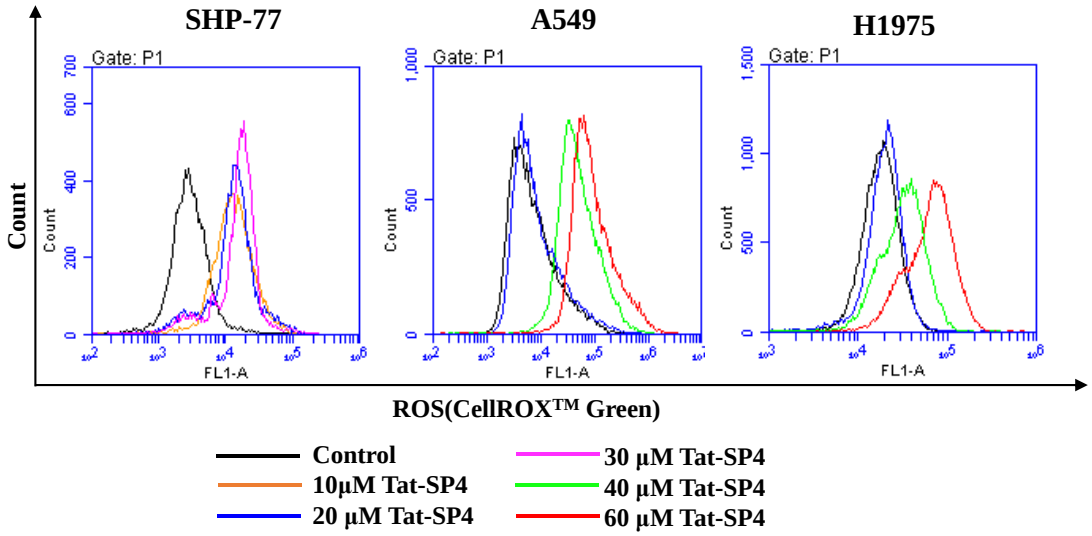

Figure 4.17 Tat-SP4 induces an increase in cellular ROS level. Representative flow cytometry plot of SHP-77 cells, A549 cells and H1975 cells treated with indicated concentrations of Tat-SP4 for an hour, followed by CellROX^{TM} green probe staining.

4.4.4 Tat-SP4 induces mitochondrial permeability transition pore (mPTP) opening

mPTP is a non-specific channel composed of the OMM and IMM, which is involved in the release of mitochondrial substances to induce apoptosis or even necrotic cell death. mPTP opening usually results from mitochondrial Ca^{2+} overloading and oxidative stress and will lead to mitochondria depolarization, mitochondria swelling and outer membrane rupture, and the release of intermembrane pro-apoptotic proteins(Kroemer, Galluzzi et al. 2007, Lim, Davidson et al. 2007).

I used the membrane permeability fluorescent probe Calcein AM to detect the opening of mPTP and Mito Tracker Deep Red to label mitochondria in A549 cells. A549 cells were pretreated with indicated concentrations of Tat-SP4 for an hour, then were stained with Calcein AM followed by calcein quencher $CoCl_2$. Calcein AM is a non-fluorescent esterase substrate and will be cleaved by esterases to release the fluorescent calcein when it enters cells. Calcein distributes all over the cell. Calcein quencher $CoCl_2$ can pass through plasma member but is stopped by mitochondrial membrane. Therefore, in normal condition, addition of $CoCl_2$ quench the fluorescence of cytosolic calcein, and fluorescence of mitochondrial calcein is reserved (Figure 4.18A.). Ionomycin was used as a positive agent to induce mPTP opening. When mPTP is opened by ionomycin, calcein in mitochondria was quenched by $CoCl_2$ leading to decreased green fluorescence (Figure 4.18A). Similar results were obtained when cells were treated with

Tat-SP4 (Figure 4.18A). The green fluorescence of calcein in mitochondria was reduced after cells were treated with Tat-SP4 for 2 hours, suggesting that Tat-SP4 could trigger mPTP opening. The state of mPTP was also analyzed by flow cytometry assay. Similarly, the fluorescence intensity of Calcein was decreased with ionomycin treatment and Tat-SP4 treatment respectively, indicating that Tat-SP4 could trigger mPTP opening (Figure 4.18B).

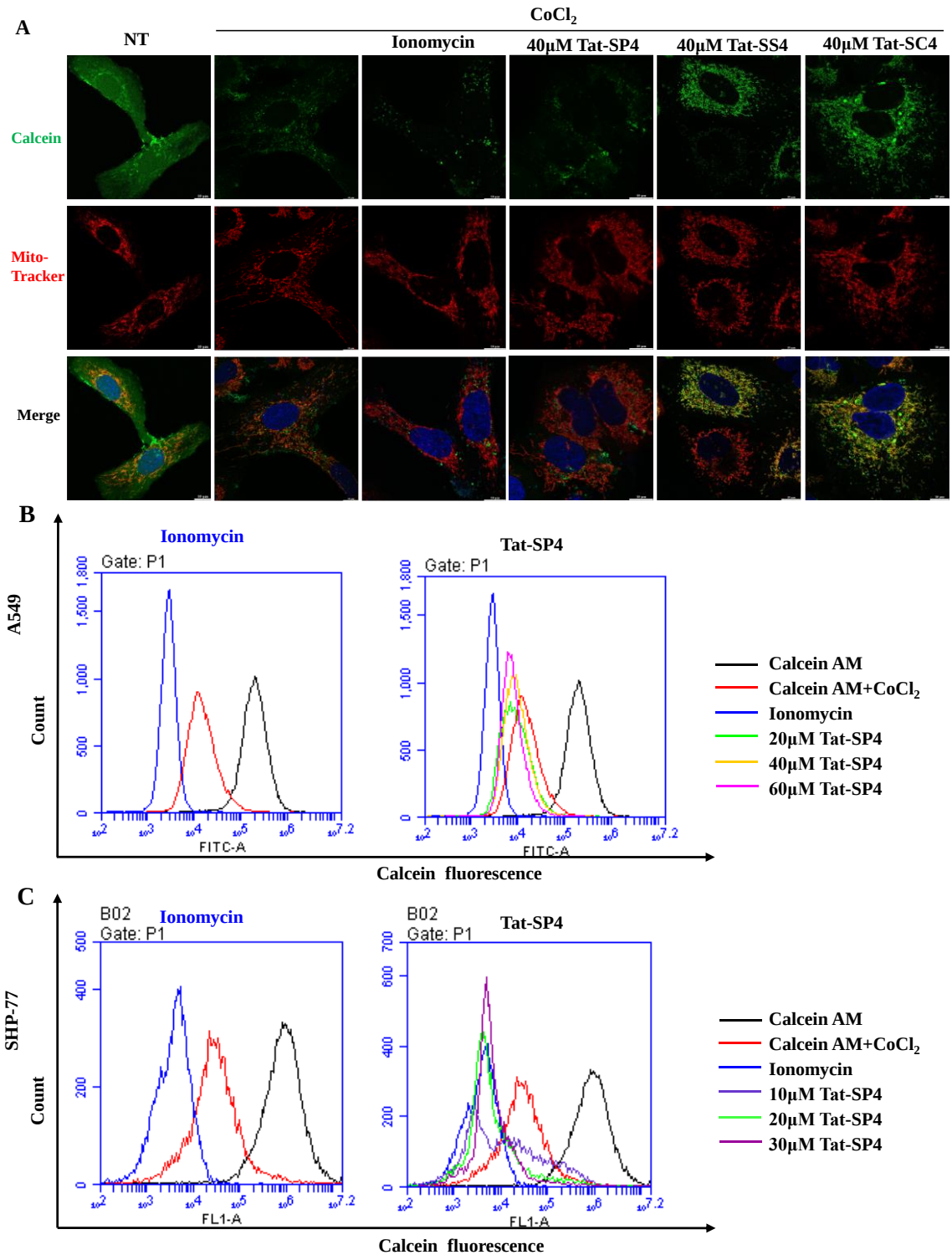

Figure 4.18 Tat-SP4 induces mitochondrial permeability transition pore (mPTP)opening. (A) Confocal imaging of state of mPTP under Tat-SP4, Tat-SS4, Tat-SC4 and ionomycin treatment in A549 cells. (Scale bar: 10 μm) **(B)** Flow cytometry plot of calcein fluorescence under Tat-SP4 or ionomycin treatment in A549 cells. **(C)** Flow cytometry plot of calcein fluorescence under Tat-SP4 or ionomycin treatment in SHP-77 cells.

Here the results showed that Tat-SP4 interferes with mitochondrial function in terms of membrane potential, ROS and OXPHOS and mPTP, and such mitochondrial dysfunction may lead to cell death. mPTP opening is rough and usually lead to irreversible necrotic cell death due to the destructive damage to mitochondria, such as mitochondrial osmotic swelling, an increase in permeability of mitochondrial membrane, the release of mitochondrial contents. Although the molecular mechanisms of mPTP are not well characterized, it is widely accepted that mPTP opening is stimulated by mitochondrial Ca^{2+} overloading, which is also proved in Figure 4.18. Since Tat-SP4 also induced mitochondrial Ca^{2+} overloading, we decided to investigate the impact of Tat-SP4 on Ca^{2+} dynamic in lung cancer model.

4.5 Tat-SP4 disrupts intracellular calcium homeostasis

4.5.1 Tat-SP4 triggers a release of Ca^{2+} from ER, and causes an increase in Ca^{2+} level in mitochondria and cytoplasm

Calcium is a survival and death signal and almost all cellular physiological activities are regulated by Ca^{2+}. The basis for Ca^{2+} as a cellular messenger is the concentration gradient between cytoplasmic Ca^{2+} and the intracellular calcium pool or extracellular Ca^{2+}. In normal cells, the intra-membrane Ca^{2+} concentration is about 10,000 times lower than the extra-membrane Ca^{2+} concentration. Mitochondria, ER and synaptic vesicles can take up and store Ca^{2+}. When cells are subjected to certain stimuli, Ca^{2+} from both extracellular and organelles may passively enter the cytoplasm, causing

the free Ca^{2+} concentration to rise to 1~10 μmol/L, thus causing certain physiological responses.

To determine the dynamic of intraorganellar Ca^{2+} level, there are two kinds of commercially available tools including chemical fluorescent probes and bioluminescent calcium indicators. Chemical fluorescent probes include Indo1, Fura2, Fluo3 and Rhod 2. Chemical fluorescent probes are the most widely used Ca^{2+} tracer, and for the same change in calcium ion concentration, they have the strongest change in signal intensity, but small molecular Ca^{2+} indicators can't be precisely targeted to the organelles. The main body of bioluminescent calcium indicators are Ca^{2+}-sensitive photoproteins, such as aequorin, obelin, clytin and mitrocomin. To make it is organelle-specific, the retention signal sequence of an organelle will be inserted into the contract of the indicators. In my project, I applied mito-GCaMP5G, G-CEPIA1er and cyto-RCaMP to real-time monitor the dynamic of Ca^{2+} level in mitochondria, ER and cytoplasm respectively.

A549 and SHP-77 cells were chosen for their high transfection ability and represent NSCLC and SCLC cells, respectively. Cells were transfected separately with mito-GCaMP5G, G-CEPIA1er and cyto-RCaMP with lipofectamine 3000 for 24 or 36 hours. Mito-GCaMP5G, G-CEPIA1er and cyto-RCaMP was highly enriched in mitochondria, ER or cytoplasm respectively in A549 and SHP-77 cells after post-

transfection. Then the culture medium was changed to Ca^{2+}-free HBSS or 1.2mM Ca^{2+}-containing HBSS buffer. Next, cells were subjected to Olympus inverted epifluorescence microscope and fluorescence images were captured every 3s. At the 60^{th} second, cells were challenged with Tat-SP4 at indicted concentrations.

As shown in Figure 4.19A, when A549 cells were challenged by Tat-SP4 at 40 μM, the fluorescence intensity of G-CEPIA1er was decreased in the presence or absence of extracellular Ca^{2+}, suggesting that Tat-SP4 could trigger a release of Ca^{2+} from the ER in A549 cells. As shown in Figure 4.19B and C, increased fluorescence intensity of mito-GCaMP5G and cyto-RCaMP were observed in the presence or absence of extracellular Ca^{2+}, when A549 cells were stimulated by Tat-SP4 at 40 μM, indicating that Tat-SP4 triggered an increase of both mitochondrial and cytosolic Ca^{2+} level.

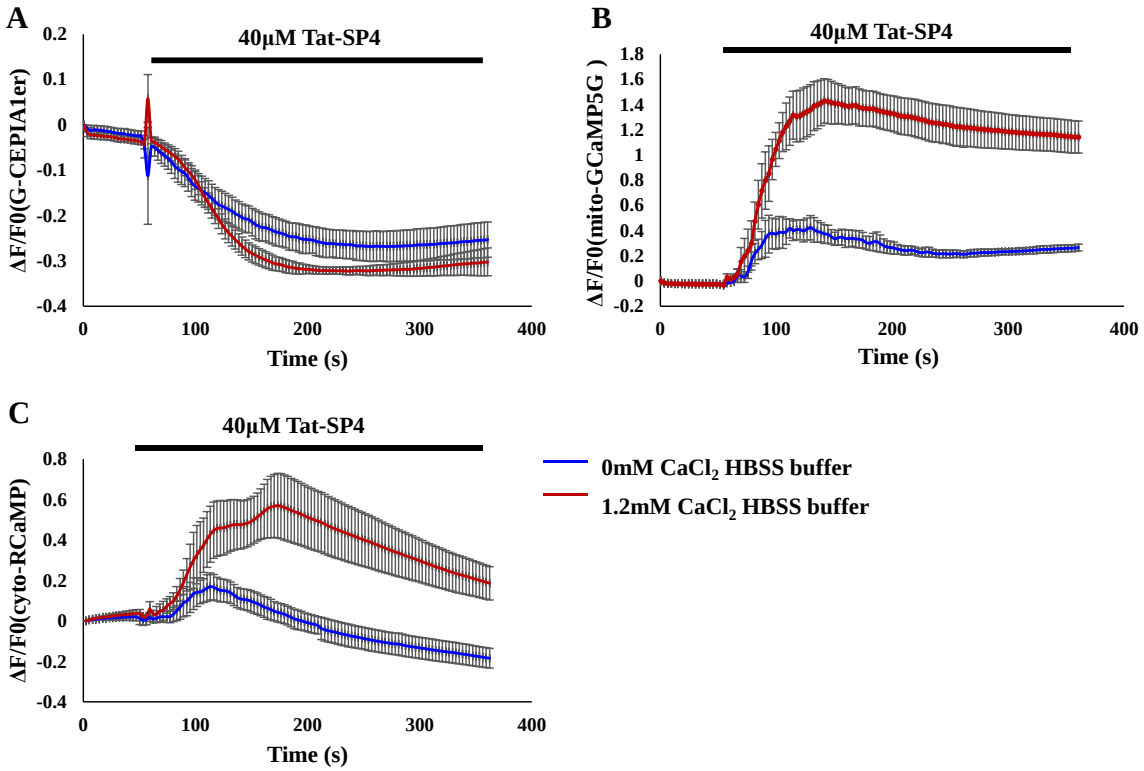

Figure 4.19 Tat-SP4 disrupts intracellular calcium homeostasis. (A) A549 cells seeded in 24-well plate were transfected with mito-GCaAMP5G for 24 hours. 40μM Tat-SP4 was added to evoke an increase of mitochondrial Ca^{2+} in A549 cells in HBSS buffer with or without $CaCl_2$. **(B)** A549 cells seeded in 24-well plate were transfected with G-CEPIA1er for 24 hours. 20 μM Tat-SP4 was added to evoke Ca^{2+} release from ER in A549 cells in HBSS buffer with or without $CaCl_2$. **(C)**A549 cells seeded in 24-well plate were transfected with cyto-RCaMP1h for 24 hours. 40 μM Tat-SP4 was added to evoke an increase of cytosolic Ca^{2+} in A549 cells in HBSS buffer with or without $CaCl_2$. F0 refers to the fluorescence intensity at the start of measurement and ΔF = Ft–F0, where Ft refers to the fluorescence intensity at time t. The data represent n=25 for each individual measurement**.** The error bars show mean ± SEM of three individual measurement.

Similar results were obtained in SHP-77 cells. When SHP-77 cells were challenged by Tat-SP4 at 10 μM, Ca^{2+} level in ER was reduced, and mitochondrial Ca^{2+} level as well as cytosolic Ca^{2+} level was elevated respectively, in the presence or absence of extracellular Ca^{2+} (Figure 4.20). In both A549 and SHP-77 cells, such changes in Ca^{2+} level in different Ca^{2+} store was more remarkable in the presence of 1.8 mM extracellular Ca^{2+} than that in absence of extracellular Ca^{2+}. However, the control peptide, Tat-SC4 didn't induce notable changes in the Ca^{2+} level in ER, mitochondria, or cytoplasm. In summary, Tat-SP4 disrupts intracellular calcium homeostasis and extracellular Ca^{2+} reduces the interference of Tat-SP4 with intracellular calcium homeostasis in both NSCLC and SCLC cells.

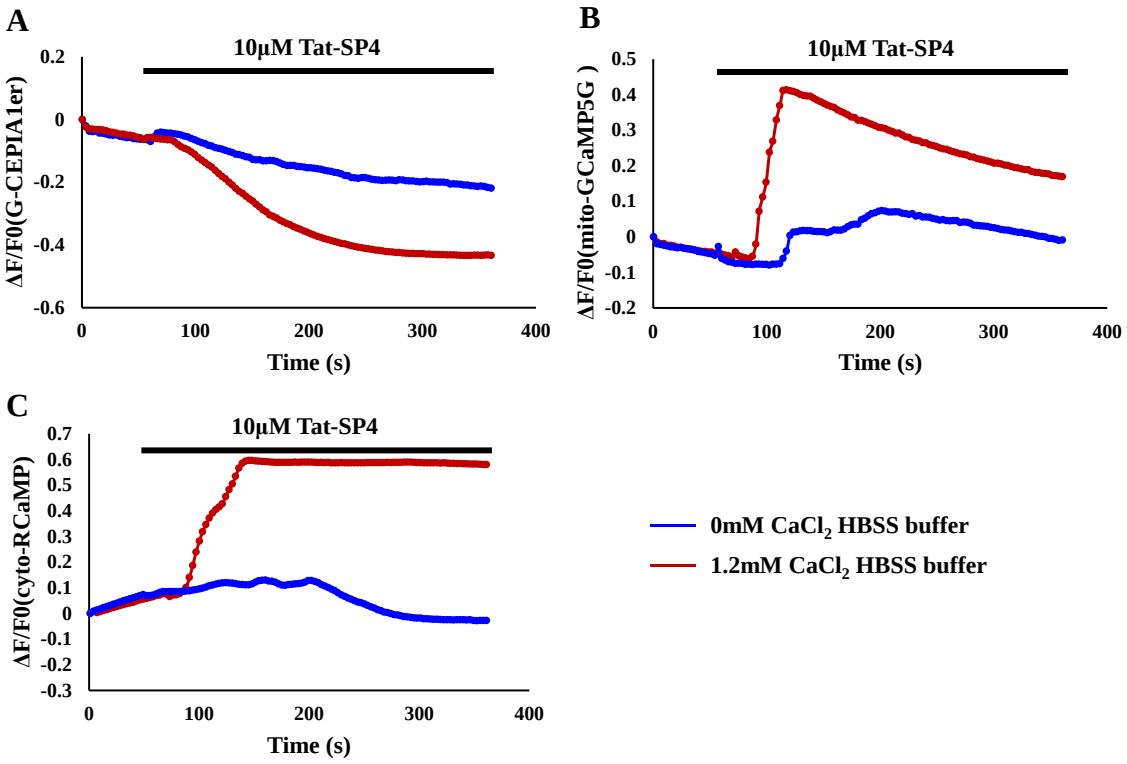

Figure 4.20 Tat-SP4 disrupts intracellular calcium homeostasis in SHP-77 cells. (A) SHP-77 cells were transfected with mito-GCaAMP5G for 36 hours. 10μM Tat-SP4 led to an increase of mitochondrial Ca^{2+} in SHP-77 cells in HBSS buffer with or without $CaCl_2$. **(B)** SHP-77 cells were transfected with G-CEPIA1er for 36 hours. 10 μM Tat-SP4 led to Ca^{2+} release from ER in SHP-77 cells in HBSS buffer with or without $CaCl_2$. **(C)** SHP-77 cells were transfected with cyto-RCaMP1h for 36 hours. 10 μM Tat-SP4 led to an increase of cytosolic Ca^{2+} in SHP-77 cells in HBSS buffer with or without $CaCl_2$. The data represent n=30 for each individual measurement**.** F0 refers to the fluorescence intensity at the start of measurement and ΔF = Ft–F0, where Ft refers to the fluorescence intensity at time t.

However, the control peptide, Tat-SC4 didn't induce notable changes in the Ca^{2+} level in ER, mitochondria, or cytoplasm (Figure 4.21). In summary, Tat-SP4 disrupts intracellular calcium homeostasis and extracellular Ca^{2+} reduces the interference of Tat-SP4 with intracellular calcium homeostasis in both NSCLC and SCLC cells.

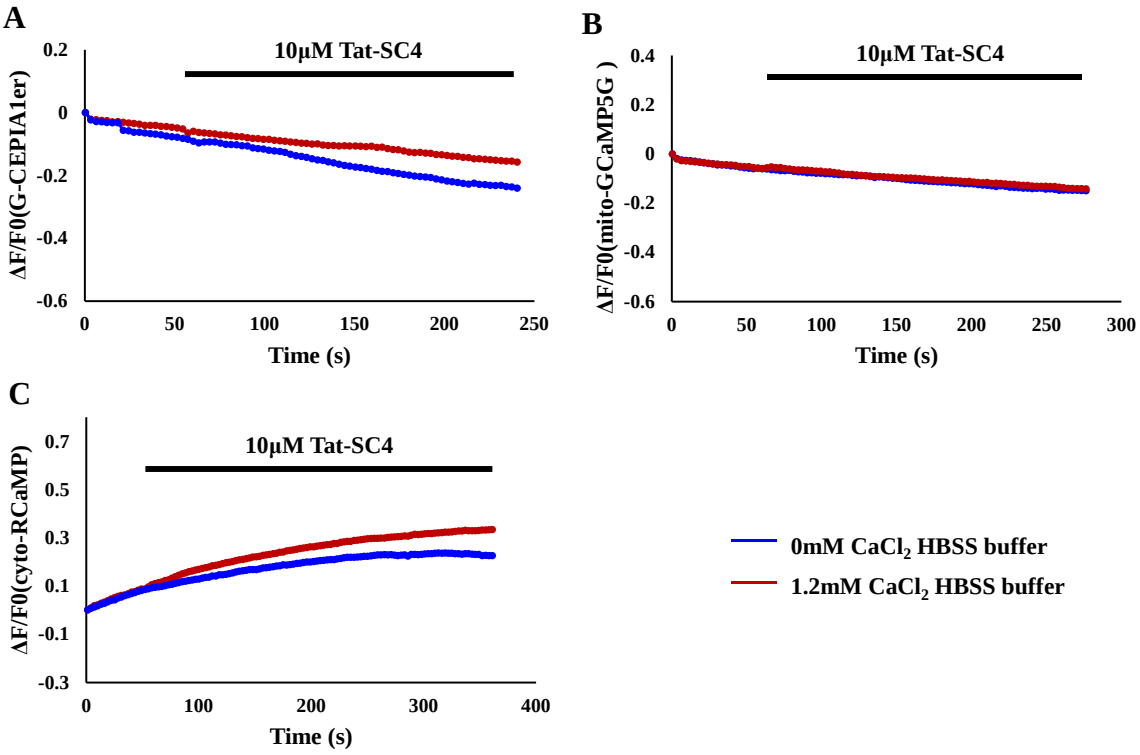

Figure 4.21 Tat-SC4 showed little effect on calcium homeostasis in SHP-77 cells. (A-C) Ca^{2+} level in mitochondria **(A)**, ER **(B)** and cytoplasm **(C)** was real-time monitored when SHP-77 cells were challenged by Tat-SC4 at 10 μM, in the presence or absence of $CaCl_2$. The data represent n=30 for each individual measurement**.** F0 refers to the fluorescence intensity at the start of measurement and ΔF = Ft–F0, where Ft refers to the fluorescence intensity at time t.

4.5.2 Digoxin moderates intracellular Ca^{2+} fluctuations induced by Tat-SP4

Digoxin is a cardiac glycoside and is Na^+,K^+-ATPase antagonists used in clinical medicine. Na^+,K^+-ATPase is responsible for the transport of potassium ions into cells and sodium ions out of cells using energy from ATP hydrolysis. Inhibiting Na^+,K^+-ATPase leads to an increase in intracellular Na^+ and Ca^{2+}. Digoxin was used to inhibit the activity of Na^+,K^+-ATPase to investigate the effect of digoxin on lung cancer cell death caused by Tat-SP4 treatment. In absence of extracellular Ca^{2+}, 40 μM Tat-SP4 stimulation reduced the Ca^{2+} level in ER (Figure 4.21A). Meanwhile, both mitochondrial Ca^{2+} levels (Figure 4.21B) and cytosolic Ca^{2+} levels (Figure 4.21C) were significantly increased by stimulation with 40 μM Tat-SP4, and then both declined to almost their basal level. Mitochondrial Ca^{2+} levels (Figure 4.21B) and cytosolic Ca^{2+} levels (Figure 4.21C) were further increased to a higher level due to the subsequent addition of 2 mM $CaCl_2$. When A549 cells were pretreated with digoxin for 3.5 hours, The Ca^{2+} level of ER (Figure 4.21A), mitochondria (Figure 4.21B), cytosol (Figure 4.21C) were not changed when cells were challenged by 40 μM Tat-SP4. Mitochondrial Ca^{2+} levels (Figure 4.21B) and cytosolic Ca^{2+} levels (Figure 4.21C) were increased significantly due to the subsequent addition of 2 mM $CaCl_2$, which is lower than that without pretreatment of digoxin. These data suggested that, in A549 cells, Tat-SP4 could trigger Ca^{2+} release form ER, which leads to an increase of mitochondrial Ca^{2+} levels and cytosolic Ca^{2+} levels. Digoxin could inhibit Tat-SP4-induced intracellular

Ca^{2+} dynamic. And high concentration of extracellular Ca^{2+} induces significant Ca^{2+} uptake into cytosol and mitochondria.

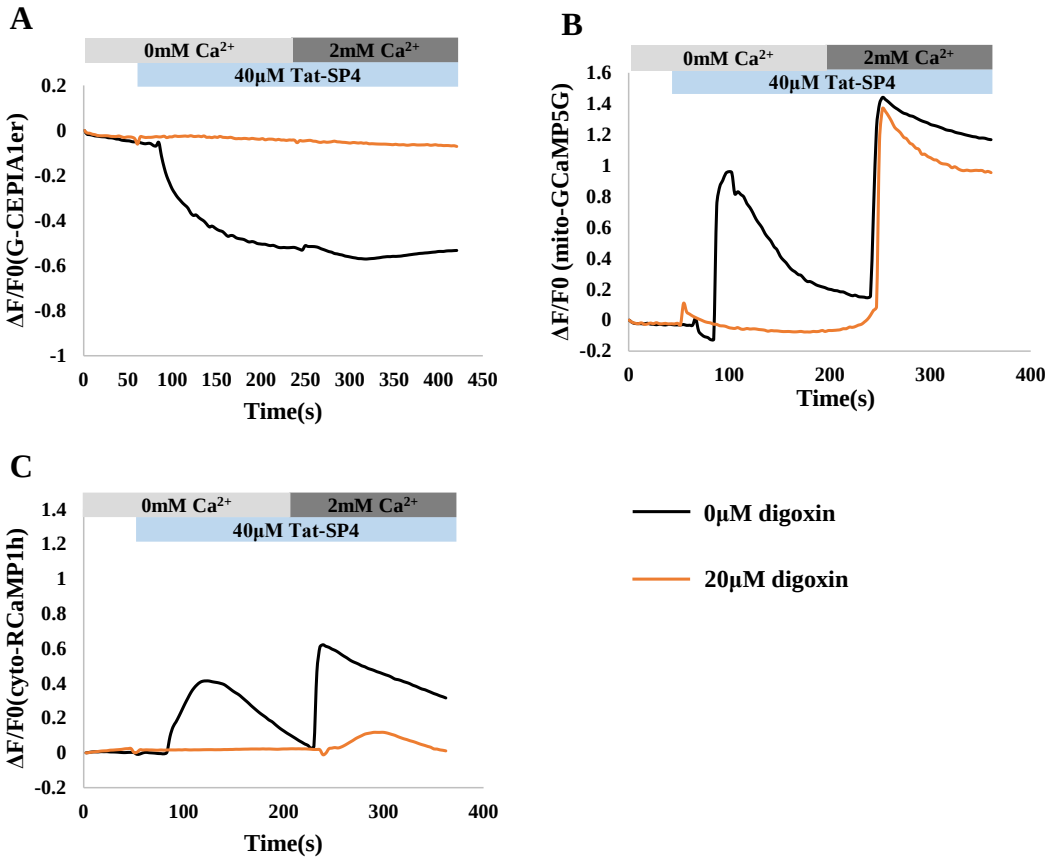

Figure 4.21 The effect of digoxin against the disruption of intracellular Ca^{2+} homeostasis caused by Tat-SP4 in A549 cells in Ca^{2+}-free HBSS buffer. (A-C) Ca^{2+} dynamics in the ER **(A)**, mitochondria**(B)**, and cytosol **(C)**in response to the sequential stimulation with 40 μM Tat-SP4 and 2 mM $CaCl_2$ with or without pretreatment with 20 μM digoxin for 3.5 hours. 20 μM digoxin keep present throughout the reaction. n=15 cells. Each curve presents the real-time Ca^{2+} dynamic under indicated stimulations of single cell. F0 refers to the fluorescence intensity at the start of measurement and ΔF = Ft–F0, where Ft refers to the fluorescence intensity at time t.

Similar results were obtained in SHP-77 cells. In absence of extracellular Ca^{2+}, when SHP-77 cells were challenged by Tat-SP4 at 10 μM, the Ca^{2+} level in ER was slightly reduced (Figure 4.22A). Meanwhile, Tat-SP4 also led to increase in mitochondrial Ca^{2+} levels (Figure 4.22B) and cytosolic Ca^{2+} levels (Figure 4.22C), and then decline back to baseline level. Subsequent addition of 2 mM $CaCl_2$ caused a further sharp and notable increase in both mitochondrial Ca^{2+} level (Figure 4.22B) and cytosolic Ca^{2+} levels (Figure 4.22C) but decreased the Ca^{2+} level in ER (Figure 4.22A). Pretreatment with digoxin for 3.5 hours totally prevent the reduction of Ca^{2+} level in ER (Figure 4.22A) as well as increase in mitochondrial Ca^{2+} level (Figure 4.22B) and cytosolic Ca^{2+} level (Figure 4.22C) when SHP-77 cells were challenged by Tat-SP4 or Ca^{2+} at 2 mM.

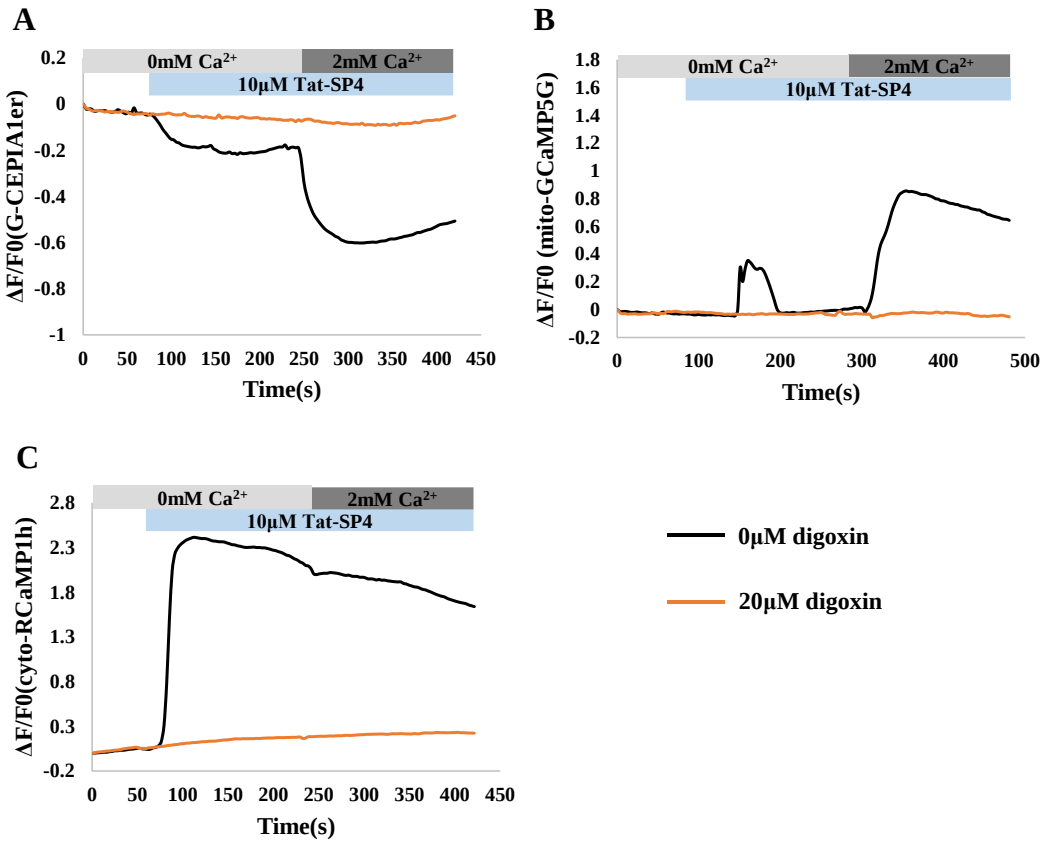

Figure 4.22 The effect of digoxin against the disruption of intracellular Ca^{2+} homeostasis caused by Tat-SP4 in SHP-77 cells in Ca^{2+}-free HBSS buffer. (A-C) Ca^{2+} dynamics in the ER **(A)**, mitochondria**(B)**, and cytosol **(C)**in response to the sequential stimulation with 10 μM Tat-SP4 and 2 mM $CaCl_2$ with or without pretreatment with 20 μM digoxin for 3.5 hours. 20 μM digoxin keep present throughout the reaction. n=15 cells. Each curve presents the real-time Ca^{2+} dynamic under indicated stimulations of single cell. F0 refers to the fluorescence intensity at the start of measurement and ΔF = Ft–F0, where Ft refers to the fluorescence intensity at time t.

In presence of 1.2 mM extracellular $CaCl_2$, 40 μM Tat-SP4 stimulation reduced the Ca^{2+} level in ER in A549 cells (Figure 4.23A). Meanwhile, when A549 cells were stimulated by 40 μM Tat-SP4, mitochondrial Ca^{2+} level and cytosolic Ca^{2+} level was increased and are maintained at high level (Figure 4.23B&C). Subsequent addition of 2 mM $CaCl_2$ didn't trigger further increase in mitochondrial Ca^{2+} level and cytosolic Ca^{2+} level (Figure 4.23B&C) but further decreased Ca^{2+} level in ER (Figure 4.23A). When A549 cells were pretreated with digoxin for 3.5 hours, the Ca^{2+} level in ER was not changed significantly by Tat-SP4 stimulation (Figure 4.23A). Unlike in the absence of extracellular Ca^{2+}, pretreatment with digoxin for 3.5 hours couldn't totally suppress the Ca^{2+} level increase in mitochondria and cytosol when A549 cells were challenged by Tat-SP4 (Figure 4.23B&C).

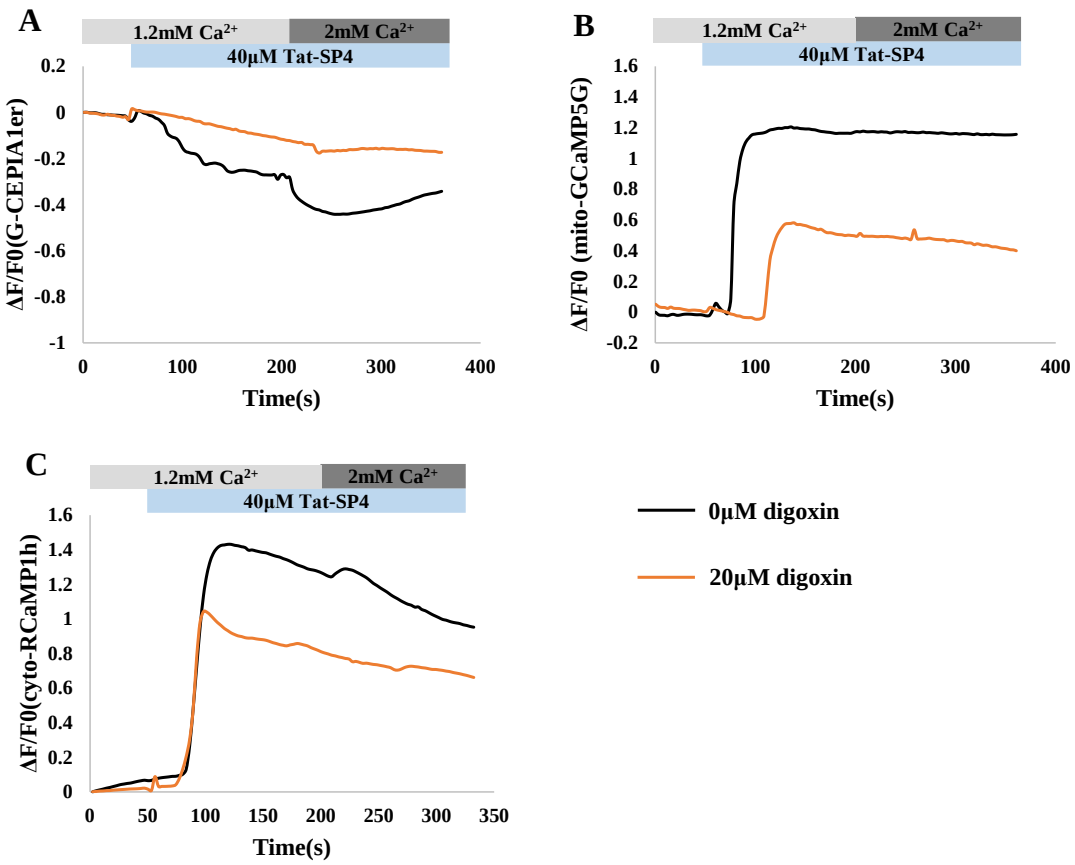

Figure 4.23 The effect of digoxin against the disruption of intracellular Ca^{2+} homeostasis caused by Tat-SP4 in A549 in HBSS buffer containing 1.2 mM Ca^{2+}. **(A-C)** Ca^{2+} dynamics in the ER **(A)**, mitochondria**(B)**, and cytosol **(C)**in response to the sequential stimulation with 40 μM Tat-SP4 and 2 mM $CaCl_2$ with or without pretreatment with 20 μM digoxin for 3.5 hours. 20 μM digoxin keep present throughout the reaction. n=15 cells. Each curve presents the real-time Ca^{2+} dynamic under indicated stimulations of single cell. F0 refers to the fluorescence intensity at the start of measurement and ΔF = Ft–F0, where Ft refers to the fluorescence intensity at time t.

Similar results were obtained in SHP-77 cells. In presence of 1.2 mM extracellular $CaCl_2$, when SHP-77 cells were challenged by Tat-SP4 at 10 μM, the Ca^{2+} level in ER decreased significantly (Figure 4.24A). The results also showed that Tat-SP4 led to increase in mitochondrial Ca^{2+} levels (Figure 4.24B) and cytosolic (Figure 4.24C) Ca^{2+} levels until saturation of Ca^{2+} level, so subsequent addition of 2 mM $CaCl_2$ didn't trigger a further increase in either mitochondrial Ca^{2+} levels (Figure 4.24B) or cytosolic (Figure 4.24C) Ca^{2+} levels. When SHP-77 cells were pretreated with digoxin for 3.5 hours, Ca^{2+} level in ER was not changed upon sequential treatment of Tat-SP4 and $CaCl_2$(Figure 4.23B). When SHP-77 cells were pretreated with digoxin for 3.5 hours, Tat-SP4 didn't induce any obvious dynamic on Ca^{2+} levels in ER (Figure 4.24A), mitochondria (Figure 4.24B), or cytosol (Figure 4.24C).

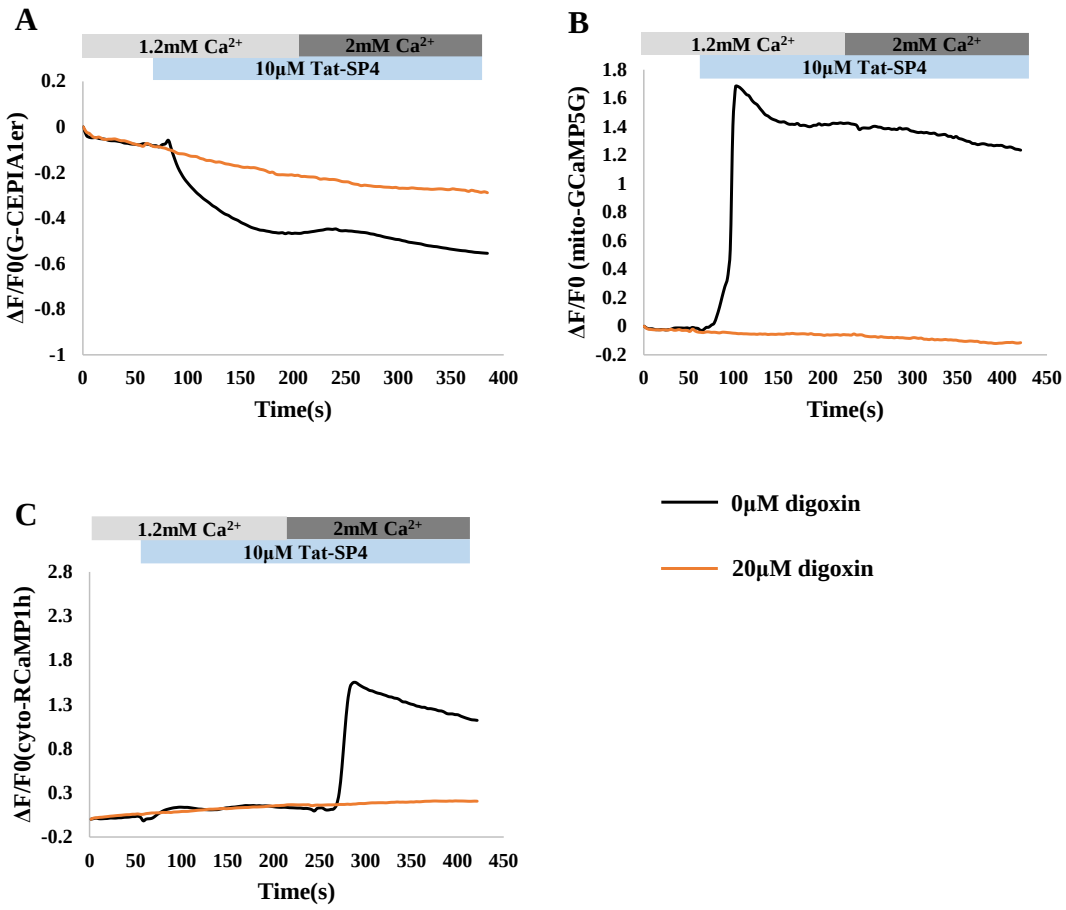

Figure 4.24 The effect of digoxin against the disruption of intracellular Ca^{2+} homeostasis caused by Tat-SP4 in SHP-77 cells in HBSS buffer containing 1.2 mM Ca^{2+}. **(A-C)** Ca^{2+} dynamics in the ER **(A)**, mitochondria**(B)**, and cytosol **(C)**in response to the sequential stimulation with 10 μM Tat-SP4 and 2 mM $CaCl_2$ with or without pretreatment with 20 μM digoxin for 3.5 hours. 20 μM digoxin keep present throughout the reaction. n=30 cells. Each curve presents the real-time Ca^{2+} dynamic under indicated stimulations of single cell. F0 refers to the fluorescence intensity at the start of measurement and ΔF = Ft–F0, where Ft refers to the fluorescence intensity at time t.

In summary, Tat-SP4 could triggered a release of Ca^{2+} from ER. IP3R is one of the key proteins that regulate Ca^{2+} released from ER, and it is to be investigate whether IP3R is a potential target of Tat-SP4. Ca^{2+} released from ER leads to an increase in both mitochondrial and cytosolic Ca^{2+} level. After Tat-SP4 treatment, extracellular Ca^{2+} induces significant Ca^{2+} uptake into mitochondria and cytosol, which may be a cytoprotective mechanism against depolarization of plasma membrane potential caused by the entry of Tat-SP4. Tat-SP4 contains a cationic CPP, and it may affect plasma membrane potential. To restore the plasma membrane potential to a normal range, cells will uptake Ca^{2+} from extracellular through some voltage dependent ion channels. Furthermore, digoxin can suppress the disruption of intracellular Ca^{2+} storage induced by Tat-SP4. Digoxin is a Na^{+},K^{+}-ATPase antagonists and may help to stabilize plasma membrane potential through inhibiting transporting Na^{+} and K^{+} when cells are challenged by Tat-SP4. At current stage of my project, the exact molecular targets involved in Tat-SP4 induced intracellular Ca^{2+} disruption is not clear and will be investigated in future studies.

4.6 Tat-SP4 induced cell death is sensitive to extracellular Ca^{2+} concentration

Our results suggested that Tat-SP4 could disrupt intracellular Ca^{2+} homeostasis in lung cancer cells, and digoxin and extracellular Ca^{2+} could reverse Ca^{2+} influx. It is well

known that Ca^{2+} signaling is involved in various cell death pathway, such as apoptosis, necrosis and autophagic cell death((Zhivotovsky and Orrenius 2011)). We would investigate whether extracellular Ca^{2+} plays a role in cell death caused by Tat-SP4.

4.6.1 Extracellular Ca^{2+} concentration affects cytotoxicity of Tat-SP4 on lung cancer cells

I accidentally found that NSCLC cell lines become more sensitive to Tat-SP4 in RMPI-1640 than in DMEM medium. In literatures, both A549 cells and H1975 cells are cultured in DMEM or RPMI-1640 medium. These two kinds of cell culture medium work for most types of mammalian cells and are the most used mediums. At first, A549 cells and H1975 cells were cultured in DMEM medium supplanted with 10% FBS. IC50 of Tat-SP4 tested with DMEM medium is 50.5 μM, 44.37 μM and 47.54 μM for A549, H1975 and H1993 cells respectively (Figure 4.25A, B and C). Another batch of A549, H1975 and H1993 cells were cultured in RPMI-1640 medium supplanted with 10% FBS. IC50 of Tat-SP4 tested with RPMI-1640 medium is 23.53 μM, 20.36 μM and 29.35 μM for A549, H1975 and H1993 cells respectively (Figure 4.25A, B and C), which is about twice lower than the IC50 test in DMEM medium. NSCLC cell lines become more sensitive to Tat-SP4 in RMPI-1640 than in DMEM medium (Figure 4.25D).

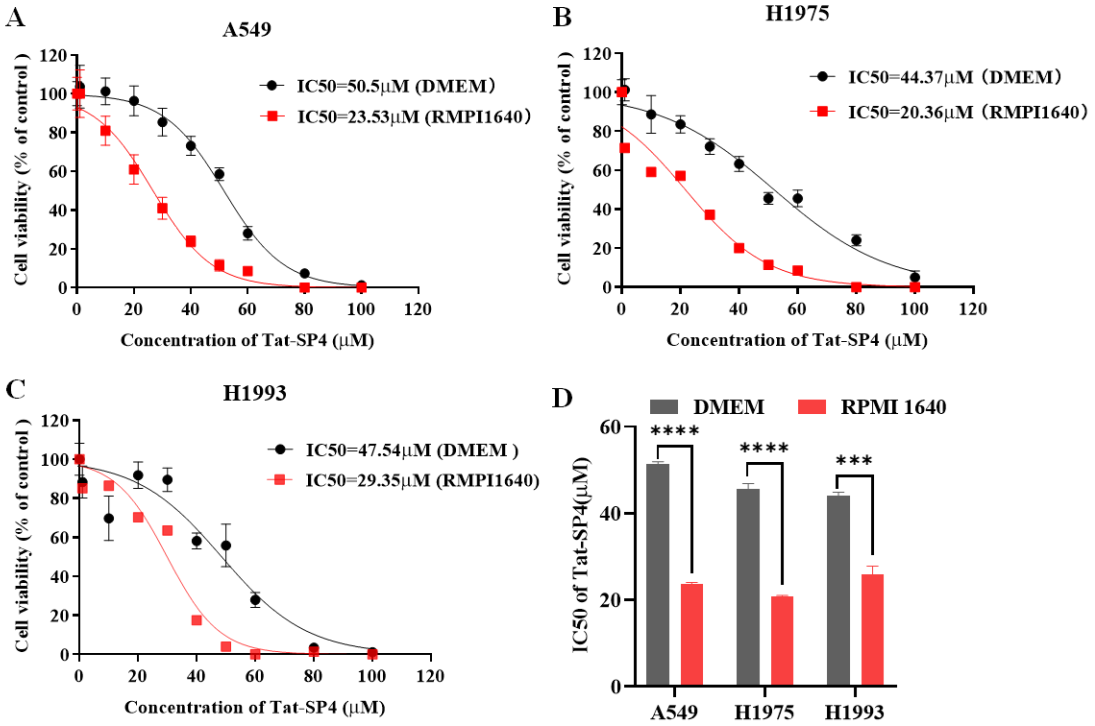

Figure 4.25 IC50 of Tat-SP4 is different in DMEM media and RPMI-1640 media. **(A-C)** lung cancer cells A549**(A)**, H1975**(B)** and H1993**(C)** were cultured in DMEM or RPMI-1640 media and treated with Tat-SP4 for 24 hours. Cell viability was assessed by Trypan Blue exclusion assay. When cells were cultured in RPMI-1640 media, they became more sensitive to Tat-SP4 compared to those cultured in DMEM. **(D)**Difference on IC50 of Tat-SP4 for a cell line cultured in DMEM media and RPMI-1640 media. Data represents mean ± SEM of three replicates. *P<0.05, **P<0.01, ***P< 0.001, ****P<0.0001; unpaired t-test.

The Ca^{2+} concentration in DMEM medium (1.8 mM $CaCl_2$) is 5 times higher than that in RPMI 1640 medium (0.4 mM Ca $(NO_3)_2$). If extracellular $CaCl_2$ is the key factor affecting the sensitivity of lung cancer cells to Tat-SP4, the protective effect of $CaCl_2$ on cell death induced by Tat-SP4 should be related to its working concentration. As shown in Figure 4.26A, in RPMI 1640 medium, the cell viability of A549 cells that were treated with Tat-SP4 at 30 μM was about 50% of the cell viability in the control group. When A549 cells were treated with Tat-SP4 at 30 μM and indicated concertation

of $CaCl_2$ together, the cell viability was increased compared with the cell viability in 30 μM Tat-SP4 only group (Figure 4.26A). $CaCl_2$ at 1.8 mM showed most protective effect against cell death caused by Tat-SP4. However, higher concentrations of $CaCl_2$ exerted some stress on cells. Therefore, within concentration of 1.8mM, $CaCl_2$ could rescue cell death caused by Tat-SP4 in a dosage-dependent manner. Next, I measured the IC50 value of Tat-SP4 with or without 1.8mM $CaCl_2$ in different lung cancer cell lines in RPMI-1640 medium. As shown in Figure 4.26B-E, in the presence of extracellular $CaCl_2$, IC50 of Tat-SP4 was higher than that measured in non-optimized RPMI1640 medium, indicating that $CaCl_2$ may have a cell-rescuing effect on Tat-SP4 induced cell death.

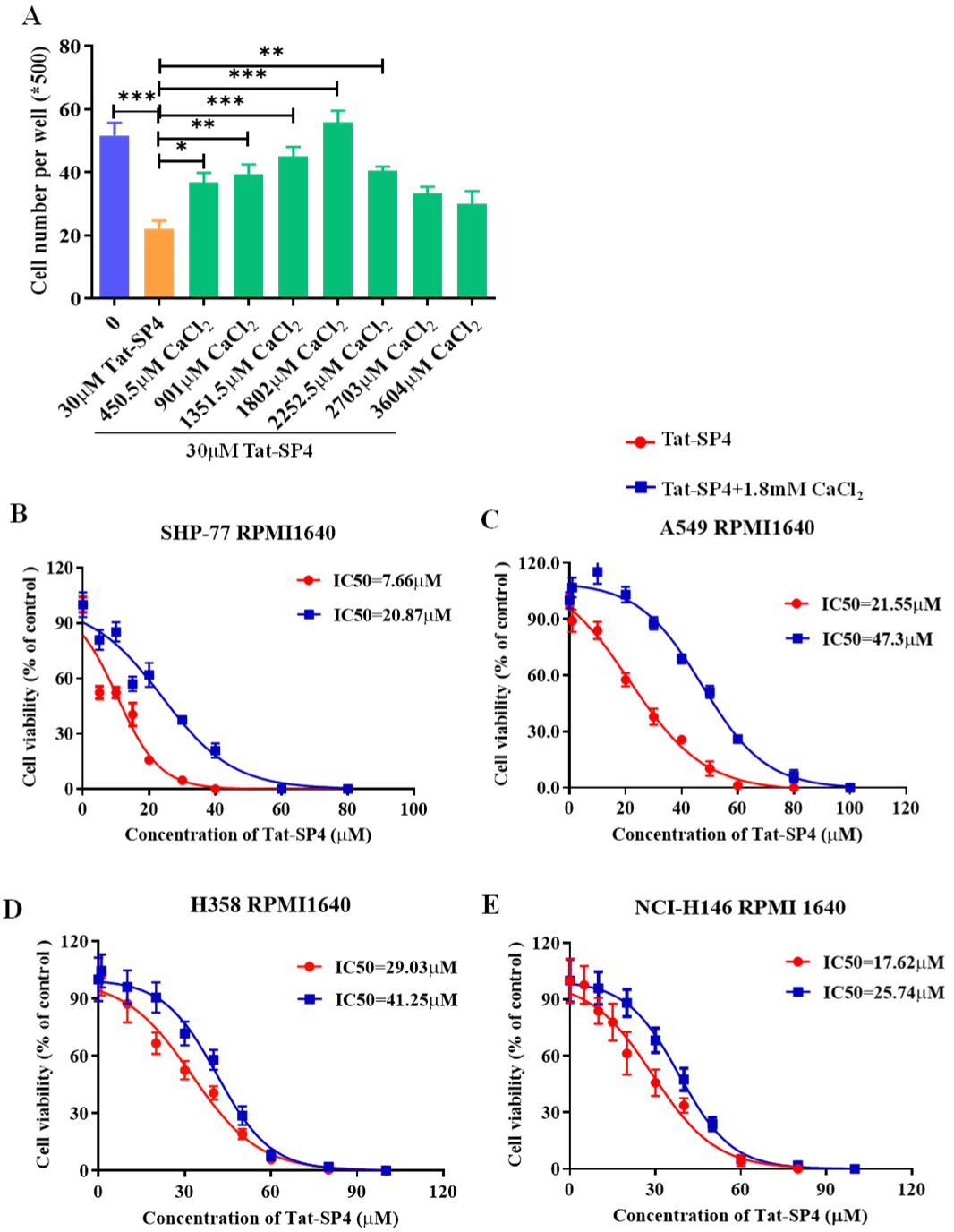

Figure 4.26 Extracellular $CaCl_2$ rescued lung cancer cell death caused by Tat-SP4. (A) A549 cells were treated with 30 μM Tat-SP4 for 24 hours in the presence or absence of different concentrations of $CaCl_2$. Cell viability was assessed by Trypan Blue exclusion assay. **(B-E)** IC50 value of Tat-SP4 with or without 1.8 mM $CaCl_2$ in different lung cancer cell lines in RPMI-1640 medium. Cells were treated with increasing concentrations of Tat-SP4 with or without 1.8 mM $CaCl_2$ for 24 hours. Cell viability was measured by trypan blue exclusion assay. Data represents mean ± SEM of three replicates. *P<0.05, **P<0.01, ***P< 0.001, ****P<0.0001; unpaired t-test.

4.6.2 Extracellular Ca^{2+} attenuates Tat-SP4-induced depolarization of MMP and impairment of OXPHOS.

Our results have proved that extracellular $CaCl_2$ rescued lung cancer cell death induced by Tat-SP4 and Tat-SP4-induced cell death was associated with depolarization of MMP and impairment of mitochondrial OXPHOS. First, the effect of $CaCl_2$ on impairment of mitochondrial respiration caused by Tat-SP4 was assessed by the Agilent Seahorse XF Analyzer in A549 and SHP-77 cells, in the presence or absence of 1.8Mm $CaCl_2$. In A549 cells, addition of 40 μM Tat-SP4 led to slightly decreased basal OCR and significantly decreased maximum OCR (Figure 4.27 A&B). And both basal and stressed ECAR level were significantly reduced by Tat-SP4 treatment (Figure 4.27 C). In the presence of 1.8 mM $CaCl_2$, when A549 cells were challenged by Tat-SP4, the basal OCR level under Tat-SP4 stimulation was comparable to that of in absence of 1.8 mM $CaCl_2$ (Figure 4.27 A&B), however the maximum OCR was rescued (Figure 4.27 A&B). The Figure 27 C showed that ECAR was suppressed with or without calcium. Similar results were obtained in SHP-77 cells. When SHP-77 cells were stimulated by Tat-SP4 at 10 μM, basal OCR and maximum OCR as well as stressed ECAR were significantly suppressed (Figure 4.27 D, E&F). $CaCl_2$ rescued the reduction of maximum OCR but not basal OCR or stressed ECAR (Figure 4.27 D, E&F). These data suggested that $CaCl_2$ showed a protective effect against Tat-SP4- induced mitochondrial respiratory damage but not against Tat-SP4-induced glycolysis damage.

Second, I assessed whether $CaCl_2$ has any protective effect on MMP against Tat-

SP4 treatment. The MMP was measured using flow cytometer with Tat-SP4 treatment in A549 cells, in the presence or absence of 1.8 mM $CaCl_2$. As shown in Figure 4.27G, in the presence of 1.8 mM $CaCl_2$, MMP was reduced less by Tat-SP4 treatment, suggesting that $CaCl_2$ attenuated Tat-SP4- induced mitochondrial depolarization.

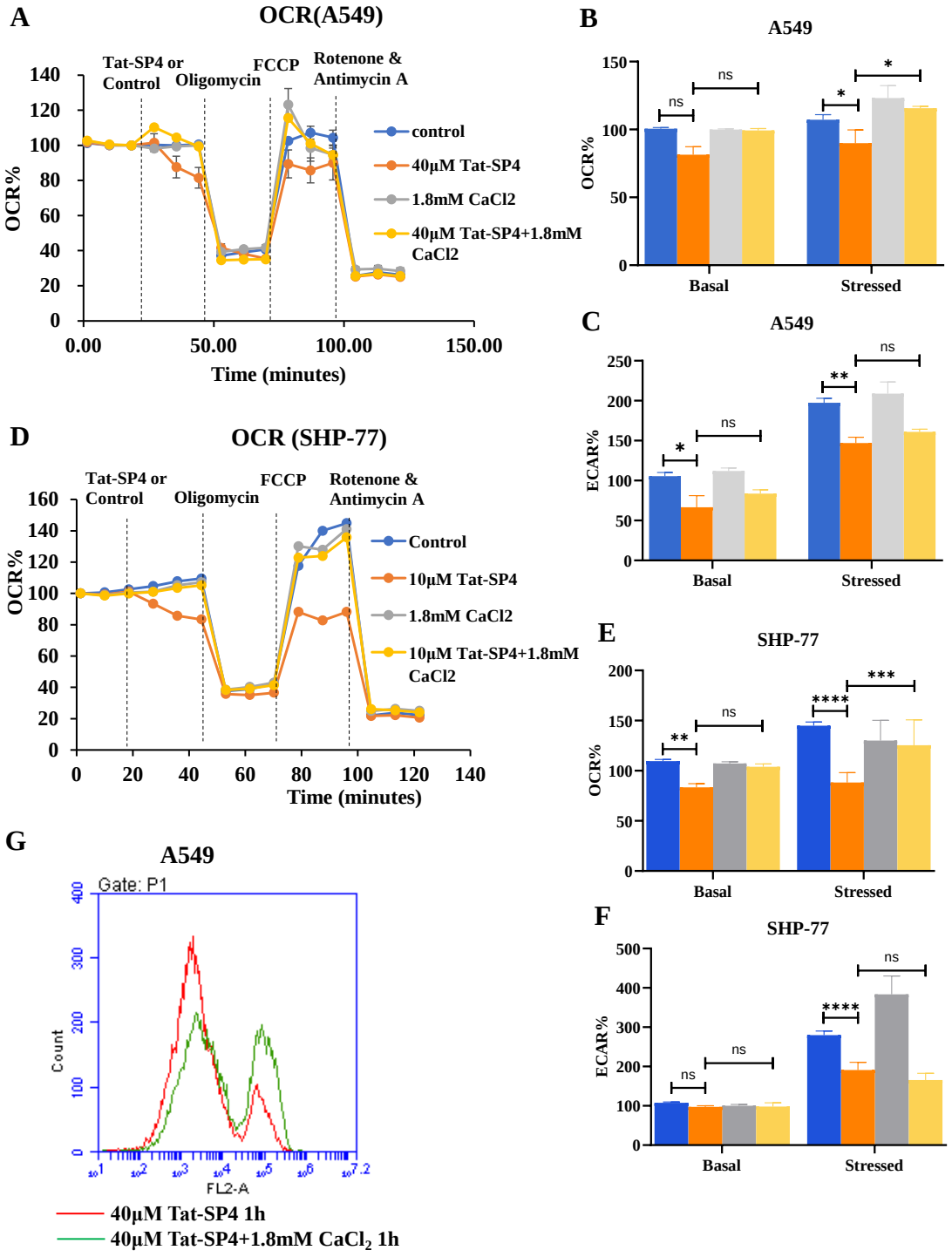

Figure 4.27 Extracellular calcium attenuates Tat-SP4-induced mitochondrial depolarization and OXPHOS inhibition. (A&D) OCR with Tat-SP4 treatment was assessed in A549**(A)** and SHP-77**(D)** cells, in the presence or absence of 1.8 mM $CaCl_2$. **(B&D)** OCR is presented before (baseline) oligomycin addition in A549**(B)** and SHP-77**(D)** cells. **(E&F)** ECAR is represented after (stressed) FCCP addition in A549**(E)**, and SHP-77**(F)** cells. **(G)** Flow cytometry plot of MMP with Tat-SP4 treatment in A549 cells, in the presence or absence of 1.8 mM $CaCl_2$. Data represents mean ± SEM of three replicates. *P<0.05, **P<0.01, ***P< 0.001, ****P<0.0001; unpaired t-test.

In summary, cell death caused by Tat-SP4 could be rescued when extracellular Ca^{2+} concentration was raised. Meanwhile, extracellular Ca^{2+} showed protective effect against Tat-SP4 induced depolarization of MMP and impairment of OXPHOS.

4.7 The cellular uptake mechanism of Tat-SP4

4.7.1 The delivery efficacy of Rhod-SP4 is energy- and time-dependent

Rhod-SP4 was developed to investigate the intracellular delivery of Tat-SP4. Rhodamine fluorophore was applied to label Tat-SP4, which makes it is possible to investigate intracellular delivery of Tat-SP4 by flow cytometry assay and confocal imaging assay. The cellular uptake mechanism of CPP cargos can be classified into direct translocation and endocytic pathways. Direct translocation is energy independent, while endocytic pathways are energy dependent.

At first, I assessed the delivery efficacy of Rhod-SP4 at 4℃, room temperature and 37℃ by flow cytometer to check whether the delivery efficacy of Tat-SP4 is energy independent or not (Figure 4.28 A-D). The signal of Rhod-SP4 in cells is strongest at

37℃ and the signal of Rhod-SP4 decreased as temperature decreased, indicating that the delivery efficacy of Rhod-SP4 is energy dependent. Next, I examined the delivery efficacy of Rhod-SP4 at indicated time points to investigate whether the delivery efficacy of Rhod-SP4 is time-dependent. At both 4℃ and 37℃, the signal of Rhod-SP4 was increased in a time-dependent manner, suggesting that delivery efficacy of Rhod-SP4 is time-dependent (Figure 4.28E).

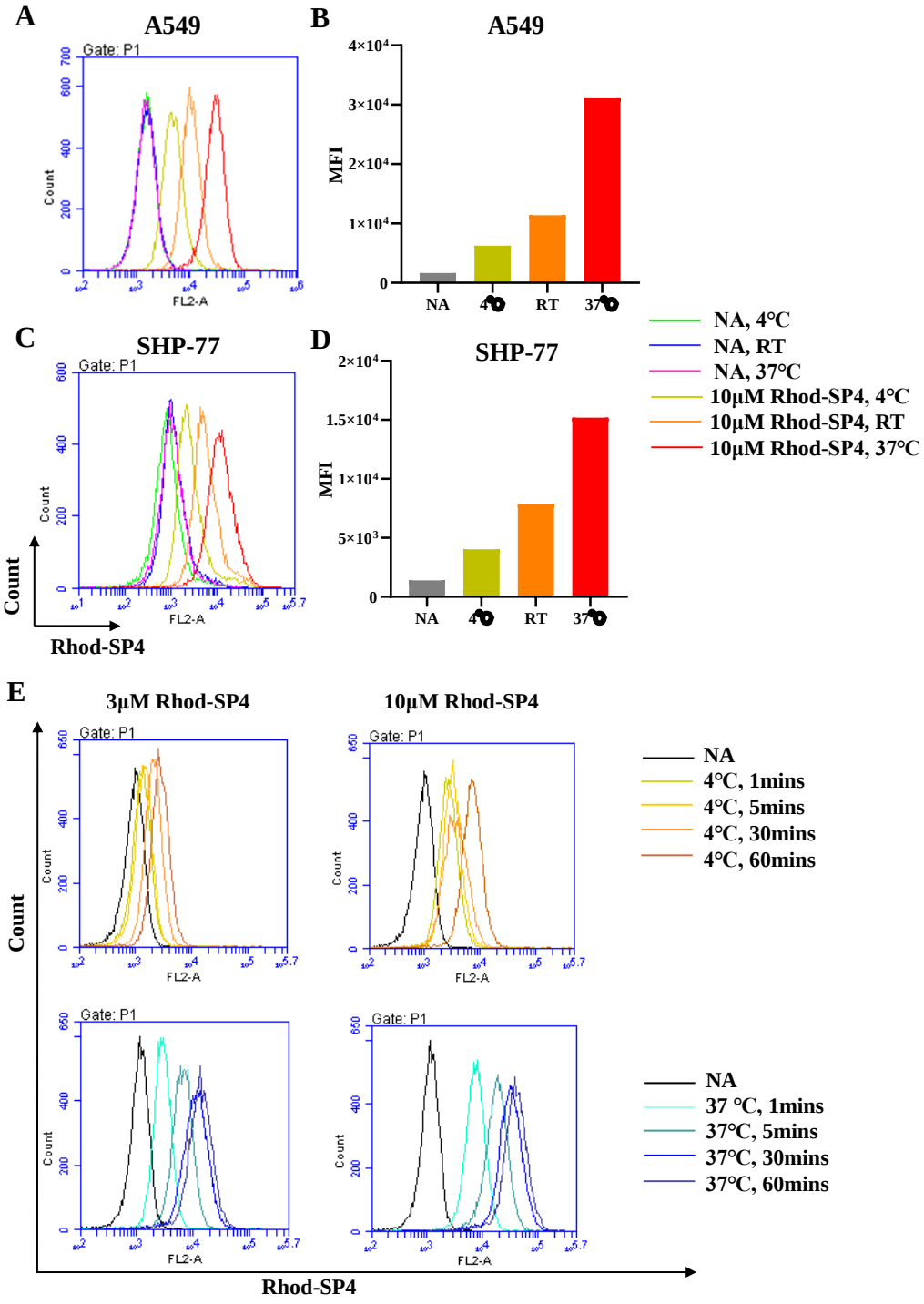

Figure 4.28. The delivery efficacy of Rhod-SP4 is energy- and time-dependent. **(A and C)** Representative flow cytometry plot of A549 and SHP-77 cells stained with Rhod-SP4 at 10 μM at 4℃, room temperature and 37℃ for an hour, respectively. Investigate whether the delivery efficacy of Rhod-SP4 is energy- dependent. **(B and D)** Mean fluorescence intensity of Rhod-SP4 from **(A)** and **(B)**, respectively. **(E)** Representative flow cytometry plot of SHP-77 cells stained with Rhod-SP4 for various incubation length (1 mins, 5 mins, 30 mins and 60 mins). Investigate whether the delivery efficacy of Rhod-SP4 is time-dependent.

4.7.2 The cellular uptake of Rhod-SP4 is mediated by macropinocytosis pathway

It was reported that cationic CPPs interact with membrane constituents, such as the glycosaminoglycans, to favor their translocation across the cell membrane(Ziegler 2008). Therefore, I investigate whether cellular uptake mechanism of Rhod-SP4 is mediated by glycosaminoglycans. In the presence of heparin, a competitive inhibitor of heparan sulphate, the signal of Rhod-SP4 didn't decrease (Figure 4.29A-D), suggesting that the cellular uptake mechanism of Rhod-SP4 is independent with glycosaminoglycans. Next, I assessed the effect of various endocytosis inhibitors on the delivery efficacy of Rhod-SP4. Methyl-beta cyclodextrin (MβCD) is an inhibitor of lipid raft-mediated endocytosis. The signal of Rhod-SP4 was not changed by pretreatment of cells with MβCD (Figure 4.29A-D), suggesting that the cellular uptake of Rhod-SP4 is independent of lipid raft-mediated endocytosis. Amiloride is an inhibitor of macropinocytosis. The signal of Rhod-SP4 was significantly reduced by pretreatment of cells with amiloride (Figure 4.29A-D), suggesting that the cellular uptake mechanism of Rhod-SP4 is mediated by a macropinocytosis pathway. Taken these data together, the cell uptake mechanism of Rhod-SP4 is energy dependent and is mediated by macropinocytosis pathway.

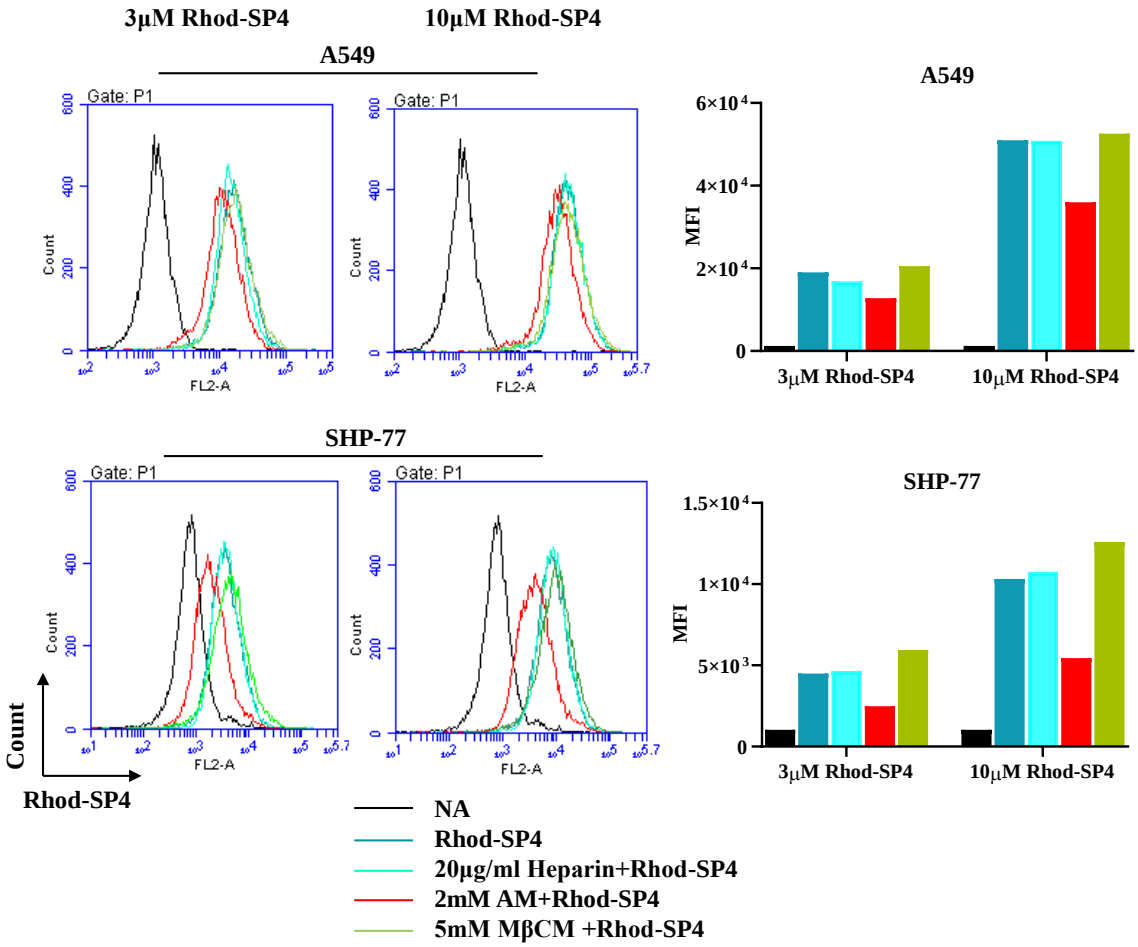

Figure 4.29. The cellular uptake of Rhod-SP4 is mediated by micropinocytosis pathway. (A and C) Representative flow cytometry plot of A549 and SHP-77 cells stained with Rhod-SP4 at 3 μM or 10 μM at 37°C for an hour, in the presence or absence of various inhibitors. AM, Amiloride; MβCD, Methyl-beta cyclodextrin. Cells were first pretreated with different inhibitors for 30 mins, followed by staining with Rhod-SP4 at 3 μM or 10 μM. **(B and D)** Mean fluorescence intensity of Rhod-SP4 from **(A)** and **(B)**, respectively.

4.8 Assessment of the anti-proliferative efficacy of Beclin1-targeting peptides in animal-based lung cancer model

4.8.1 Tat-SP4 shows potent anti-proliferative efficacy in SHP-77 xenograft model

The *in vivo* anti-proliferative efficacy of Tat-SP4 was investigate on SHP-77 xenograft model. SHP-77 cell line was most sensitive to Tat-SP4 among the lung cancer cell lines I tested, so SHP-77 cell line was used for xenograft model to study the anti-proliferative efficacy of Tat-SP4 *in vivo.* SHP-77 cells were implanted subcutaneously on 5-week-old male nude mice in a number of 5×10^6. The administration of Tat-SP4 was started when tumor volume reached 60 mm^3 with a dosage of 40 mg/kg via daily intraperitoneal (i.p.) injection. PBS was injected to mice in control group as placebo. The anti-proliferative efficacy of Tat-SP4 *in vivo* was evaluated by measuring tumor volume. After 34 days post-treatment, the tumors were harvested. As shown in Figure 4.30A, Tat-SP4 inhibited tumor growth remarkably as compared with PBS. The tumor weight in Tat-SP4 treatment group was significantly reduced (Figure 4.30B). Figure 4.30C illustrated that the gradual increase in body weight of mice in treatment group was consistent with that in control group. Besides, there were no obvious color or morphological abnormalities in the organs.

In summary, the animal experiment in vivo showed that Tat-SP4 significant anti-proliferative efficacy in SHP-77 cell-driven xenograft model with little toxic side effect.

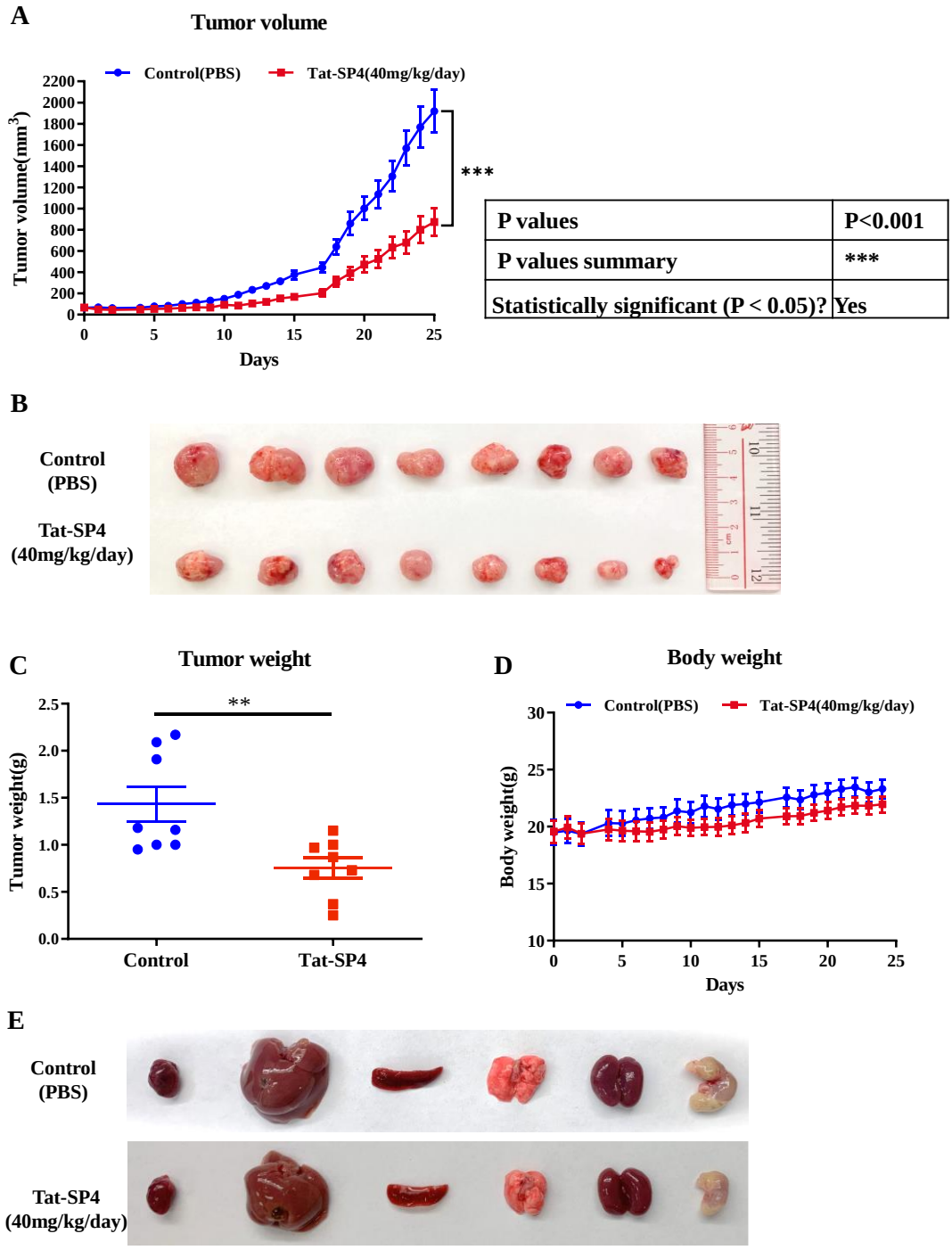

Figure 4.30 The anti-proliferative efficacy of Tat-SP4 in SHP-77 xenograft model. **(A)** SHP-77 cells were subcutaneously injected into nude mice in a number of 5×10^6.The administration of 40 mg/kg Tat-SP4 (treatment) or PBS (control) was started when the tumor volume reached about 60 mm^3. The tumor volume was recorded every other day. The tumor volume was defined as $width^2 \times length/2$.Data represents mean ± SEM, n=8; *P<0.05, **P<0.01, ***P< 0.001, ****P<0.0001; Two-way ANOVA. **(B)** Image of tumors at the end of time point from control and Tat-SP4 treatment groups. **(C)**Tumor weight on Day 25. Data represents mean ± SEM, n=8; *P<0.05, **P<0.01, ***P< 0.001, ****P<0.0001; unpaired t-test. **(D)** The changes of mice body weight during treatment for each group. Two-way ANOVA. **(E)** The samples of vital organs.

5. Discussion and future study

Autophagy is regarded as a double-edged sword for cancer treatment and the role of autophagy in cancer depends on the cancer type and stage of cancer. Autophagy plays a different role in cancer treatment, and the correct use of autophagy can effectively improve anti-tumor efficacy and suppress tumor recurrence. The treatment by modulating autophagy of tumor cells is a hot topic in tumor therapy research today. Beclin1 has an important role in the regulation of autophagy. Beclin1 acts together with other factors, such as Atg14L, UVRAG, Rubicon, and Ambra1, to regulate lipid kinase Vps34 protein, promoting the formation of Beclin1-Vps34/Vps15 core complex, thus regulating autophagic activity. (Kang, Zeh et al. 2011). Atg14L and UVRAG bind to Beclin1 coiled-coil domains in a mutually exclusive manner(Li, He et al. 2012). A previous study of our lab showed that Beclin1 coiled-coil domain could form readily dissociable homodimer, which facilitated ATG14 and UVRAG binding to the Beclin1 coiled-coil domain (Li, He et al. 2012). Although Beclin1 has long been identified as a tumor suppressor, it is rare and challenging to modulate Beclin1 or the Beclin1-mediated autophagy activity for cancer therapy. Our study is the first to design stapled peptide that disrupts the self-association of Beclin1 and promotes the formation of Beclin1-Atg14L or -UVRAG complex to regulate the autophagy process.

We designed a group of Beclin1-derived stapled peptides targeting at the coiled-

coil domain of Beclin1 based on the previous structural study of Beclin1–UVRAG coiled-coil complex in our lab. Our *in vitro* study showed that the Beclin1-derived stapled peptides not only bound to Beclin1 with strong binding affinity but also significantly suppressed the self-association of Beclin1 coiled-coil domain and promoted the formation of Beclin1–Atg14L/UVRAG complex. Our data shows that Tat-SP4 upregulated autophagy activity at moderate concentration in lung cancer cell lines. Endosomal trafficking, another membrane-mediated transport process, was also tightly regulated by Beclin1-UVRAG-Vps34 complex II. Therefore, it was expected that Tat-SP4 remarkably promoted the endolysosomal degradation oncogenic receptors including EGFR and c-Met, while inhibiting their downstream signaling transduction.

Furthermore, Tat-SP4 shows the potential to synergize with TKIs like Erlotinib to overcome drug resistance in NSCLC. Targeted therapy focusing on tyrosine kinase receptors has achieved breakthrough in treatment of NSCLC in the past decade. Although they exhibit good initial therapeutic effect and fewer side effects, acquired drug resistance always happen because of mutation in multiple driven oncogenes, such as EGFR, c-Met, and HER2, which is a big challenge for the development of targeted therapy(Kobayashi, Boggon et al. 2005). Our novel designed Tat-SP4 significantly promoted endolysosomal degradation of oncogenic receptors on plasma membrane, indicating that Tat-SP4 had the potential to synergize with TKIs like Erlotinib to overcome drug resistance in NSCLC. Erlotinib is the first generation of EGFR-TKIs

and is reported to be effective in patients with EGFR-sensitive mutations(Kobayashi, Boggon et al. 2005). A549 is EGFR-WT NSCLC cell line and H1975 harbors the sensitive L858R and resistant T790M mutations of EGFR. Indeed, the cell-based results showed that Tat-SP4 alone demonstrated moderate anti-proliferative efficacy on different subtypes of lung cancer. Erlotinib was chosen as a candidate to combine with Tat-SP4, and the interesting results showed that the combined administration of Tat-SP4 and Erlotinib at moderate concentration exhibited synergistic effect in inhibiting the proliferation of A549 and H1975 cells. This data is highly encouraging and suggests that our Beclin1-targeting stapled peptides, through its distinct mechanism, may synergize with TKIs like Erlotinib to enhance their efficacy, particularly for NSCLC subtypes refractory to current regiments. The exact molecular mechanism of the synergistic effect of combined administration of Tat-SP4 and Erlotinib will be investigated in future studies.

For mechanistic studies of Tat-SP4-caused cell death, our findings showed that Tat-SP4-induced necrotic cell death could be rescued by a cardiac glycoside, digoxin, but not other inhibitors of other programmed cell death. Besides, necrotic cell death induced by Tat-SP4 in lung cancer cells (A549 cells) presented some morphological features similar to that of autosis, including perinuclear accumulation of numerous vacuoles, shrinkage of nucleus, rupture of plasma membrane and extracellular extrusion of cytoplasmic contents, continuous adhesion to the culture dish, suggesting that Tat-

SP4 induces necrotic cell death through an autosis-related pathway.

Meanwhile, Tat-SP4 induced necrotic cell death was accompanied by mitochondrial dysfunction including depolarization of mitochondria membrane potential, increased ROS level and reduction in OXPHOS activity and mPTP opening. TAT, a cationic CPP was added at the N-terminal to improve cell penetration, so it is possible that Tat-SP4 may associate with membrane-bound organelles due to non-specific binding to negatively charged phospholipids through electrostatic interaction (Xie, Bi et al. 2020). Although TAT sequence didn't show significant cytotoxicity, its positive charge residues was a potential threat to normal cellular physiological activity. First, direct translocation of CPPs can decrease the plasma membrane potential(Vm)(Trofimenko, Grasso et al. 2021). Vm affects many voltage-dependent ion channels, so depolarization of Vm may lead to disturbance of intracellular ion homoeostasis and even cell death. Second, positively charged Tat-SP4 is likely to be driven to mitochondria and lead to mitochondrial depolarization, which causes mitochondrial dysfunction.

Tat-SP4 also triggers a release of Ca^{2+} from ER, and an increase in mitochondrial and cytosolic Ca^{2+} level. After Tat-SP4 treatment, extracellular Ca^{2+} induces significant Ca^{2+} uptake into mitochondria and cytosol, which may be a cytoprotective mechanism against depolarization of plasma membrane potential caused by the entry of Tat-SP4.

Tat-SP4 contains a cationic CPP and it may affect plasma membrane potential. To restore the plasma membrane potential to a normal range, cells will uptake Ca^{2+} from extracellular through some voltage dependent ion channels. Furthermore, digoxin can suppress the disruption of intracellular Ca^{2+} storage induced by Tat-SP4. Digoxin is a Na^{+},K^{+}-ATPase antagonists and may help to stabilize plasma membrane potential through inhibiting transporting Na^{+} and K^{+} when cells are challenged by Tat-SP4. At current stage of my project, the exact molecular targets involved in Tat-SP4 induced intracellular Ca^{2+} disruption is not clear and will be investigated in future studies.

Since Ca^{2+} plays multiple roles in regulating ion channels, such as Ca^{2+} ATPase, Na^{+}/Ca^{2+} exchanger and K^{+}/Na^{+} -ATPase etc(Hagiwara and Byerly 1981), we wonder whether extracellular Ca^{2+} have any effect on the cell death induced by Tat-SP4. Our results show that elevating the concentration of extracellular Ca^{2+} not only can reduce lung cancer cell sensitivity to Tat-SP4, also can attenuate Tat-SP4-induced mitochondrial depolarization and impairment of OXPHOS, which may be due to extracellular Ca^{2+} help cells to stabilize plasma membrane potential when cells are stimulated by Tat-SP4. The exact molecular mechanism of both protective effect of digoxin and extracellular Ca^{2+} against Tat-SP4 in lung cancer cells will be identified in future studies.

The effect of Tat-SP4 founded in lung cancer cell models has been validated in

other cancer cell models, such as triple negative breast cancer cells, hepatocellular carcinoma cells, ovarian cancer cells and pancreatic cancer cell. Tat-SP4 also induces autophagy and endolysosomal trafficking of membrane oncogenic proteins, impairs mitochondrial function and shows potent anti-proliferative effect on triple negative breast cancer cells, hepatocellular carcinoma cells(Gao, Li et al. 2023), ovarian cancer cells(Brown, Chung et al. 2022) and pancreatic cancer cells(Li, Zhang et al. 2023). Tat-SP4-induced disruption of intracellular Ca^{2+} homeostasis is also observed in hepatocellular carcinoma cells and ovarian cancer cells. Tat-SP4 also induces triple negative breast cancer cell death through autosis and Tat-SP4 treated triple negative breast cancer cell shows morphological features of autotic cells, which has been reported in a paper that is under review. These data demonstrate that the effect of Tat-SP4 is consistent across cancer cells.

The animal assay result confirmed that Tat-SP4 had potent anti-tumor effect in lung cancer cell line driven xenograft nude mice model without obvious toxicity. This *in vivo* result suggested that high proliferative cancer cells or tumor tissues were sensitive to our stapled peptides, however, normal cells such as cardiomyocytes and neurons might be resistant to our stapled peptides since no obvious cardiotoxicity or neurotoxicity was observed in the animal assay. The sensitivity of different cell types to our stapled peptides might be related to their ability to regulate calcium signaling. It is well known that excitable cells such as cardiomyocytes and neurons are capable of

regulating high-magnitude Ca^{2+} release and uptake as part of the stimulatory signals for muscle contraction or synaptic transmission, so they may be resistant to our stapled peptides.

For future studies on our stapled peptides, the following aspects will be explored. First, I will investigate other molecular targets of Tat-SP4.Based on the mechanistic study of cell death induced by Tat-SP4, it seems that Tat-SP4 may have other targets because Tat-SP4 not only promotes autophagy and endolysosmal trafficking through interacting with Beclin1 with strong binding affinity and enhancing the formation of Beclin1-Atg14L/ UVRAG complex, but also significantly disrupts intracellular Ca^{2+} homeostasis and induces mitochondrial dysfunction. Tat-SP4 may affect plasma membrane potential because of the cationic CPP, TAT, which leads to Ca^{2+} influx. When Tat-SP4 enter cells through direct translocation or endocytosis(Xie, Bi et al. 2020), it may associate with membrane-bound organelles like ER and mitochondria due to non-specific binding to lipids since Tat-SP4 is positive charged. The potential targets may be Ca^{2+} channel regulatory protein, such as IP3R, TOM20 and Na^{+}/K^{+} ATPase. A method is to use the inhibitor of specific Ca^{2+} channels. If blocking a specific Ca^{2+} channel could prevent cell death from Tat-SP4 treatment, it means that channel is the target of Tat-SP4. However, the exact molecular processes need more effort to identify.

Second, I would like to investigate the major factors that determine the sensitivity

of different cancer model to Tat-SP4. Different cancer cells have different resting membrane potential. It was reported that cancer cells usually have a higher resting membrane potential than non-cancer cells(Kadir, Stacey et al. 2018). Our results shows that the IC50 of Tat-SP4 in normal bronchial epithelial cell (Beas-2b) is about four times higher than that in lung cancer cells. We will investigate whether resting membrane potential has some association with the sensitivity of Tat-SP4 in different cell types.

Next, I will investigate the combinative effect of Tat-SP4 and Erlotinib in NSCLC xenograft model. The synergetic effect of Tat-SP4 plus Erlotinib has been confirmed in vitro in my project. If Tat-SP4 could synergizes with Erlotinib to potently inhibit proliferation in NSCLC xenograft model, Tat-SP4 presents a new approach to inhibit EGFR orthogonal to that utilized by TKI and thus may offer possible synergy. Chemotherapy is the most traditional and widely used treatment for various types of cancer. I am also interested in investigating combinative effect of Tat-SP4 and chemotherapeutic drugs in NSCLC models.

Finally, the safety profile of our stapled peptides will be assessed in both cell- and animal-based models. The cytotoxicity of Tat-SP4 should be tested not only in multiple cell lines, including normal somatic cells and primary lung cells, but also in BALB/c mice for acute toxicity. Additionally, hematological tests and histological structural

analysis of vital organs will be carried out at the end of animal experiment to evaluate the cytotoxicity of Tat-SP4.

In summary, the work of my PhD study has provided a design strategy of stapled peptides targeting to Beclin1 coiled coil domain to enhance autophagy activity and endolysosomal trafficking. Our Beclin1-targeting stapled peptide shows potent anti-proliferative efficacy in lung cancer models, as well as the potential to synergize with TKIs like Erlotinib to overcome drug resistance in NSCLC. The mechanistic studies demonstrates that Tat-SP4 induces necrotic cell death that is accompanied by mitochondrial dysfunction and disruption of intracellular Ca^{2+} homeostasis. The finding of my project not only provides a new strategy to target Beclin1 to regulate autophagy, but also suggests that our Beclin1-targeting stapled peptides, through its distinct mechanism, may synergize with TKIs like Erlotinib to enhance their efficacy, particularly for NSCLC subtypes refractory to current regiments. Since SCLC cancer cells is very sensitive to Tat-SP4, our designed peptides may also serve as potential therapeutic candidates against SCLC by targeting this vulnerability.

References

Introduction to Lung Cancer and Mesothelioma. Lung Cancer**:** 1-14.

(2012). "Comprehensive genomic characterization of squamous cell lung cancers." Nature **489**(7417): 519-525.

Abedin, M., D. Wang, M. McDonnell, U. Lehmann and A. Kelekar (2007). "Autophagy delays apoptotic death in breast cancer cells following DNA damage." Cell Death & Differentiation **14**(3): 500-510.

Aita, V. M., X. H. Liang, V. Murty, D. L. Pincus, W. Yu, E. Cayanis, S. Kalachikov, T. C. Gilliam and B. Levine (1999). "Cloning and genomic organization of beclin 1, a candidate tumor suppressor gene on chromosome 17q21." Genomics **59**(1): 59-65.

Al Soraj, M., L. He, K. Peynshaert, J. Cousaert, D. Vercauteren, K. Braeckmans, S. C. De Smedt and A. T. Jones (2012). "siRNA and pharmacological inhibition of endocytic pathways to characterize the differential role of macropinocytosis and the actin cytoskeleton on cellular uptake of dextran and cationic cell penetrating peptides octaarginine (R8) and HIV-Tat." J Control Release **161**(1): 132-141.

Axe, E. L., S. A. Walker, M. Manifava, P. Chandra, H. L. Roderick, A. Habermann, G. Griffiths and N. T. Ktistakis (2008). "Autophagosome formation from membrane compartments enriched in phosphatidylinositol 3-phosphate and dynamically connected to the endoplasmic reticulum." The Journal of cell biology **182**(4): 685-701.

Bernales, S., K. L. McDonald and P. Walter (2006). "Autophagy counterbalances endoplasmic reticulum expansion during the unfolded protein response." PLoS biology **4**(12): e423.

Berón, W., M. G. Gutierrez, M. Rabinovitch and M. I. Colombo (2002). "Coxiella burnetii Localizes in a Rab7-Labeled Compartment with Autophagic Characteristics." Infection and Immunity **70**(10): 5816-5821.

Bishayee, S. (2000). "Role of conformational alteration in the epidermal growth factor receptor (EGFR) function." Biochemical pharmacology **60**(8): 1217-1223.

Borromeo, Mark D., Trisha K. Savage, Rahul K. Kollipara, M. He, A. Augustyn, Jihan K. Osborne, L. Girard, John D. Minna, Adi F. Gazdar, Melanie H. Cobb and Jane E. Johnson (2016). "ASCL1 and NEUROD1 Reveal Heterogeneity in Pulmonary Neuroendocrine Tumors and Regulate Distinct Genetic Programs." Cell Reports **16**(5): 1259-1272.

Brown, H., M. Chung, A. Üffing, N. Batistatou, T. Tsang, S. Doskocil, W. Mao, D. Willbold, R. C. Bast, Jr., Z. Lu, O. H. Weiergräber and J. A. Kritzer (2022). "Structure-Based Design of Stapled Peptides That Bind GABARAP and Inhibit Autophagy." Journal of the American Chemical Society **144**(32): 14687-14697.

Budanov, A. V. and M. Karin (2008). "p53 target genes sestrin1 and sestrin2 connect genotoxic stress and mTOR signaling." Cell **134**(3): 451-460.

Carew, J. S., E. C. Medina, J. A. Esquivel II, D. Mahalingam, R. Swords, K. Kelly, H. Zhang, P. Huang, A. C. Mita and M. M. Mita (2010). "Autophagy inhibition

enhances vorinostat-induced apoptosis via ubiquitinated protein accumulation." Journal of cellular and molecular medicine **14**(10): 2448-2459.

Cheng, L., R. E. Alexander, G. T. MacLennan, O. W. Cummings, R. Montironi, A. Lopez-Beltran, H. M. Cramer, D. D. Davidson and S. Zhang (2012). "Molecular pathology of lung cancer: key to personalized medicine." Modern Pathology **25**(3): 347.

chengY, W. (2018). "Anlotinibasthird lineorfurther line treatmentinrelapsedScLc: amulticentre, randomized, double blind phase2trial." JThoracOncol **13**(10Supple): S351.

Chevallier, M., M. Borgeaud, A. Addeo and A. Friedlaender (2021). "Oncogenic driver mutations in non-small cell lung cancer: Past, present and future." World J Clin Oncol **12**(4): 217-237.

Christofferson, D. E., Y. Li and J. Yuan (2014). "Control of life-or-death decisions by RIP1 kinase." Annual review of physiology **76**: 129-150.

Chude, C. I. and R. K. Amaravadi (2017). "Targeting autophagy in cancer: update on clinical trials and novel inhibitors." International journal of molecular sciences **18**(6): 1279.

Couraud, S., G. Zalcman, B. Milleron, F. Morin and P.-J. Souquet (2012). "Lung cancer in never smokers – A review." European Journal of Cancer **48**(9): 1299-1311.

Davies, A. M., P. N. Lara, D. H. Lau and D. R. Gandara (2004). "Treatment of extensive small cell lung cancer." Hematology/Oncology Clinics **18**(2): 373-385.

de Cássia S. Alves, R., R. T. Meurer and A. V. Roehe (2014). "MYC amplification is associated with poor survival in small cell lung cancer: a chromogenic in situ hybridization study." Journal of Cancer Research and Clinical Oncology **140**(12): 2021-2025.

Degenhardt, K., R. Mathew, B. Beaudoin, K. Bray, D. Anderson, G. Chen, C. Mukherjee, Y. Shi, C. Gélinas and Y. Fan (2006). "Autophagy promotes tumor cell survival and restricts necrosis, inflammation, and tumorigenesis." Cancer cell **10**(1): 51-64.

Degenhardt, K., R. Mathew, B. Beaudoin, K. Bray, D. Anderson, G. Chen, C. Mukherjee, Y. Shi, C. Gélinas, Y. Fan, D. A. Nelson, S. Jin and E. White (2006). "Autophagy promotes tumor cell survival and restricts necrosis, inflammation, and tumorigenesis." Cancer Cell **10**(1): 51-64.

Deng, Z., J. Lim, Q. Wang, K. Purtell, S. Wu, G. M. Palomo, H. Tan, G. Manfredi, Y. Zhao, J. Peng, B. Hu, S. Chen and Z. Yue (2020). "ALS-FTLD-linked mutations of SQSTM1/p62 disrupt selective autophagy and NFE2L2/NRF2 anti-oxidative stress pathway." Autophagy **16**(5): 917-931.

Dong, L. X., L. L. Sun, X. Zhang, L. Pan, L. J. Lian, Z. Chen and D. S. Zhong (2013). "Negative regulation of mTOR activity by LKB1-AMPK signaling in non-small cell lung cancer cells." Acta Pharmacol Sin **34**(2): 314-318.

Drilon, A., F. Cappuzzo, S.-H. I. Ou and D. R. Camidge (2017). "Targeting MET in lung cancer: will expectations finally be MET?" Journal of Thoracic Oncology **12**(1): 15-26.

Duran, A., J. F. Linares, A. S. Galvez, K. Wikenheiser, J. M. Flores, M. T. Diaz-Meco and J. Moscat (2008). "The signaling adaptor p62 is an important NF-κB mediator in tumorigenesis." Cancer cell **13**(4): 343-354.

Eberhard, D. A., B. E. Johnson, L. C. Amler, A. D. Goddard, S. L. Heldens, R. S. Herbst, W. L. Ince, P. A. Jänne, T. Januario and D. H. Johnson (2005). "Mutations in the epidermal growth factor receptor and in KRAS are predictive and prognostic indicators in patients with non–small-cell lung cancer treated with chemotherapy alone and in combination with erlotinib." Journal of clinical oncology **23**(25): 5900-5909.

Fawell, S., J. Seery, Y. Daikh, C. Moore, L. L. Chen, B. Pepinsky and J. Barsoum (1994). "Tat-mediated delivery of heterologous proteins into cells." Proc Natl Acad Sci U S A **91**(2): 664-668.

Finlay, B. B., B. R. Dorn, W. A. Dunn and A. Progulske-Fox (2001). "Porphyromonas gingivalis Traffics to Autophagosomes in Human Coronary Artery Endothelial Cells." Infection and Immunity **69**(9): 5698-5708.

Fu, L.-l., Y. Cheng and B. Liu (2013). "Beclin-1: Autophagic regulator and therapeutic target in cancer." The International Journal of Biochemistry & Cell Biology **45**(5): 921-924.

Furuya, N., J. Yu, M. Byfield, S. Pattingre and B. Levine (2005). "The evolutionarily conserved domain of Beclin 1 is required for Vps34 binding, autophagy, and tumor suppressor function." Autophagy **1**(1): 46-52.

Gainor, J. F., A. M. Varghese, S.-H. I. Ou, S. Kabraji, M. M. Awad, R. Katayama, A. Pawlak, M. Mino-Kenudson, B. Y. Yeap and G. J. Riely (2013). "ALK Rearrangements Are Mutually Exclusive with Mutations in EGFR or KRAS: An Analysis of 1,683 Patients with Non–Small Cell Lung CancerALK-Positive Tumors Lack EGFR or KRAS Mutations." Clinical cancer research **19**(15): 4273-4281.

Galluzzi, L., I. Vitale, S. A. Aaronson, J. M. Abrams, D. Adam, P. Agostinis, E. S. Alnemri, L. Altucci, I. Amelio, D. W. Andrews, M. Annicchiarico-Petruzzelli, A. V. Antonov, E. Arama, E. H. Baehrecke, N. A. Barlev, N. G. Bazan, F. Bernassola, M. J. M. Bertrand, K. Bianchi, M. V. Blagosklonny, K. Blomgren, C. Borner, P. Boya, C. Brenner, M. Campanella, E. Candi, D. Carmona-Gutierrez, F. Cecconi, F. K. Chan, N. S. Chandel, E. H. Cheng, J. E. Chipuk, J. A. Cidlowski, A. Ciechanover, G. M. Cohen, M. Conrad, J. R. Cubillos-Ruiz, P. E. Czabotar, V. D'Angiolella, T. M. Dawson, V. L. Dawson, V. De Laurenzi, R. De Maria, K. M. Debatin, R. J. DeBerardinis, M. Deshmukh, N. Di Daniele, F. Di Virgilio, V. M. Dixit, S. J. Dixon, C. S. Duckett, B. D. Dynlacht, W. S. El-Deiry, J. W. Elrod, G. M. Fimia, S. Fulda, A. J. Garcia-Saez, A. D. Garg, C. Garrido, E. Gavathiotis, P. Golstein, E. Gottlieb, D. R. Green, L. A. Greene, H. Gronemeyer, A. Gross, G. Hajnoczky, J. M. Hardwick, I. S. Harris, M. O. Hengartner, C. Hetz, H. Ichijo, M. Jaattela, B. Joseph, P. J. Jost, P. P. Juin, W. J. Kaiser, M. Karin, T. Kaufmann, O. Kepp, A. Kimchi, R. N. Kitsis, D. J. Klionsky, R. A. Knight, S. Kumar, S. W. Lee, J. J. Lemasters, B. Levine, A. Linkermann, S. A. Lipton, R. A. Lockshin, C. Lopez-Otin, S. W. Lowe, T. Luedde, E. Lugli, M. MacFarlane, F. Madeo, M. Malewicz, W. Malorni, G. Manic, J. C. Marine, S. J. Martin, J. C. Martinou, J. P. Medema, P.

Mehlen, P. Meier, S. Melino, E. A. Miao, J. D. Molkentin, U. M. Moll, C. Munoz-Pinedo, S. Nagata, G. Nunez, A. Oberst, M. Oren, M. Overholtzer, M. Pagano, T. Panaretakis, M. Pasparakis, J. M. Penninger, D. M. Pereira, S. Pervaiz, M. E. Peter, M. Piacentini, P. Pinton, J. H. M. Prehn, H. Puthalakath, G. A. Rabinovich, M. Rehm, R. Rizzuto, C. M. P. Rodrigues, D. C. Rubinsztein, T. Rudel, K. M. Ryan, E. Sayan, L. Scorrano, F. Shao, Y. Shi, J. Silke, H. U. Simon, A. Sistigu, B. R. Stockwell, A. Strasser, G. Szabadkai, S. W. G. Tait, D. Tang, N. Tavernarakis, A. Thorburn, Y. Tsujimoto, B. Turk, T. Vanden Berghe, P. Vandenabeele, M. G. Vander Heiden, A. Villunger, H. W. Virgin, K. H. Vousden, D. Vucic, E. F. Wagner, H. Walczak, D. Wallach, Y. Wang, J. A. Wells, W. Wood, J. Yuan, Z. Zakeri, B. Zhivotovsky, L. Zitvogel, G. Melino and G. Kroemer (2018). "Molecular mechanisms of cell death: recommendations of the Nomenclature Committee on Cell Death 2018." Cell Death Differ **25**(3): 486-541.

Gao, P., C. Mei, L. He, Z. Xiao, L. Chan, D. Zhang, C. Shi, T. Chen and L. Luo (2018). "Designing multifunctional cancer-targeted nanosystem for magnetic resonance molecular imaging-guided theranostics of lung cancer." Drug delivery **25**(1): 1811-1825.

Gao, S., N. Li, X. Zhang, J. Chen, B. C. B. Ko and Y. Zhao (2023). "An autophagy-inducing stapled peptide promotes c-MET degradation and overrides adaptive resistance to sorafenib in c-MET(+) hepatocellular carcinoma." Biochem Biophys Rep **33**: 101412.

George, J., J. S. Lim, S. J. Jang, Y. Cun, L. Ozretić, G. Kong, F. Leenders, X. Lu, L. Fernández-Cuesta and G. Bosco (2015). "Comprehensive genomic profiles of small cell lung cancer." Nature **524**(7563): 47-53.

Glick, D., S. Barth and K. F. Macleod (2010). "Autophagy: cellular and molecular mechanisms." The Journal of pathology **221**(1): 3-12.

Gomez, J. A., J. Chen, J. Ngo, D. Hajkova, I.-J. Yeh, V. Gama, M. Miyagi and S. Matsuyama (2010). "Cell-penetrating penta-peptides (CPP5s): measurement of cell entry and protein-transduction activity." Pharmaceuticals **3**(12): 3594-3613.

Govindan, R., N. Page, D. Morgensztern, W. Read, R. Tierney, A. Vlahiotis, E. L. Spitznagel and J. Piccirillo (2006). "Changing epidemiology of small-cell lung cancer in the United States over the last 30 years: analysis of the surveillance, epidemiologic, and end results database." J Clin Oncol **24**(28): 4539-4544.

Gridelli, C., A. Ardizzoni, J. Y. Douillard, N. Hanna, C. Manegold, F. Perrone, R. Pirker, R. Rosell, F. A. Shepherd, L. De Petris, M. Di Maio and F. de Marinis (2010). "Recent issues in first-line treatment of advanced non-small-cell lung cancer: Results of an International Expert Panel Meeting of the Italian Association of Thoracic Oncology." Lung Cancer **68**(3): 319-331.

Guo, J. Y., H.-Y. Chen, R. Mathew, J. Fan, A. M. Strohecker, G. Karsli-Uzunbas, J. J. Kamphorst, G. Chen, J. M. Lemons and V. Karantza (2011). "Activated Ras requires autophagy to maintain oxidative metabolism and tumorigenesis." Genes & development **25**(5): 460-470.

Hagiwara, S. and L. Byerly (1981). "Calcium channel." Annual review of

neuroscience **4**(1): 69-125.

Han, W., H. Pan, Y. Chen, J. Sun, Y. Wang, J. Li, W. Ge, L. Feng, X. Lin, X. Wang, X. Wang and H. Jin (2011). "EGFR tyrosine kinase inhibitors activate autophagy as a cytoprotective response in human lung cancer cells." PLoS One **6**(6): e18691.

He, C. and B. Levine (2010). "The beclin 1 interactome." Current opinion in cell biology **22**(2): 140-149.

Hecht, S. S. (2012). "Lung carcinogenesis by tobacco smoke." International journal of cancer **131**(12): 2724-2732.

Herbst, R. S., D. Morgensztern and C. Boshoff (2018). "The biology and management of non-small cell lung cancer." Nature **553**(7689): 446-454.

Hong, D. S., S. G. DuBois, S. Kummar, A. F. Farago, C. M. Albert, K. S. Rohrberg, C. M. van Tilburg, R. Nagasubramanian, J. D. Berlin and N. Federman (2020). "Larotrectinib in patients with TRK fusion-positive solid tumours: a pooled analysis of three phase 1/2 clinical trials." The Lancet Oncology **21**(4): 531-540.

Huang, J., C. H. Ngai, Y. Deng, M. S. Tin, V. Lok, L. Zhang, J. Yuan, W. Xu, Z. J. Zheng and M. C. S. Wong (2022). "Cancer Incidence and Mortality in Asian Countries: A Trend Analysis." Cancer Control **29**: 10732748221095955.

Huang, W., W. Choi, W. Hu, N. Mi, Q. Guo, M. Ma, M. Liu, Y. Tian, P. Lu, F.-L. Wang, H. Deng, L. Liu, N. Gao, L. Yu and Y. Shi (2012). "Crystal structure and biochemical analyses reveal Beclin 1 as a novel membrane binding proteinOpen." Cell research **22**: 473-489.

Islam, M. Z., S. Sharmin, M. Moniruzzaman and M. Yamazaki (2018). "Elementary processes for the entry of cell-penetrating peptides into lipid bilayer vesicles and bacterial cells." Appl Microbiol Biotechnol **102**(9): 3879-3892.

J, S., Z. Y, W. K, S. X, W. Y, H. H, Z. Y, C. T, W. F and S. F (2015). "Cleavage of GSDMD by inflammatory caspases determines pyroptotic cell death." Nature **526**(7575): 660-665.

Jackson, W. T., T. H. Giddings Jr, M. P. Taylor, S. Mulinyawe, M. Rabinovitch, R. R. Kopito and K. Kirkegaard (2005). "Subversion of cellular autophagosomal machinery by RNA viruses." PLoS biology **3**(5): e156.

Janes, M. R., J. J. Limon, L. So, J. Chen, R. J. Lim, M. A. Chavez, C. Vu, M. B. Lilly, S. Mallya and S. T. Ong (2010). "Effective and selective targeting of leukemia cells using a TORC1/2 kinase inhibitor." Nature medicine **16**(2): 205-213.

Jänne, P. A., B. Freidlin, S. Saxman, D. H. Johnson, R. B. Livingston, F. A. Shepherd and B. E. Johnson (2002). "Twenty-five years of clinical research for patients with limited-stage small cell lung carcinoma in North America: Meaningful improvements in survival." Cancer **95**(7): 1528-1538.

Jiang, M., L. Qi, L. Li and Y. Li (2020). "The caspase-3/GSDME signal pathway as a switch between apoptosis and pyroptosis in cancer." Cell Death Discovery **6**(1): 112.

Kadir, L. A., M. Stacey and R. Barrett-Jolley (2018). "Emerging Roles of the Membrane Potential: Action Beyond the Action Potential." Frontiers in Physiology **9**:

1661.

Kang, R., H. Zeh, M. Lotze and D. Tang (2011). "The Beclin 1 network regulates autophagy and apoptosis." Cell Death & Differentiation **18**(4): 571-580.

Kastan, M. B. (2008). "DNA Damage Responses: Mechanisms and Roles in Human Disease." Molecular Cancer Research **6**(4): 517.

Kheloufi, M., C. M. Boulanger, P. Codogno and P. E. Rautou (2015). "Autosis occurs in the liver of patients with severe anorexia nervosa." Hepatology **62**(2): 657-658.

Kim, D.-W., N. Wu, Y.-C. Kim, P. F. Cheng, R. Basom, D. Kim, C. T. Dunn, A. Y. Lee, K. Kim and C. S. Lee (2016). "Genetic requirement for Mycl and efficacy of RNA Pol I inhibition in mouse models of small cell lung cancer." Genes & development **30**(11): 1289-1299.

Kim, I., S. Rodriguez-Enriquez and J. J. Lemasters (2007). "Selective degradation of mitochondria by mitophagy." Archives of biochemistry and biophysics **462**(2): 245-253.

Kim, J., M. Kundu, B. Viollet and K.-L. Guan (2011). "AMPK and mTOR regulate autophagy through direct phosphorylation of Ulk1." Nature Cell Biology **13**(2): 132-141.

Kim, K.-B., C. T. Dunn and K.-S. Park (2019). "Recent progress in mapping the emerging landscape of the small-cell lung cancer genome." Experimental & Molecular Medicine **51**(12): 1-13.

Kim, K. W., L. Moretti, L. R. Mitchell, D. K. Jung and B. Lu (2009). "Combined Bcl-2/Mammalian Target of Rapamycin Inhibition Leads to Enhanced Radiosensitization via Induction of Apoptosis and Autophagy in Non–Small Cell Lung Tumor Xenograft Model." Clinical Cancer Research **15**(19): 6096-6105.

Kobayashi, S., T. J. Boggon, T. Dayaram, P. A. Jänne, O. Kocher, M. Meyerson, B. E. Johnson, M. J. Eck, D. G. Tenen and B. Halmos (2005). "EGFR mutation and resistance of non-small-cell lung cancer to gefitinib." N Engl J Med **352**(8): 786-792.

Komatsu, M., S. Waguri, M. Koike, Y. S. Sou, T. Ueno, T. Hara, N. Mizushima, J. Iwata, J. Ezaki, S. Murata, J. Hamazaki, Y. Nishito, S. Iemura, T. Natsume, T. Yanagawa, J. Uwayama, E. Warabi, H. Yoshida, T. Ishii, A. Kobayashi, M. Yamamoto, Z. Yue, Y. Uchiyama, E. Kominami and K. Tanaka (2007). "Homeostatic levels of p62 control cytoplasmic inclusion body formation in autophagy-deficient mice." Cell **131**(6): 1149-1163.

Kongara, S., O. Kravchuk, I. Teplova, F. Lozy, J. Schulte, D. Moore, N. Barnard, C. A. Neumann, E. White and V. Karantza (2010). "Autophagy Regulates Keratin 8 Homeostasis in Mammary Epithelial Cells and in Breast Tumors." Molecular Cancer Research **8**(6): 873-884.

Kosaka, T., Y. Yatabe, H. Endoh, H. Kuwano, T. Takahashi and T. Mitsudomi (2004). "Mutations of the epidermal growth factor receptor gene in lung cancer: biological and clinical implications." Cancer Res **64**(24): 8919-8923.

Kroemer, G., L. Galluzzi and C. Brenner (2007). "Mitochondrial Membrane

Permeabilization in Cell Death." Physiological Reviews **87**(1): 99-163.

Lara Jr, P. N., R. Natale, J. Crowley, H. J. Lenz, M. W. Redman, J. E. Carleton, J. Jett, C. J. Langer, J. P. Kuebler and S. R. Dakhil (2009). "Phase III trial of irinotecan/cisplatin compared with etoposide/cisplatin in extensive-stage small-cell lung cancer: clinical and pharmacogenomic results from SWOG S0124." Journal of clinical oncology **27**(15): 2530.

Larsen, J. E. and J. D. Minna (2011). "Molecular biology of lung cancer: clinical implications." Clinics in chest medicine **32**(4): 703-740.

LeCher, J. C., S. J. Nowak and J. L. McMurry (2017). "Breaking in and busting out: cell-penetrating peptides and the endosomal escape problem." Biomol Concepts **8**(3-4): 131-141.

Lee, B., B. Lee, G. Han, M. J. Kwon, J. Han and Y.-L. Choi (2014). "KRAS mutation detection in non-small cell lung cancer using a peptide nucleic acid-mediated polymerase chain reaction clamping method and comparative validation with next-generation sequencing." Korean journal of pathology **48**(2): 100.

Lee, E. F., M. A. Perugini, A. Pettikiriarachchi, M. Evangelista, D. W. Keizer, S. Yao and W. D. Fairlie (2016). "The BECN1 N-terminal domain is intrinsically disordered." Autophagy **12**(3): 460-471.

Lee, J.-H., D.-S. Yang, C. N. Goulbourne, E. Im, P. Stavrides, A. Pensalfini, H. Chan, C. Bouchet-Marquis, C. Bleiwas, M. J. Berg, C. Huo, J. Peddy, M. Pawlik, E. Levy, M. Rao, M. Staufenbiel and R. A. Nixon (2022). "Faulty autolysosome acidification in Alzheimer's disease mouse models induces autophagic build-up of Aβ in neurons, yielding senile plaques." Nature Neuroscience **25**(6): 688-701.

Li, N., X. Zhang, J. Chen, S. Gao, L. Wang and Y. Zhao (2023). "Perturbation of Autophagy by a Beclin 1-Targeting Stapled Peptide Induces Mitochondria Stress and Inhibits Proliferation of Pancreatic Cancer Cells." Cancers (Basel) **15**(3).

Li, X. and Z. Fan (2010). "The epidermal growth factor receptor antibody cetuximab induces autophagy in cancer cells by downregulating HIF-1α and Bcl-2 and activating the beclin 1/hVps34 complex." Cancer research **70**(14): 5942-5952.

Li, X., L. He, K. H. Che, S. F. Funderburk, L. Pan, N. Pan, M. Zhang, Z. Yue and Y. Zhao (2012). "Imperfect interface of Beclin1 coiled-coil domain regulates homodimer and heterodimer formation with Atg14L and UVRAG." Nat Commun **3**: 662.

Li, X., L. He, K. H. Che, S. F. Funderburk, L. Pan, N. Pan, M. Zhang, Z. Yue and Y. Zhao (2012). "Imperfect interface of Beclin1 coiled-coil domain regulates homodimer and heterodimer formation with Atg14L and UVRAG." Nature Communications **3**(1): 662.

Li, X., L. He, K. H. Che, S. F. Funderburk, L. Pan, N. Pan, M. Zhang, Z. Yue and Y. Zhao (2012). "Imperfect interface of Beclin1 coiled-coil domain regulates homodimer and heterodimer formation with Atg14L and UVRAG." Nature communications **3**(1): 1-11.

Li, X., L. He, M. Zhang, Z. Yue and Y. Zhao (2012). "The BECN1 coiled coil

domain: An “imperfect” homodimer interface that facilitates ATG14 and UVRAG binding." Autophagy **8**(8): 1258-1260.

Liang, C., P. Feng, B. Ku, I. Dotan, D. Canaani, B. H. Oh and J. U. Jung (2006). "Autophagic and tumour suppressor activity of a novel Beclin1-binding protein UVRAG." Nat Cell Biol **8**(7): 688-699.

Liang, X. H., S. Jackson, M. Seaman, K. Brown, B. Kempkes, H. Hibshoosh and B. Levine (1999). "Induction of autophagy and inhibition of tumorigenesis by beclin 1." Nature **402**(6762): 672-676.

Liang, X. H., L. K. Kleeman, H. H. Jiang, G. Gordon, J. E. Goldman, G. Berry, B. Herman and B. Levine (1998). "Protection against fatal Sindbis virus encephalitis by beclin, a novel Bcl-2-interacting protein." Journal of virology **72**(11): 8586-8596.

Lim, J., M. L. Lachenmayer, S. Wu, W. Liu, M. Kundu, R. Wang, M. Komatsu, Y. J. Oh, Y. Zhao and Z. Yue (2015). "Proteotoxic stress induces phosphorylation of p62/SQSTM1 by ULK1 to regulate selective autophagic clearance of protein aggregates." PLoS Genet **11**(2): e1004987.

Lim, S. Y., S. M. Davidson, D. J. Hausenloy and D. M. Yellon (2007). "Preconditioning and postconditioning: The essential role of the mitochondrial permeability transition pore." Cardiovascular Research **75**(3): 530-535.

Liu, S.-Y., L.-Y. Gou, A.-N. Li, N.-N. Lou, H.-F. Gao, J. Su, J.-J. Yang, X.-C. Zhang, Y. Shao and Z.-Y. Dong (2016). "The unique characteristics of MET exon 14 mutation in Chinese patients with NSCLC." Journal of Thoracic Oncology **11**(9): 1503-1510.

Liu, Y. and B. Levine (2015). "Autosis and autophagic cell death: the dark side of autophagy." Cell Death Differ **22**(3): 367-376.

Liu, Y., S. Shoji-Kawata, R. M. Sumpter, Jr., Y. Wei, V. Ginet, L. Zhang, B. Posner, K. A. Tran, D. R. Green, R. J. Xavier, S. Y. Shaw, P. G. Clarke, J. Puyal and B. Levine (2013). "Autosis is a Na+,K+-ATPase-regulated form of cell death triggered by autophagy-inducing peptides, starvation, and hypoxia-ischemia." Proc Natl Acad Sci U S A **110**(51): 20364-20371.

Liu, Y., S. Shoji-Kawata, R. M. Sumpter, Y. Wei, V. Ginet, L. Zhang, B. Posner, K. A. Tran, D. R. Green, R. J. Xavier, S. Y. Shaw, P. G. H. Clarke, J. Puyal and B. Levine (2013). "Autosis is a Na⁺,K⁺-ATPase–regulated form of cell death triggered by autophagy-inducing peptides, starvation, and hypoxia–ischemia." Proceedings of the National Academy of Sciences **110**(51): 20364-20371.

Lu, H., S. Zhang, J. Wu, M. Chen, M.-C. Cai, Y. Fu, W. Li, J. Wang, X. Zhao, Z. Yu, P. Ma and G. Zhuang (2018). "Molecular Targeted Therapies Elicit Concurrent Apoptotic and GSDME-Dependent Pyroptotic Tumor Cell Death." Clinical Cancer Research **24**(23): 6066-6077.

Lu, Z., R. Z. Luo, Y. Lu, X. Zhang, Q. Yu, S. Khare, S. Kondo, Y. Kondo, Y. Yu and G. B. Mills (2008). "The tumor suppressor gene ARHI regulates autophagy and tumor dormancy in human ovarian cancer cells." The Journal of clinical investigation

118(12): 3917-3929.

Lynch, T. J., D. W. Bell, R. Sordella, S. Gurubhagavatula, R. A. Okimoto, B. W. Brannigan, P. L. Harris, S. M. Haserlat, J. G. Supko, F. G. Haluska, D. N. Louis, D. C. Christiani, J. Settleman and D. A. Haber (2004). "Activating mutations in the epidermal growth factor receptor underlying responsiveness of non-small-cell lung cancer to gefitinib." N Engl J Med **350**(21): 2129-2139.

Mason, R. C., J. F. Murray, J. A. Nadel and M. Gotway (2015). Murray & Nadel's Textbook of Respiratory Medicine E-Book, Elsevier Health Sciences.

Matsunaga, K., T. Saitoh, K. Tabata, H. Omori, T. Satoh, N. Kurotori, I. Maejima, K. Shirahama-Noda, T. Ichimura, T. Isobe, S. Akira, T. Noda and T. Yoshimori (2009). "Two Beclin 1-binding proteins, Atg14L and Rubicon, reciprocally regulate autophagy at different stages." Nat Cell Biol **11**(4): 385-396.

Meric-Bernstam, F. and A. M. Gonzalez-Angulo (2009). "Targeting the mTOR signaling network for cancer therapy." Journal of clinical oncology : official journal of the American Society of Clinical Oncology **27**(13): 2278-2287.

Milletti, F. (2012). "Cell-penetrating peptides: classes, origin, and current landscape." Drug Discov Today **17**(15-16): 850-860.

Mizushima, N. (2007). "Autophagy: process and function." Genes & development **21**(22): 2861-2873.

Muscat, J. E., S. D. Stellman, Z. F. Zhang, A. I. Neugut and E. L. Wynder (1997). "Cigarette smoking and large cell carcinoma of the lung." Cancer Epidemiology Biomarkers & Prevention **6**(7): 477.

N, K., S. IB, L. BL, O. R. K, A. K, W. S, C. T, H. B, R.-G. M, P. QT, L. PS, L. JR, L. H, W. J, K. S, Z. J, L. WP, S. SJ, S. GS, M. LX, F. L, Z. Y, B. EM, G. CC and D. VM (2015). "Caspase-11 cleaves gasdermin D for non-canonical inflammasome signalling." Nature **526**(7575): 666-671.

Niederst, M. J., H. Hu, H. E. Mulvey, E. L. Lockerman, A. R. Garcia, Z. Piotrowska, L. V. Sequist and J. A. Engelman (2015). "The Allelic Context of the C797S Mutation Acquired upon Treatment with Third-Generation EGFR Inhibitors Impacts Sensitivity to Subsequent Treatment Strategies." Clin Cancer Res **21**(17): 3924-3933.

Noda, K., Y. Nishiwaki, M. Kawahara, S. Negoro, T. Sugiura, A. Yokoyama, M. Fukuoka, K. Mori, K. Watanabe and T. Tamura (2002). "Irinotecan plus cisplatin compared with etoposide plus cisplatin for extensive small-cell lung cancer." New England Journal of Medicine **346**(2): 85-91.

O'Reilly, K., A. M. Mclaughlin, W. S. Beckett and P. J. Sime (2007). "Asbestos-related lung disease." American family physician **75**(5).

Oberstein, A., P. D. Jeffrey and Y. Shi (2007). "Crystal structure of the Bcl-XL-Beclin 1 peptide complex: Beclin 1 is a novel BH3-only protein." Journal of Biological Chemistry **282**(17): 13123-13132.

Ohe, Y., Y. Ohashi, K. Kubota, T. Tamura, K. Nakagawa, S. Negoro, Y. Nishiwaki, N. Saijo, Y. Ariyoshi and M. Fukuoka (2007). "Randomized phase III study of cisplatin plus irinotecan versus carboplatin plus paclitaxel, cisplatin plus gemcitabine, and

cisplatin plus vinorelbine for advanced non-small-cell lung cancer: Four-Arm Cooperative Study in Japan." Annals of oncology **18**(2): 317-323.

Onitsuka, T., H. Uramoto, N. Nose, M. Takenoyama, T. Hanagiri, K. Sugio and K. Yasumoto (2010). "Acquired resistance to gefitinib: the contribution of mechanisms other than the T790M, MET, and HGF status." Lung Cancer **68**(2): 198-203.

Onodera, J. and Y. Ohsumi (2005). "Autophagy Is Required for Maintenance of Amino Acid Levels and Protein Synthesis under Nitrogen Starvation*." Journal of Biological Chemistry **280**(36): 31582-31586.

Pao, W., V. Miller, M. Zakowski, J. Doherty, K. Politi, I. Sarkaria, B. Singh, R. Heelan, V. Rusch, L. Fulton, E. Mardis, D. Kupfer, R. Wilson, M. Kris and H. Varmus (2004). "EGF receptor gene mutations are common in lung cancers from "never smokers" and are associated with sensitivity of tumors to gefitinib and erlotinib." Proc Natl Acad Sci U S A **101**(36): 13306-13311.

Pardo, J., A. M. Martinez-Peñuela, J. J. Sola, A. Panizo, A. Gúrpide, J. M. Martinez-Peñuela and M. D. Lozano (2009). "Large cell carcinoma of the lung: an endangered species?" Appl Immunohistochem Mol Morphol **17**(5): 383-392.

Paumelle, R., D. Tulashe, Z. Kherrouche, S. Plaza, C. Leroy, S. Reveneau, B. Vandenbunder and V. Fafeur (2002). "Hepatocyte growth factor/scatter factor activates the ETS1 transcription factor by a RAS-RAF-MEK-ERK signaling pathway." Oncogene **21**(15): 2309.

Perez-Moreno, P., E. Brambilla, R. Thomas and J. C. Soria (2012). "Squamous cell carcinoma of the lung: molecular subtypes and therapeutic opportunities." Clin Cancer Res **18**(9): 2443-2451.

Pescina, S., C. Ostacolo, I. M. Gomez-Monterrey, M. Sala, A. Bertamino, F. Sonvico, C. Padula, P. Santi, A. Bianchera and S. Nicoli (2018). "Cell penetrating peptides in ocular drug delivery: State of the art." J Control Release **284**: 84-102.

Peto, R., J. Boreham and A. D. Lopez (1996). Mortality from smoking in developed countries, Oxford University Press.

Pignon, J. P., R. Arriagada, D. C. Ihde, D. H. Johnson, M. C. Perry, R. L. Souhami, O. Brodin, R. A. Joss, M. S. Kies, B. Lebeau and et al. (1992). "A meta-analysis of thoracic radiotherapy for small-cell lung cancer." N Engl J Med **327**(23): 1618-1624.

Pizarro-Cerdá, J., E. Moreno, V. Sanguedolce, J.-L. Mege and J.-P. Gorvel (1998). "Virulent Brucella abortus Prevents Lysosome Fusion and Is Distributed within Autophagosome-Like Compartments." Infection and Immunity **66**(5): 2387-2392.

Popper, H. H. (2011). "Large cell carcinoma of the lung – a vanishing entity?" memo - Magazine of European Medical Oncology **4**(1): 4-9.

Puglisi, M., S. Dolly, A. Faria, J. Myerson, S. Popat and M. O'brien (2010). "Treatment options for small cell lung cancer–do we have more choice?" British journal of cancer **102**(4): 629-638.

Qu, X., J. Yu, G. Bhagat, N. Furuya, H. Hibshoosh, A. Troxel, J. Rosen, E.-L. Eskelinen, N. Mizushima and Y. Ohsumi (2003). "Promotion of tumorigenesis by heterozygous disruption of the beclin 1 autophagy gene." The Journal of clinical

investigation **112**(12): 1809-1820.

Rao, S., L. Tortola, T. Perlot, G. Wirnsberger, M. Novatchkova, R. Nitsch, P. Sykacek, L. Frank, D. Schramek, V. Komnenovic, V. Sigl, K. Aumayr, G. Schmauss, N. Fellner, S. Handschuh, M. Glösmann, P. Pasierbek, M. Schlederer, G. P. Resch, Y. Ma, H. Yang, H. Popper, L. Kenner, G. Kroemer and J. M. Penninger (2014). "A dual role for autophagy in a murine model of lung cancer." Nature Communications **5**(1): 3056.

Raucher, D. and J. S. Ryu (2015). "Cell-penetrating peptides: strategies for anticancer treatment." Trends Mol Med **21**(9): 560-570.

Rhee, M. and P. Davis (2006). "Mechanism of uptake of C105Y, a novel cell-penetrating peptide." Journal of Biological Chemistry **281**(2): 1233-1240.

Rogers, C., D. A. Erkes, A. Nardone, A. E. Aplin, T. Fernandes-Alnemri and E. S. Alnemri (2019). "Gasdermin pores permeabilize mitochondria to augment caspase-3 activation during apoptosis and inflammasome activation." Nature Communications **10**(1): 1689.

Rowell, N. P. and C. J. Williams (2001). "Radical radiotherapy for stage I/II non-small cell lung cancer in patients not sufficiently fit for or declining surgery (medically inoperable): a systematic review." Thorax **56**(8): 628-638.

Rudin, C. M., M. C. Pietanza, T. M. Bauer, N. Ready, D. Morgensztern, B. S. Glisson, L. A. Byers, M. L. Johnson, H. A. Burris, III, F. Robert, T. H. Han, S. Bheddah, N. Theiss, S. Watson, D. Mathur, B. Vennapusa, H. Zayed, S. Lally, D. K. Strickland, R. Govindan, S. J. Dylla, S. L. Peng and D. R. Spigel (2017). "Rovalpituzumab tesirine, a DLL3-targeted antibody-drug conjugate, in recurrent small-cell lung cancer: a first-in-human, first-in-class, open-label, phase 1 study." The Lancet Oncology **18**(1): 42-51.

Rudin, C. M., J. T. Poirier, L. A. Byers, C. Dive, A. Dowlati, J. George, J. V. Heymach, J. E. Johnson, J. M. Lehman and D. MacPherson (2019). "Molecular subtypes of small cell lung cancer: a synthesis of human and mouse model data." Nature Reviews Cancer **19**(5): 289-297.

Saltos, A., M. Shafique and A. Chiappori (2020). "Update on the Biology, Management, and Treatment of Small Cell Lung Cancer (SCLC)." Frontiers in Oncology **10**.

Saunders, L. R., A. J. Bankovich, W. C. Anderson, M. A. Aujay, S. Bheddah, K. Black, R. Desai, P. A. Escarpe, J. Hampl, A. Laysang, D. Liu, J. Lopez-Molina, M. Milton, A. Park, M. A. Pysz, H. Shao, B. Slingerland, M. Torgov, S. A. Williams, O. Foord, P. Howard, J. Jassem, A. Badzio, P. Czapiewski, D. H. Harpole, A. Dowlati, P. P. Massion, W. D. Travis, M. C. Pietanza, J. T. Poirier, C. M. Rudin, R. A. Stull and S. J. Dylla (2015). "A DLL3-targeted antibody-drug conjugate eradicates high-grade pulmonary neuroendocrine tumor-initiating cells in vivo." Science Translational Medicine **7**(302): 302ra136-302ra136.

Schiller, J. H., D. Harrington, C. P. Belani, C. Langer, A. Sandler, J. Krook, J. Zhu and D. H. Johnson (2002). "Comparison of four chemotherapy regimens for advanced non–small-cell lung cancer." New England Journal of Medicine **346**(2): 92-98.

Schläfli, A. M., O. Adams, J. A. Galván, M. Gugger, S. Savic, L. Bubendorf, R. A.

Schmid, K.-F. Becker, M. P. Tschan and R. Langer (2016). "Prognostic value of the autophagy markers LC3 and p62/SQSTM1 in early-stage non-small cell lung cancer." Oncotarget **7**(26): 39544.

Sequist, L. V., R. G. Martins, D. Spigel, S. M. Grunberg, A. Spira, P. A. Janne, V. A. Joshi, D. McCollum, T. L. Evans and A. Muzikansky (2008). "First-line gefitinib in patients with advanced non-small-cell lung cancer harboring somatic EGFR mutations." Journal of clinical oncology **26**(15): 2442-2449.

Simon, G. R. and H. Wagner (2003). "Small cell lung cancer." Chest **123**(1): 259S-271S.

Simonsen, A. and S. A. Tooze (2009). "Coordination of membrane events during autophagy by multiple class III PI3-kinase complexes." Journal of cell biology **186**(6): 773-782.

Slotman, B., C. Faivre-Finn, G. Kramer, E. Rankin, M. Snee, M. Hatton, P. Postmus, L. Collette, E. Musat and S. Senan (2007). "Prophylactic cranial irradiation in extensive small-cell lung cancer." N Engl J Med **357**(7): 664-672.

Smythe, W. R. (2003). "Treatment of stage I non-small cell lung carcinoma." Chest **123**(1): 181S-187S.

Soda, M., Y. L. Choi, M. Enomoto, S. Takada, Y. Yamashita, S. Ishikawa, S.-i. Fujiwara, H. Watanabe, K. Kurashina and H. Hatanaka (2007). "Identification of the transforming EML4–ALK fusion gene in non-small-cell lung cancer." Nature **448**(7153): 561-566.

Solomon, B., K. Wilner and A. Shaw (2014). "Current status of targeted therapy for anaplastic lymphoma kinase–rearranged non–small cell lung cancer." CLINICAL PHARmACOLOgy & THeRAPeuTICS **95**(1): 15-23.

Soria, J.-C., Y. Ohe, J. Vansteenkiste, T. Reungwetwattana, B. Chewaskulyong, K. H. Lee, A. Dechaphunkul, F. Imamura, N. Nogami, T. Kurata, I. Okamoto, C. Zhou, B. C. Cho, Y. Cheng, E. K. Cho, P. J. Voon, D. Planchard, W.-C. Su, J. E. Gray, S.-M. Lee, R. Hodge, M. Marotti, Y. Rukazenkov and S. S. Ramalingam (2017). "Osimertinib in Untreated EGFR-Mutated Advanced Non–Small-Cell Lung Cancer." New England Journal of Medicine **378**(2): 113-125.

Stalmans, S., N. Bracke, E. Wynendaele, B. Gevaert, K. Peremans, C. Burvenich, I. Polis and B. De Spiegeleer (2015). "Cell-Penetrating Peptides Selectively Cross the Blood-Brain Barrier In Vivo." PLoS One **10**(10): e0139652.

Sun, B. and M. Karin (2013). "Inflammation and liver tumorigenesis." Frontiers of medicine **7**(2): 242-254.

Swanson, M. S. and E. Fernandez-Moreia (2002). "A microbial strategy to multiply in macrophages: the pregnant pause." Traffic **3**(3): 170-177.

Tallóczy, Z., W. Jiang, H. W. Virgin, D. A. Leib, D. Scheuner, R. J. Kaufman, E.-L. Eskelinen and B. Levine (2002). "Regulation of starvation- and virus-induced autophagy by the eIF2α kinase signaling pathway." Proceedings of the National Academy of Sciences **99**(1): 190-195.

Tang, D., R. Kang, K. M. Livesey, C.-W. Cheh, A. Farkas, P. Loughran, G. Hoppe,

M. E. Bianchi, K. J. Tracey and H. J. Zeh III (2010). "Endogenous HMGB1 regulates autophagy." Journal of Cell Biology **190**(5): 881-892.

Taylor, R., F. Najafi and A. Dobson (2007). "Meta-analysis of studies of passive smoking and lung cancer: effects of study type and continent." International journal of epidemiology **36**(5): 1048-1059.

Thai, A. A., B. J. Solomon, L. V. Sequist, J. F. Gainor and R. S. Heist (2021). "Lung cancer." Lancet **398**(10299): 535-554.

Tiseo, M., L. Boni, F. Ambrosio, A. Camerini, M. G. Vitale, E. Baldini, S. Cinieri, F. Zanelli, E. Defraia, R. Passalacqua, L. Crino, C. Dazzi, C. Tibaldi, G. M. Turolla, V. D'Alessandro, N. Zilembo, F. Riccardi and A. Ardizzoni (2015). "Italian multicenter phase III randomized study of cisplatin-etoposide with or without bevacizumab as first-line treatment in extensive stage small cell lung cancer: treatment rationale and protocol design of the GOIRC-AIFA FARM6PMFJM trial." Clin Lung Cancer **16**(1): 67-70.

Tomas, A., C. E. Futter and E. R. Eden (2014). "EGF receptor trafficking: consequences for signaling and cancer." Trends Cell Biol **24**(1): 26-34.

Trofimenko, E., G. Grasso, M. Heulot, N. Chevalier, M. A. Deriu, G. Dubuis, Y. Arribat, M. Serulla, S. Michel, G. Vantomme, F. Ory, L. C. Dam, J. Puyal, F. Amati, A. Lüthi, A. Danani and C. Widmann (2021). "Genetic, cellular, and structural characterization of the membrane potential-dependent cell-penetrating peptide translocation pore." eLife **10**: e69832.

Tsao, M. S., A. Sakurada, J. C. Cutz, C. Q. Zhu, S. Kamel-Reid, J. Squire, I. Lorimer, T. Zhang, N. Liu, M. Daneshmand, P. Marrano, G. da Cunha Santos, A. Lagarde, F. Richardson, L. Seymour, M. Whitehead, K. Ding, J. Pater and F. A. Shepherd (2005). "Erlotinib in lung cancer - molecular and clinical predictors of outcome." N Engl J Med **353**(2): 133-144.

Tsukada, M. and Y. Ohsumi (1993). "Isolation and characterization of autophagy-defective mutants of Saccharomyces cerevisiae." FEBS letters **333**(1-2): 169-174.

Umemura, S., S. Mimaki, H. Makinoshima, S. Tada, G. Ishii, H. Ohmatsu, S. Niho, K. Yoh, S. Matsumoto, A. Takahashi, M. Morise, Y. Nakamura, A. Ochiai, K. Nagai, R. Iwakawa, T. Kohno, J. Yokota, Y. Ohe, H. Esumi, K. Tsuchihara and K. Goto (2014). "Therapeutic priority of the PI3K/AKT/mTOR pathway in small cell lung cancers as revealed by a comprehensive genomic analysis." J Thorac Oncol **9**(9): 1324-1331.

Umemura, S., S. Mimaki, H. Makinoshima, S. Tada, G. Ishii, H. Ohmatsu, S. Niho, K. Yoh, S. Matsumoto, A. Takahashi, M. Morise, Y. Nakamura, A. Ochiai, K. Nagai, R. Iwakawa, T. Kohno, J. Yokota, Y. Ohe, H. Esumi, K. Tsuchihara and K. Goto (2014). "Therapeutic Priority of the PI3K/AKT/mTOR Pathway in Small Cell Lung Cancers as Revealed by a Comprehensive Genomic Analysis." Journal of Thoracic Oncology **9**(9): 1324-1331.

Van Raemdonck, D. E., A. Schneider and R. J. Ginsberg (1992). "Surgical treatment for higher stage non-small cell lung cancer." The Annals of thoracic surgery **54**(5): 999-1013.

Verbaanderd, C., H. Maes, M. B. Schaaf, V. P. Sukhatme, P. Pantziarka, V.

Sukhatme, P. Agostinis and G. Bouche (2017). "Repurposing Drugs in Oncology (ReDO)-chloroquine and hydroxychloroquine as anti-cancer agents." Ecancermedicalscience **11**: 781-781.

Wei, Y., Z. Zou, N. Becker, M. Anderson, R. Sumpter, G. Xiao, L. Kinch, P. Koduru, C. S. Christudass, R. W. Veltri, N. V. Grishin, M. Peyton, J. Minna, G. Bhagat and B. Levine (2013). "EGFR-mediated Beclin 1 phosphorylation in autophagy suppression, tumor progression, and tumor chemoresistance." Cell **154**(6): 1269-1284.

Wei, Y., Z. Zou, N. Becker, M. Anderson, R. Sumpter, G. Xiao, L. Kinch, P. Koduru, C. S. Christudass, R. W. Veltri, N. V. Grishin, M. Peyton, J. Minna, G. Bhagat and B. Levine (2013). "EGFR-mediated Beclin 1 phosphorylation in autophagy suppression, tumor progression, and tumor chemoresistance." Cell **154**(6): 1269-1284.

Wender, P. A., D. J. Mitchell, K. Pattabiraman, E. T. Pelkey, L. Steinman and J. B. Rothbard (2000). "The design, synthesis, and evaluation of molecules that enable or enhance cellular uptake: Peptoid molecular transporters." Proceedings of the National Academy of Sciences **97**(24): 13003-13008.

Wu, H.-M., L.-J. Shao, Z.-F. Jiang and R.-Y. Liu (2016). "Gemcitabine-induced autophagy protects human lung cancer cells from apoptotic death." Lung **194**(6): 959-966.

Wu, S., Y. He, X. Qiu, W. Yang, W. Liu, X. Li, Y. Li, H.-M. Shen, R. Wang, Z. Yue and Y. Zhao (2018). "Targeting the potent Beclin 1–UVRAG coiled-coil interaction with designed peptides enhances autophagy and endolysosomal trafficking." Proceedings of the National Academy of Sciences **115**(25): E5669-E5678.

Wu, S., Y. He, X. Qiu, W. Yang, W. Liu, X. Li, Y. Li, H. M. Shen, R. Wang, Z. Yue and Y. Zhao (2018). "Targeting the potent Beclin 1-UVRAG coiled-coil interaction with designed peptides enhances autophagy and endolysosomal trafficking." Proc Natl Acad Sci U S A **115**(25): E5669-e5678.

Wu, Z., P.-C. Chang, J. C. Yang, C.-Y. Chu, L.-Y. Wang, N.-T. Chen, A.-H. Ma, S. J. Desai, S. H. Lo and C. P. Evans (2010). "Autophagy blockade sensitizes prostate cancer cells towards Src family kinase inhibitors." Genes & cancer **1**(1): 40-49.

Xie, J., Y. Bi, H. Zhang, S. Dong, L. Teng, R. J. Lee and Z. Yang (2020). "Cell-Penetrating Peptides in Diagnosis and Treatment of Human Diseases: From Preclinical Research to Clinical Application." Frontiers in Pharmacology **11**.

Xie, T., W. Peng, C. Yan, J. Wu, X. Gong and Y. Shi (2013). "Structural insights into RIP3-mediated necroptotic signaling." Cell reports **5**(1): 70-78.

Xu, Y., Z. Huang, H. Lu, X. Yu, Y. Li, W. Li, J. Chen, M. Chen, L. Gong and K. Chen (2019). "Apatinib in patients with extensive-stage small-cell lung cancer after second-line or third-line chemotherapy: a phase II, single-arm, multicentre, prospective study." British journal of cancer **121**(8): 640-646.

Yang, I. A., J. W. Holloway and K. M. Fong (2013). "Genetic susceptibility to lung cancer and co-morbidities." Journal of thoracic disease **5**(Suppl 5): S454.

Yang, Q., X. Qiu, X. Zhang, Y. Yu, N. Li, X. Wei, G. Feng, Y. Li, Y. Zhao and R. Wang (2021). "Optimization of Beclin 1-Targeting Stapled Peptides by Staple Scanning

Leads to Enhanced Antiproliferative Potency in Cancer Cells." Journal of Medicinal Chemistry **64**(18): 13475-13486.

Yang, Q., X. Qiu, X. Zhang, Y. Yu, N. Li, X. Wei, G. Feng, Y. Li, Y. Zhao and R. Wang (2021). "Optimization of Beclin 1-Targeting Stapled Peptides by Staple Scanning Leads to Enhanced Antiproliferative Potency in Cancer Cells." J Med Chem **64**(18): 13475-13486.

Yang, S., X. Wang, G. Contino, M. Liesa, E. Sahin, H. Ying, A. Bause, Y. Li, J. M. Stommel and G. Dell'Antonio (2011). "Pancreatic cancers require autophagy for tumor growth." Genes & development **25**(7): 717-729.

Yao, S., E. F. Lee, A. Pettikiriarachchi, M. Evangelista, D. W. Keizer and W. D. Fairlie (2016). "Characterisation of the conformational preference and dynamics of the intrinsically disordered N-terminal region of Beclin 1 by NMR spectroscopy." Biochimica et Biophysica Acta (BBA)-Proteins and Proteomics **1864**(9): 1128-1137.

Yarden, Y. and J. Schlessinger (1987). "Epidermal growth factor induces rapid, reversible aggregation of the purified epidermal growth factor receptor." Biochemistry **26**(5): 1443-1451.

Yin, R., H. Wang, C. Li, L. Wang, S. Lai, X. Yang, D. Hong and W. Zhang (2022). "Induction of apoptosis and autosis in cardiomyocytes by the combination of homocysteine and copper via NOX-mediated p62 expression." Cell Death Discov **8**(1): 75.

Yu, K., C. Shi, L. Toral-Barza, J. Lucas, B. Shor, J. E. Kim, W.-G. Zhang, R. Mahoney, C. Gaydos and L. Tardio (2010). "Beyond rapalog therapy: preclinical pharmacology and antitumor activity of WYE-125132, an ATP-competitive and specific inhibitor of mTORC1 and mTORC2." Cancer research **70**(2): 621-631.

Zhang, G., B. T. Luk, X. Wei, G. R. Campbell, R. H. Fang, L. Zhang and S. A. Spector (2019). "Selective cell death of latently HIV-infected CD4(+) T cells mediated by autosis inducing nanopeptides." Cell Death Dis **10**(6): 419.

Zhang, Y., T. Zheng and W. Zhang (2018). "Report of cancer incidence and mortality in China, 2012." Advances in Modern Oncology Research **4**(3): 1-7.

Zheng, N., J. Fang, G. Xue, Z. Wang, X. Li, M. Zhou, G. Jin, M. M. Rahman, G. McFadden and Y. Lu (2022). "Induction of tumor cell autosis by myxoma virus-infected CAR-T and TCR-T cells to overcome primary and acquired resistance." Cancer Cell **40**(9): 973-985 e977.

Zhivotovsky, B. and S. Orrenius (2011). "Calcium and cell death mechanisms: A perspective from the cell death community." Cell Calcium **50**(3): 211-221.

Zhong, Y., Q. J. Wang, X. Li, Y. Yan, J. M. Backer, B. T. Chait, N. Heintz and Z. Yue (2009). "Distinct regulation of autophagic activity by Atg14L and Rubicon associated with Beclin 1-phosphatidylinositol-3-kinase complex." Nat Cell Biol **11**(4): 468-476.

Ziegler, A. (2008). "Thermodynamic studies and binding mechanisms of cell-penetrating peptides with lipids and glycosaminoglycans." Advanced drug delivery reviews **60**(4-5): 580-597.